AD-A054 434 GTE LABS INC WALTHAM MASS F/G 20/5
ND MINI LASER BASED ON STOICHIOMETRIC RARE EARTHS COMPOUNDS.(U)
APR 78 A LEMPICKI, E JOHNSON, B MCCOLLUM DAAC29-75-C-0028
UNCLASSIFIED ARO-13299.3-P NL

1 OF 2
AD A054434

GTE

(12)

Nd MINI LASERS BASED ON STOICHIOMETRIC RARE EARTHS COMPOUNDS

A. Lempicki
E. Johnson
B. McCollum

Final Report

Contract No. ~~DAAC04-75-C-0028~~
25 JUNE 1975-24 JUNE 1977

Submitted to

U.S. Army Research Office
Box 12211
Research Triangle Park, NC 27709

GTE LABORATORIES INCORPORATED
Waltham, Massachusetts 02154

(6) Nd MINI LASERS BASED ON STOICHIOMETRIC RARE EARTHS COMPOUNDS

by

(10) A. Lempicki
E. Johnson
B. McCollum

(9) Final Report, 25 Jun 75 - 24 Jun 77

Contract No. DAAC04-75-C-0028

25 JUNE 1975 - 24 JUNE 1977

Submitted to

(11) Apr 78

U.S. Army Research Office
Box 12211
Research Triangle Park, NC 27709

(12) 155 P.

(15) DAAG29-75-C-0028

GTE LABORATORIES INCORPORATED
40 Sylvan Road
Waltham, Massachusetts 02154

(18) ARO (19) 13299.3-P

DISTRIBUTION STATEMENT A
Approved for public release;
Distribution Unlimited

406 462 JOB

PREFACE

This report contains an account of the principal results of an investtigation into new stoichiometric compounds of Nd over a two-year period. The overall objective of this program was to develop new high concentration Nd materials for miniature lasers emitting at 1.06μ. At the present time there are only a few such compounds,[1] Nd pentaphosphate being the most widely known. Although remarkable in its efficiency, relative lack of concentration quenching and high gain, the growth of pentaphosphate crystals has proved to be difficult.[2] The crystal growth problems of the pentaphosphate coupled with the possibilities for improved performance by new materials were motivating factors in our research.

The publication of a paper[3] on cubic (ordered perovskite) $Cs_2NaNdCl_6$ in 1974 gave us the idea that the remarkable properties of this material could be used as a starting point for the development of a new class of stoichiometric compounds possibly superior to anything known at the time. The unusual property of $Cs_2NaNdCl_6$ is the exceedingly long lifetime of luminescence (1.2 ms) in the undiluted compound. The length of the decay was ascribed to a large Nd-Nd separation, no sharing of nearest neighbors and the presence of a center of inversion at the Nd site.

As reported in Ref. 3 the new material is of no particular interest to miniature laser technology because of a low emission cross section (and therefore gain) and poor stability in air. However, the isolating properties of the lattice permitting such a long lifetime gave us an idea of how concentration quenching can be suppressed. The initial course of our work was therefore directed at maintaining a similar, ordered perovskite lattice but removing the inversion center. It was thought that a compound with these characteristics might result in a enhancement of the transition probability while still maintaining the lack of concentration quenching.

Our work in the $KF-LiF-NdF_3$ system did not produce an ordered perovskite structure with a distorted site symmetry. However, a new and interesting phase was discovered which may prove a valuable addition to the list of isolated Nd compounds. Since the completion of the contract period the new compound, $K_5NdLi_2F_{10}$, has been isolated with properties that challenge NdP_5O_{14} as a miniature laser material. Prompted by a desire to eliminate active or passive Q-switching while still retaining fast and high peak power pulse operation, we explored the dynamics of laser operation in a system having two centers of similar spectral characteristics but having different lifetimes. A system of that kind could be pictured as containing a low

threshold subsystem based on the high gain centers and an energy storage subsystem based on the low gain centers, all in one material. As it turned out the merits of this scheme are very limited. However, this effort gave rise to a new and comprehensive analytical treatment of pulse operation in optically pumped lasers.

This report is organized as a series of Sections each largely self-contained and dealing with various phases of the work. We summarize the main achievements by presenting an abstract for each Section in turn:

SECTION I

NEW LUMINESCENT Nd^{3+} COMPOUNDS FOR LASER APPLICATIONS;

I. ORDERED CESIUM SODIUM NEODYMIUM HALIDES

A number of polycrystalline elpasolite halides of the general formula $A_2BB'X_6$ have been prepared and investigated as possible candidate materials for miniature Nd lasers. The chief base materials have been $Cs_2NaNdCl_6$ and Cs_2NaNdF_6. X-ray diffraction and emission spectroscopy have been used to follow the effects of various attempts to distort the O_h site symmetry in the parent-ordered-perovskite materials. The combination of excitation line narrowing (using monochromatic excitation) and time resolution (using a boxcar integrator gated at selected delay times) have been very effective in the elucidation of the emission spectra of elpasolite fluorides.

All the fluorides investigated contain two Nd^{3+} sites. At the highest Nd^{3+} concentration, one has a fluorescence lifetime of about 3 μs; the other has a much longer lifetime of 2 ms. The short lifetime species is badly quenched and has been ascribed to $NaNd_xY_{1-x}F_4$ impurity in $Cs_2NaNd_xY_{1-x}F_6$. The quenching constant, k_{cn}, is more than two orders of magnitude higher than for stoichiometric Nd materials. The long lifetime centers show a much smaller deviation of k_{cn} (a factor of 3 or 4) from other stoichiometric materials. The emission spectrum of the long lifetime site has been discussed in terms of nearly O_h symmetry but with the presence of some lines which are likely of vibronic origin.

The design of a stoichiometric material based on the elpasolite structure but with increased radiative probability is evidently much more difficult than originally anticipated. The various attempts to reduce the

Nd^{3+} site symmetry by cationic and anionic substitution have been largely unsuccessful. A further difficulty has been the sensitivity of cesium elpasolites (both chlorides and fluorides) to moisture. This work does indicate that a better understanding of the quenching process would be helpful in future materials design. Finally, the usefulness of the methods of investigation are shown both in this section and very successfully in Section 2, which covers the investigation of the KF-LiF-NdF_3 system.

SECTION II

NEW Nd^{3+} COMPOUNDS FOR LASER APPLICATIONS;

II. POTASSIUM LITHIUM NEODYMIUM FLUORIDES

The KF-LiF-NdF_3 system was investigated with the objective of determining whether a new stoichiometric Nd material might be found. With the aid of selective excitation with a dye laser, the fluorescence spectrum of a new interesting phase was obtained. The fluorescence lifetime for Nd ion in this phase was found to be 280 μs, which is more than twice that of the leading candidate material for miniature lasers, neodymium pentaphosphate (NdP_5O_{14}). A comparison of the emission spectra of single crystalline NdP_5O_{14} and the polycrystalline potassium neodymium lithium fluoride show the two to be very similar with the NPP emission at 1.05μ a bit more intense, but the KNLF phase exhibits a much better branching ratio. Preliminary dilution studies with cerium ion indicates that concentration quenching may be much less in KNLF than in NPP.

Since the end of the contract period some additional information has been obtained in cooperation with S.R. Chinn and H. Y-P. Hong of the MIT Lincoln Laboratory with the use of single crystals.[4] The composition of KNLF has been found as a consequence of an x-ray structural determination to be $K_5NdLi_2F_{10}$. The unit cell is orthorhombic with the space group Pnma. The lattice parameters are: a = 2.065 nm, b = 0.778 nm, and c = 0.690 nm. Nd^{3+} is coordinated to eight fluoride ions with the point symmetry m. The Nd^{3+} concentration is 3.61×10^{21} cm^{-3} and the closest Nd-Nd distance is 0.673 nm. Laser emission has been obtained with a platelet pumped by a dye laser. This is the first high concentration fluoride material in which lasing has been observed.

SECTION III

CONCENTRATION QUENCHING IN Nd^{3+} STOICHIOMETRIC MATERIALS

The basic experimental facts concerning the luminescence of stoichiometric compounds have been reviewed and further confirmed in the case of $Nd_xLa_{1-x}P_5O_{14}$. In particular we draw attention to a quenching rate which is linear in x and the exponential nature of the decay for all x. We point out that the conventional models of concentration quenching based on energy migration governed by a diffusion equation can only account for observations if it is assumed that the stoichiometric materials (specifically the pentaphosphate) contain a fixed impurity concentration ($\sim 10^{17}$ cm^{-3}) independent of x.

This model is considered artificial and another one is proposed based on quenching by nearby Nd-Nd pairs. This too leads to difficulties. A conclusion is reached that there is at present no clear theoretical picture capable of explaining the results. Experiments are suggested for the measurement of energy migration rates as a function of concentration. These could give rise to a major revision of conventional concepts of energy transfer and concentration quenching.

SECTION IV

APPROXIMATE ANALYTIC APPROACH TO LASER PULSE PHENOMENA

We have suceeded in obtaining approximate analytic expressions that describe a wide variety of laser pulse phenomena that can be handled using the laser rate equations. Using these expressions we can examine these phenomena without recourse to the catalogs of numerical computer data that have been the traditional approach to laser pulse phenomena.

For laser materials with long spontaneous lifetimes the Q-switch mode is to be preferred since it gives the highest peak intensity. The enhancement of the peak intensity over cw is approximately equal to the ratio of the spontaneous lifetime to the cavity lifetime.

As the spontaneous lifetime approaches the cavity lifetime the preferred mode is cavity dumping, if the residual cavity losses are small enough. In this case the enhancement over cw is proportional to the ratio of the cavity lifetime with zero output coupling to the cavity round trip time.

Transient spike operation is useful in roughly the same range as Q-switching. However, the enhancement factor over cw operation is low relative to that achievable with Q-switching. Transient spike operation is useful if one is interested in moderate pulse intensities and in dispensing with extra intracavity elements or if one is principly interested in obtaining narrow pulses. If there are lasing centers of different lifetimes present, transient spike operation is dominated by the fast centers and no enhancement of peak intensity results from adding long lifetimes centers for energy storage.

Where one is interested principally in obtaining laser pulses short relative to those of a pump laser transient, pulse operation can be used to advantage even where the spontaneous lifetime approaches the cavity lifetime. With this approach subnanosecond pulses can be obtained in dye lasers.

SECTION V

SPECTROSCOPY OF A HIGH Nd CONCENTRATION Al-PHOSPHATE GLASS

As an extension of the work on stoichiometric materials, we have investigated a Nd glass containing up to 2.7×10^{21} Nd ions per cm^3, or 23 wt % of Nd, and thus approaching the concentration in Nd pentaphosphate (which is 3.9×10^{21} Nd/cm^3). This work was not part of the contract since it was carried out on internally provided funds. We include it in this report in order to draw attention to high concentration glasses as possible candidates for minilasers. Contrary to widely-held beliefs, glasses containing such high concentrations of Nd can still show substantial efficiency. The luminescence decay times were of the order of 40 μs, thus only a factor of three lower than for the pentaphosphate.

Laser experiments performed subsequently to the writing of this report showed that thresholds are between one and two orders of magnitude higher than for the pentaphosphate, when both are pumped with a tunable dye laser.[5] From this it is estimated that thresholds for flashlamp-pumped rods (of the order of 1-cm length) should be below 10J.

REFERENCES

1. S.R. Chinn, H.Y.P. Hong and J.W. Pierce, "Laser Focus," 64 (May 1976).

2. B.C. Tofield, H.P. Weber, T.C. Damen, and G.A. Pasteur, Mat. Res. Bull. 9, 435 (1974).

3. B.C. Tofield and H.P. Wever, Phys. Rev. 10B, 4560 (1974).

4. A Lempicki, B. McCollum, S.R. Chinn, and H.Y-P. Hong, Extended Abstracts, International Quantum Electronics Conf., Atlanta (1978).

5. A. Lempicki, R.M. Klein and S.R. Chinn, IEEE J. Quant. Electr. (to be published).

TABLE OF CONTENTS

TABLE OF CONTENTS (Cont'd)

LIST OF ILLUSTRATIONS

LIST OF ILLUSTRATIONS (Cont'd)

LIST OF ILLUSTRATIONS (Cont'd)

LIST OF ILLUSTRATIONS (Cont'd)

LIST OF TABLES

SECTION I

ORDERED CESIUM SODIUM NEODYMIUM HALIDES

1. INTRODUCTION

The purpose of the present study is to investigate new kinds of materials with stoichiometric or near stoichiometric concentrations of Nd ions. These materials are excellent candidates for the development of miniaturized lasers, emitting around 1.06 μm.

Recently excellent review articles describing the work done to date in several laboratories have been published by Chinn, Hong and Pierce[1] and by Danielmeyer.[2] From these the following criteria for the development of new stoichiometric materials appear to emerge: (a) the distance between Nd-Nd pairs should be large, (b) the Nd ions should not share nearest neighbors and (c) the energy level scheme should be such as to prevent efficient pair relaxation. While these criteria may not be totally sufficient and (c) may not be easily controllable, (a) and (b) are eminently reasonable in terms of what is known about concentration quenching.

Table 1, which summarizes the main properties of known stoichiometric materials is reproduced here from Ref. 1. We wish to draw particular attention to the column labeled "Fluorescence Lifetime." It will be noticed that for all materials with the exception of the aluminum borate, the lifetimes at 1% dilution ($x = 0.01$) are of the order of 200 μs to 400 μs, a value which appears to be characteristic for electric dipole transitions in Nd^{+3}. The aluminum borate has a lower coordination and a stronger departure from inversion symmetry than the rest.[1]

The last entry in the table represents a special case. The unusually long lifetime of $Cs_2NaNdCl_6$ is due to the presence of an inversion center at the Nd site (O_h site symmetry) which makes electric dipole transitions symmetry forbidden.[2] We have chosen the material, or rather materials structurally similar to the hexachloride as the main subject of this investigation. These materials (known as elpasolites) have the general formula $A_2BB'X_6$.[3] The cation A is larger than cations B and B' which are nearly the same size and occupy identical octahedral sites in an ordered manner. This serves to double the cell parameter of the simple cubic ABX_3 perovskite structure and, importantly, to greatly increase the separation of Nd^{3+} sites.

Again referring to Table 1, we see that as the concentration of Nd increases toward a purely stoichiometric composition, the lifetime shortens. This is a well-known manifestation of concentration quenching which is expressible in terms of the lifetime ratio. In an ideal material, this

TABLE 1

COMPARISON OF STOICHIOMETRIC Nd MATERIALS

(From Ref. 1)

Material		Space group	Nd site symmetry	No. of nearest cations	Laser wavelength (μm)	Fluorescence Lifetime (μs) x = 0.01	x = 1.0	Lifetime ratio	Maximum Nd concentration (cm^{-3})
$Nd_xLa_{1-x}P_5O_{14}$	(NPP)	$P2_1/c$	1	8	1.051	320	115	2.78	3.9×10^{21}
$LiNd_xLa_{1-x}P_4O_{12}$	(LNP)	$C2/c$	2	8	1.048	325	135	2.41	4.4×10^{21}
$KNd_xGd_{1-x}P_4O_{12}$	(KNP)	$P2_1$	1	8	1.052	275	100	2.75	4.1×10^{21}
$Nd_xGd_{1-x}Al_3(BO_3)_4$	(NAB)	$I32$	32	6	1.064	50	19	2.63	5.4×10^{21}
$Nd_xLa_{1-x}Na_5(WO_4)_4$	(NST)	$I4_1/a$	$\bar{4}$	8	———	220	85	2.59	2.6×10^{21}
$Nd_xLa_{1-x}P_3O_9$		$C222_1$	2	8	———	375	5	75	5.8×10^{21}
$Cs_2Nd_xY_{1-x}NaCl_6$		$Fm3m$	m3m	6	———	4100	1230	3.33	3.2×10^{21}

ratio would be equal to unity, i.e., there would be no concentration quenching. The table indicates that by this criterion, there should be room for about a threefold improvement. The lifetime ratio of the hexachloride does not appear to be particularly low and, in fact, is the second highest of the materials listed. There is, however, another consideration which makes this structure of particular interest and provides the main motivation for the work reported here.

The observed decay time of fluorescence τ_d is given by the expression:

$$\frac{1}{\tau_d} = \frac{1}{\tau_r} + \frac{1}{\tau_n} \qquad (1)$$

where τ_r and τ_n are the radiative and nonradiative lifetimes, respectively. Assuming that at 1% dilution the observed lifetime is essentially due to radiative processes (i.e., τ_r = 4100 μs), we obtain from Ref. 1 for the stoichiometric (x = 1) material τ_n = 1757 μs). This is an unusually long time indicating a very low probability of nonradiative deactivation. It may represent a consequence of the large distance between Nd ions in this structure (0.77 nm) and the lack of any sharing of nearest neighbors between Nd pairs.[2] The structure of the hexachloride must thus have excellent isolating characteristics which prevent deactivation.

Suppose now that this property of the lattice can be maintained by keeping interionic distances approximately fixed while at the same time removing the center of inversion from the Nd site. This should be achievable, for instance, by substitution of a different halogen (say a fluorine for a chlorine in the nearest neighbor shell). Such a substitution should result mainly in a change of τ_r leaving τ_n unchanged. Suppose that τ_r can be reduced tenfold to a value similar to that encountered in noncentrosymmetric environments. Using Eq. (1), this should result in $\tau_d \sim 300$ μs, and thus a considerable improvement in the ratio τ_r/τ_d. The idea of manipulating the immediate environment of Nd to enhance radiative (electric dipole) transitions while retaining the highly isolating characteristics of the expanded perovskite lattice is thus an intriguing one.

The limited success which we report here is due to rather formidable chemical problems encountered in the preparation of mixed materials. The results provide, however, useful insights into the mechanisms of quenching and for further extension of the same ideas to other systems.

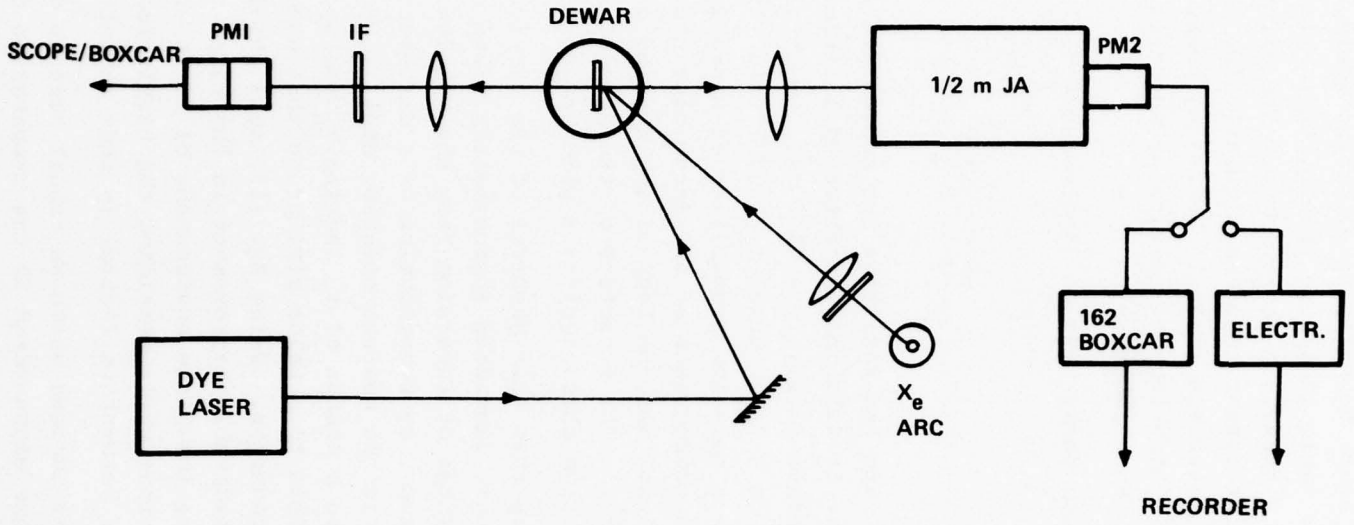

Figure 1. Schematic Layout of Apparatus for Measuring Lifetimes and Time Resolved Spectroscopy

2. EXPERIMENTAL

2.1 SPECTROSCOPY

The experimental setup for spectroscopy shown on Figure 1 enables us to perform a variety of measurements. The sample is located in a gas flow dewar whose temperature can be regulated anywhere between room and liquid nitrogen temperature. For ordinary emission spectra a 150W Xe arc lamp with a BG18 filter is used for front excitation. Spectra are analyzed with a 1/2m Jarrell Ash spectrometer, and detected with a cooled photomultiplier. In the course of this work, two different (PM2) tubes of vastly different responses were used. Earlier spectra were taken with an ITT, FW 118 photomultiplier; later ones with a Varian. Since the Varian response is very nearly flat in the range 800 nm to 1080 nm, the spectra obtained with it show very nearly the correct intensity distribution between the resonance region (850 nm to 950 nm) and the laser transition region (1020 nm to 1080 nm). The S-1 response of the ITT tube tends to emphasize the resonance region by a factor of about 2.5. Since in this paper we are not concerned with branching ratios, no need for spectral correction of the traces was necessary. In all traces the number given on the extreme left identifies the original chart recording and the conditions of experiment. All charts starting with #130 (for Nd samples) and #E26 (for Eu samples) were taken with the Varian tube. All lower numbers were taken with the ITT tube.

An alternative excitation source is provided by a tunable dye laser of conventional design pumped by a nitrogen laser. Depending upon the desired excitation wavelength, rhodamine 6G, coumarin 120, or coumarin 102 were used as dyes. The line width of the dye laser was typically 0.1 nm to 0.2 nm, the repetition rate 60 pps and the tuning range typical of rhodamine 6G. With monochromatic excitation we can obtain "line-narrowed" emission spectra and thus detect the presence of different luminescent sites.[4] Often, however, line narrowing is not sufficient to separate spectra due to different ionic environments because the absorption bands of the different species may still overlap. If the different sites result in luminescence characterized by sufficiently different lifetimes, one can combine excitation line narrowing with time resolution of the detected spectra. This is provided by a boxcar integrator (PAR 162) whose gate can be set up for different delay times. This technique has been used extensively to separate the spectra of sites giving rise to short (microsecond)

and long (millisecond) lifetimes in a series of materials described in Section 2.2. In general, therefore, three types of emission spectra were taken; broadband (Xenon arc) excited to take advantage of all pump bands; monochromatically excited (dye laser) but time averaged by the detection system and finally monochromatically excited and time resolved (boxcar).

The decay times can be measured in two different ways. Fluorescence emanating from the back side of the sample is focused into a photomultiplier through an interference filter isolating the 1.06μ group of lines. The output of the PM can be displayed directly on an oscilloscope or sampled with the boxcar. In the case of Nd^{+3}, this is adequate since the lifetime of the two main groups of lines terminating on $^4I_{9/2}$ and $^4I_{11/2}$ states both originate from the same upper level $^4F_{3/2}$ which in cubic symmetry is not split. In a distorted symmetry, the splitting is usually quite small and the populations in the two possible components are thermalized. Alternately it is possible to measure the decay of a particular line by using the spectrometer and the PM2 tube. The condition of excitation and the measured lifetime (where appropriate) are given on the right side of each emission trace.

2.2 MATERIAL PREPARATION

The goal of the materials part of this project has been the preparation of an ordered perovskite neodymium compound in which the Nd^{3+} site symmetry is reduced so as to enhance radiative transitions. The basic idea is to distort the Nd^{3+} environment of something like $Cs_2NaNdCl_6$ in which Na^+ and Nd^{3+} occupy octahedral sites in an ordered manner as shown in Figure 2.[5] One approach would be to partially substitute the halide sphere such that the anion neighbors are made up of two different elements, such as Br^- and Cl^-. Another approach would be substitution of the cations in the A or B sites in the general $A_2BB'X_6$ formula. Finally a solution to the problem was sought in widening the range of elements such that certain component size restrictions for the perovskite structure are approached. For example, the following tolerance factor has been used:

$$t = \frac{R_A + R_X}{\sqrt{2}\,(R_B + R_X)}$$

where R_A, R_B, and R_X refer to the ionic radii in the perovskite formula ABX_3. For cubic oxide perovskites $0.8 < t < 0.9$, but a somewhat wider range has been reported for the noncubic structures found mainly among oxides.[6]

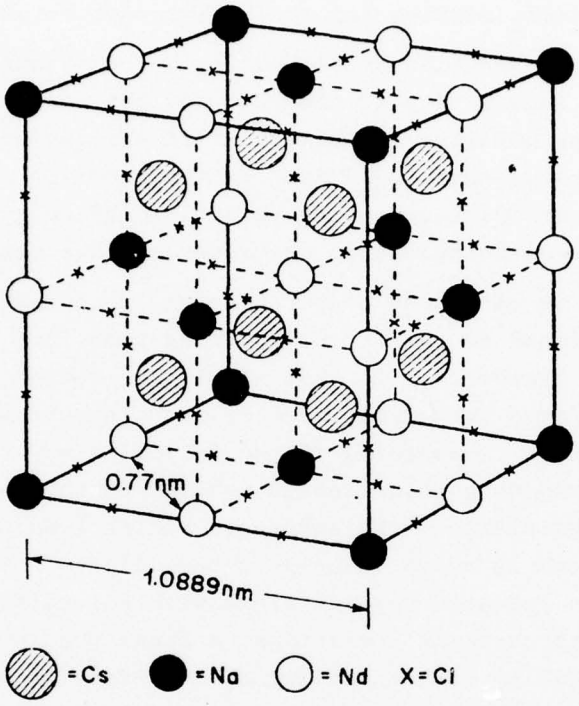

Figure 2. Crystal Structure of $Cs_2NaNdCl_6$

Our approach has been to first investigate samples which were expected to be cubic and then attempt distortion of the Nd^{3+} site. Of course, a simple distortion of the unit cell as indicated by x-ray powder diffraction data does not necessarily imply a distortion of the Nd^{3+} site. In order to follow local changes in the Nd^{3+} environment, emission spectra of samples were routinely taken as reported in the Spectroscopy and Spectroscopy Results sections. The details of the preparations of the various perovskite samples are provided on the following pages.

$Cs_2NaNdCl_6$

This material is the prototype of the ordered perovskites containing Nd^{3+} which are of interest (see Figure 2). The preparation of this material and the growth of single crystals of ordered Cs_2NaMCl_6 compounds (where M represents a number of trivalent metal cations) were first reported by Morss, et al.[7] Samples were reportedly prepared by evaporation of an HCl

solution of the cations to dryness or by combination of the anhydrous halides under vacuum or inert atmosphere conditions. These preparative techniques were later used by Tofield and Weber to obtain polycrystalline and single crystalline $Cs_2NaNdCl_6$ samples for their fluorescence studies.[5]

We found the preparation of $Cs_2NaNdCl_6$ to be rather difficult, not so much from the air sensitivity of the product, but because moisture is introduced readily by handling the reactants in air (especially $NdCl_3$). The attempted formation of pure $Cs_2NaNdCl_6$ by the reaction of CsCl, NaCl, and Nd_2O_3 in a stream of HCl has demonstrated the difficulty of the complete conversion of rare-earth oxides to chlorides by this method.

The alternative method of evaporating an appropriate HCl solution to dryness has been found to result in impure samples, but the method might be acceptable if the evaporation is done slowly, or better, under reduced pressure. An improved procedure, greatly reducing the water content of the final precipitate is achieved in the following way.[8] The volume of an HCl solution of component chlorides is reduced to the point where $Cs_2NaNdCl_6$ just begins to precipitate. The sample is redissolved by the addition of methanol, the volume is again reduced to the point of precipitate formation, and the process is repeated several times with HCl being bubbled through the solution. After several iterations, a final precipitation is made by reducing the solubility of the product by the addition of isopropanol. This is dried under an HCl flow by gentle heating followed by somewhat higher temperatures to remove the last traces of solvent. Even this did not prove entirely satisfactory because impurities were always shown to be present by x-ray powder diffraction data.

The direct, and probably best, preparation of $Cs_2NaNdCl_6$ involves the reaction of the component chlorides in a stream of HCl, or in a sealed ampule. In either case some precautions should be taken to avoid sample contamination. An argon filled glove box and vacuum line techniques were used during and after sample preparations in order to minimize atmospheric contaminants.

Cesium chloride is somewhat volatile at preparation temperatures of 800° to $850^{\circ}C$; thus, precise control of stoichiometry is a bit difficult in an HCl flow because of loss of CsCl. Therefore, both polycrystalline and samples with single crystalline sections were prepared by heating dried anhydrous chlorides in sealed, evacuated quartz ampules. Best results were obtained, especially in crystal growth experiments, after the melting point of $Cs_2NaNdCl_6$ was found to be about $715^{\circ}C$ (the sample was observed to be

liquid at 720°) rather than 800° to 850°C as implied elsewhere.[5] Knowing this, samples were heated above 800°C for only a few hours (to allow complete reaction of the components) and then brought to about 730° to 750° for the crystal-growth process. By this procedure, attack of the quartz ampules was visibly reduced.

The crystal-growth procedure employed the gradient freeze method in a zoned vertical furnace with gradients of about 5° to 40°C per inch. Samples were equilibrated 25° to 50° above the melting point for six to ten hours prior to controlled cooling at 2° to 5°/hour. The quartz sample containers were 6 mm to 10 mm I.D. with a conical tip drawn at about 30° to 45° angles. Best results were obtained when a constriction was provided about one-half inch above the sample tip in order to reduce crystal defects and twinning. The samples were susceptible to attack by moist air, were rather soft, and proved difficult to polish. Chloride samples grown by this method included $Cs_2NaNdCl_6$, $Cs_2LiNdCl_6$, and $Cs_2Na_{0.9}Mg_{0.2}Cl_6$. All showed clean x-ray patterns for the ordered perovskite phase. Emission spectra showed evidence that Nd^{3+} is located only in an Oh symmetry octahedral environment.

$Cs_2NaNd_xY_{1-x}F_6$

Initially, preparation of Cs_2NaNdF_6 was attempted by substitution of $Cs_2NaNdCl_6$ by various fluorinating agents but without notable success. It was apparent that a preparation from the component fluorides or from appropriate carbonates or oxides by the action of HF in a Monel apparatus would be best. To this end, the apparatus diagrammed in Figure 3 was constructed. The gas line inputs were Monel and allowed the use of argon as a flushing gas prior to heating the sample. A screw-on Monel cap fitted with a Teflon washer on the upstream end of the reaction tube provided access for sample loading and withdrawal as well as cleaning prior to use. A nitrogen flow was maintained over the section of the outer wall of the Monel tube inside the furnace to minimize external oxidation of the tube at reaction temperatures. Both graphite boats and platinum lined alumina combustion boats have been used satisfactorily in the formation of ordered perovskite fluorides.

Preparation of pure Cs_2NaNdF_6 has never been satisfactory. Early in the program, before the argon filled glove box and vacuum line were available for sample handling, it was unclear whether pure Cs_2NaNdF_6 did not form because of thermodynamic considerations or whether the hygroscopic samples deteriorated so quickly that good x-ray or spectroscopic data could not be obtained. Subsequent work with adequate facilities has shown the former to

be the case, in that anhydrous samples continued to exhibit two Nd^{3+} sites in fluorescence spectra and the x-ray powder diffraction patterns always revealed small amounts of impurities were present.

Aleonard and Pouzet[9] have indicated that the larger rare earth ions do not form cubic perovskites of the Cs_2NaMF_6 composition. Accordingly, a preparation of Cs_2NaYF_6 was made in the same manner as the Cs_2NaNdF_6 samples previously indicated. The product was nonhygroscopic and x-ray data agreed with those listed for Cs_2NaYF_6 in Ref. 9. This result is excellent evidence that the difference in size of Nd^{3+} (0.107 nm) and Y^{3+} (0.095 nm) is an important factor in the formation of stable ordered perovskite fluorides.

Subsequent preparations of a range of compositions in the $Cs_2NaNd_xY_{1-x}F_6$ system have shown that the hygroscopic nature of the product varies with the Nd content. Powdered samples with x = 0.5 or less present no particular handling problems in air, but extended exposure of powdered samples with x greater than 0.25 results in some deterioration. One or more samples have been prepared at each of the compositions with x = 1, 0.75, 0.50, 0.25, 0.10, 0.05, 0.01 and 0.001. Each, with the exception of the pure Nd material discussed earlier, has the ordered perovskite structure as determined by x-ray powder diffraction data. These samples have been examined in some detail spectroscopically and the experiments are reported in the Spectroscopic Results section.

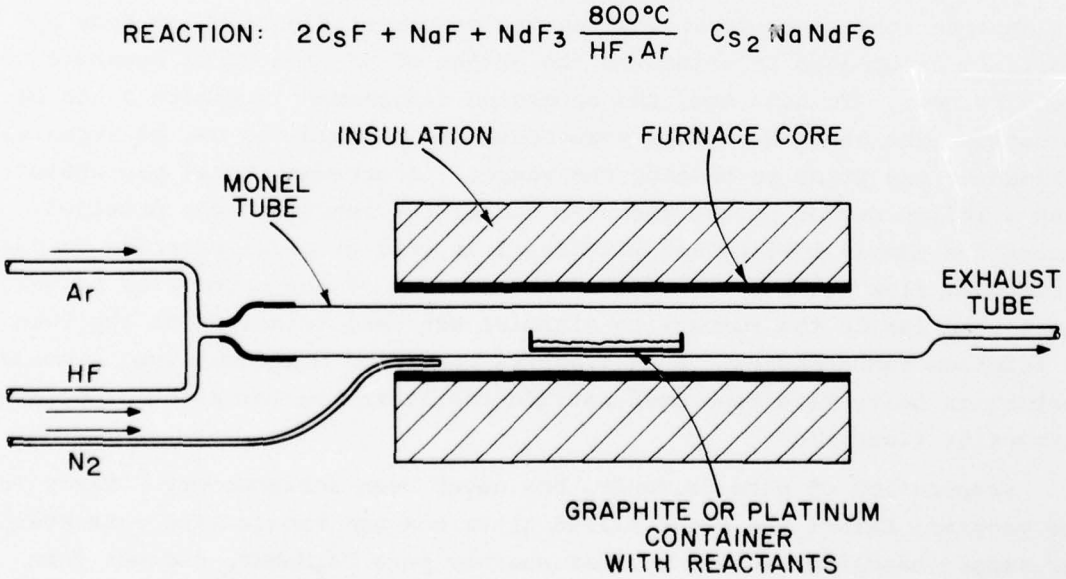

Figure 3. Preparation of Perovskite Fluorides

$NaNd_xY_{1-x}F_4$ and $NaEu_xY_{1-x}F_4$

Polycrystalline samples of these materials were made by the same procedure used for $Cs_2NaNd_xY_{1-x}F_6$, except that somewhat higher temperatures (900° to 950°C) were required. The $NaNd_xY_{1-x}F_4$ and $NaEu_xY_{1-x}F_4$ series were prepared at compositions with x = 1, 0.25, and 0.01 for spectroscopic studies in order to trace the identity of impurities in $Cs_2NaNd_xY_{1-x}F_6$ materials.

Mixed Halides

The mixed halide materials, $Cs_2NaNd_xY_{1-x}F_{6-y}Cl_y$ and $Cs_2NaNd_xY_{1-x}Br_{6-y}Cl_y$, were specific attempts to reduce the site symmetry of the Nd^{3+} ion. The preparation of fluoride-chloride samples was tried under an argon flow in the manner described for the $Cs_2NaNd_xY_{1-x}F_6$ system (except no HF flow was used). Later when high-density graphite containers with tight-fitting lids became available, the attempted preparation from component fluorides and chlorides was repeated. A third method simply involved heating the components for reaction in an evacuated quartz ampule. The result of this last method was extensive quartz attack. The other samples were shown to be impure by x-ray data. Fluorescence spectra were characteristic of $Cs_2NaNdCl_6$ with no reduction of lifetime. Despite a number of attempts, including slowly cooling (3°/hr) a sample in a closed high purity graphite container, no preparation of a mixed fluoride-chloride ordered perovskite was successful.

The preparations of mixed bromide-chlorides were made in evacuated quartz ampules by heating the components at 850° for several hours and then cooling the samples at perhaps 100°/hour. The x-ray data were correct for ordered perovskites and the lattice parameters were suitably intermediate between those of $Cs_2NaNdCl_6$ and that expected for $Cs_2NaNdBr_6$. However, as indicated in the Spectroscopy Results section, the emission spectra consisted of rather broad bands and were essentially the same as spectra for the pure chloride. It is likely that this resulted in a range of bromide-chloride Nd^{3+} environments.

Crystal Growth Experiments

A number of attempts were made to grow crystals of Cs_2NaNdF_6 by the gradient freeze method in a zoned furnace as described for $Cs_2NaNdCl_6$ growth. In this case, a special graphite of high purity and density (Poco DFP-3-2*) was used to construct the closed containers for both

*Union Poco Graphite, Inc., Decater, Texas.

horizontal and vertical use shown in Figure 4. The graphite containers were cleaned prior to use in a stream of argon and HCl at 900°C for several hours, and then transferred to an argon-filled glove box for sample loading. The closed containers were effective in limiting CsF loss even when subjected to temperatures above 800°C for several days. Losses were typically a few tenths of a gram from a sample charge of 7 to 8 grams. Temperature zones of from 40° to about 150°C over the 4 in. container length were tried at a cooling rate of about 3°C/hr. Perhaps the most crystalline samples were obtained with the higher gradients, but nothing approaching single crystalline material was obtained. The x-ray powder data always indicated small amounts of impurities (nonperovskite phase) to be present. This was confirmed in the spectroscopic data because the hexagonal form of $NaNdF_4$ was always present. It seems likely that $Cs_2NaNd_xY_{1-x}F_6$ melts incongruently. In retrospect, perhaps single crystals might be obtained using CsF or CsF-NaF eutectic as a solvent for normal flux growth procedures.

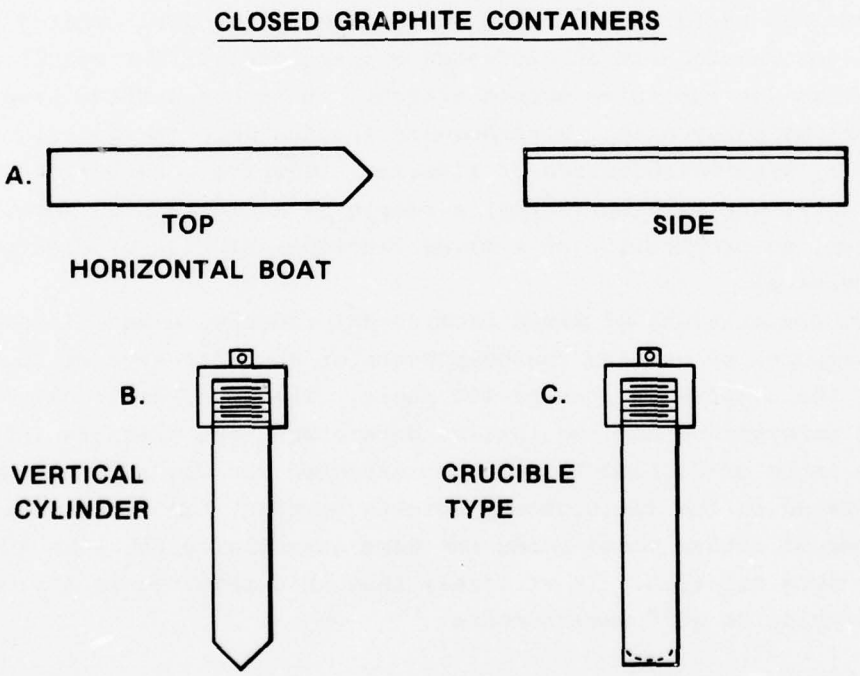

Figure 4. Containers Used for Fluoride Crystal Growth

2.3 SPECTROSCOPIC RESULTS

$Cs_2NaNdCl_6$

Emission and absorption spectra of this material have been reported by Tofield and Weber[5] who interpreted them as magnetic dipole and forced electric (vibronic) transitions. Although there is little doubt that the environment represents a true O_h symmetry [see for instance, the work on the corresponding Eu^{+3} compound by Serra and Thompson (Ref. 10)], the Nd^{+3} spectrum is far more complicated and the vibronic contributions make the assignments somewhat tentative. Using an Xe arc as excitation the spectrum appears to be identical to that reported in Ref. 5 (Figure 5 top trace*). For comparison purposes, we also give an emission spectrum of the same sample excited by the dye laser. The differences are indeed minor except for the change of intensity in the shoulders of the dominant line in the resonance transition group (850 nm to 950 nm).

Cs_2NaNdF_6

As noted in Section 2.2, this material is not stable, is highly hygroscopic and over a period of time in air loses the appearance of crystallinity. Figure 6 shows two emission spectra taken with an Xe arc excitation. The top trace has been obtained on a fresh sample and has a rather poorly resolved structure. The decay time of the luminescence is, however, 1.28 ms characteristic of a site with inversion symmetry. The lower trace was taken after a few weeks exposure of the sample to laboratory air. We notice a radical change in the spectrum, accompanied by a decrease in intensity. The lifetime of this sample has decreased to 2.5 μs.

$Cs_2NaY_{1-x}Nd_xF_6$

Depending on the value of x, emission spectra and decay times can be divided into fairly distinct categories which we shall designate as follows:

Type A: $0.1 < x < 0.75$
Type B: $0.01 < x < 0.1$
Type C: $x < 0.01$

For $x \leq 0.75$ the compounds are considerably more stable than for $x = 1$ and can be left for weeks without appreciable change. Eventually Type A compounds do undergo some change in the same direction as the undiluted

*Excitation conditions and observed decay times (τ_d) are given on the right side of the spectra.

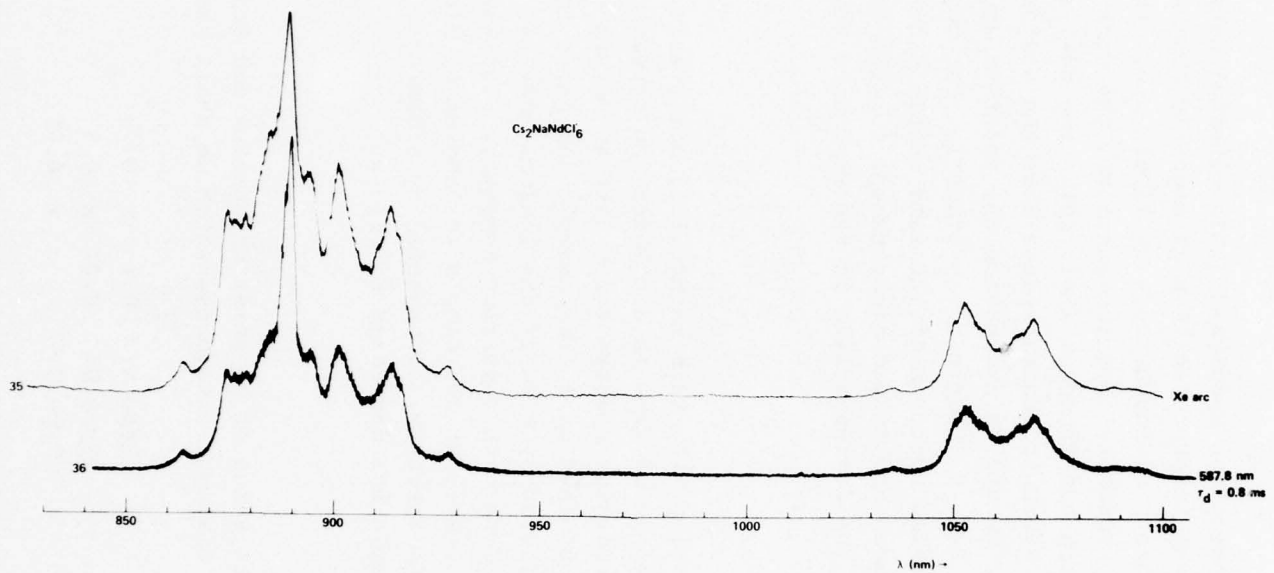

Figure 5. Room Temperature Spectra of Pure Perovskite Chloride Material Under Broadband and Monochromatic Excitation

compound, but the process is very much slower. An immediate characteristic of the Type A compounds is the appearance of two different lifetimes depending upon the excitation wavelength. In Figure 7, we see two oscilloscope decay traces taken under identical conditions except for the wavelength setting of the dye laser. The top trace shows a very rapid decay from a high peak level whereas the bottom trace shows only a low intensity rapid component followed by a long lifetime component. The two lifetimes are 2.4 μs and 2.2 ms, respectively.

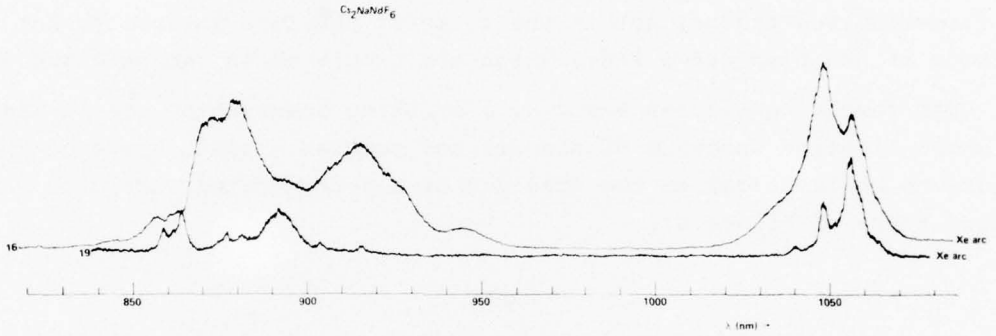

Figure 6. Room Temperature Emission on Spectra (Broadband Excitation). The Top Trace is for a Fresh Sample. The bottom trace represents the same sample after a few weeks.

$Cs_2NaY_{0.5}Nd_{0.5}F_6$

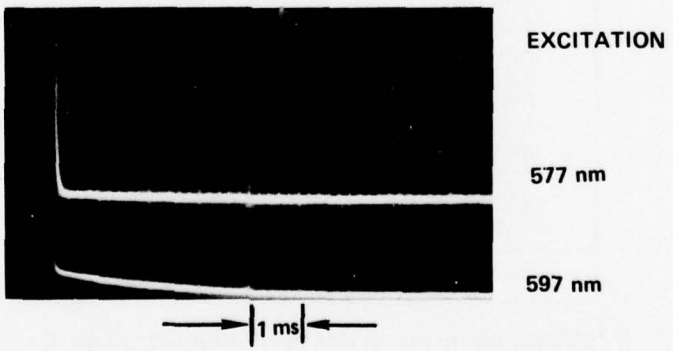

Figure 7. Decay Current for Two Different Excitation Wavelengths Showing the Existence of Two Lifetimes

Representative emission of Type A compounds are shown on Figure 8. The top trace is obtained with Xe arc excitation and shows a multitude of lines. A greatly simplified spectrum can be obtained by tuning the dye laser to a wavelength which maximizes the fast or the slow component of the decay. A further simplification resulting in the two lower traces is obtained with the boxcar whose gate is adjusted to time resolve either the fast or the slow component of the delay. By judicious choice of excitation wavelengths and gates, one can almost completely eliminate any overlap of lines in the two spectra. Overall, however, the Xenon excited spectrum is dominated by the long-lifetime species especially in the resonance region (note the similarity of the 47 and 28 trace in the range of 850 nm to 950 nm). Upon closer examination the Xe excited trace represents a summation of the two time-resolved traces, not in the sense of absolute intensity, but the presence of the respective lines which are tabulated in Tables 2 and 3.

Upon comparing Figures 6 and 8, a striking observation can be made. The short lifetime spectrum of the diluted samples (middle trace of Figure 8) appears to be identical to the spectrum of a deteriorated undiluted sample (bottom trace of Figure 6).

TABLE 2

SHORT LIFETIME LINES (nm)*

$(Cs_2NaY_{0.75}Nd_{0.25}F_6)$

$^4F_{3/2} \rightarrow {}^4I_{9/2}$	$^4F_{3/2} \rightarrow {}^4I_{11/2}$
896.0 (L?)	1065.0 VW
893.6 S	1062.4 W
890.4 S	1060.4 W
888.0 (L?)	1058.8 S
880.0 S	1057.0 S
877.0 S	1055.0 S
874.5 W	1053.0 VW
870.4 W	1050.6 W
864.6 S	1048.4 S
863.2 W	1047.4 S
861.6 S	1043.8 W
859.0 S	1039.8 W
10 (12?) Lines	12 Lines

*Obtained from spectra taken at liquid nitrogen temperature

S - Strong
W - Weak
VW - Very Weak
(L?) - Possibly belonging to long lifetime spectrum

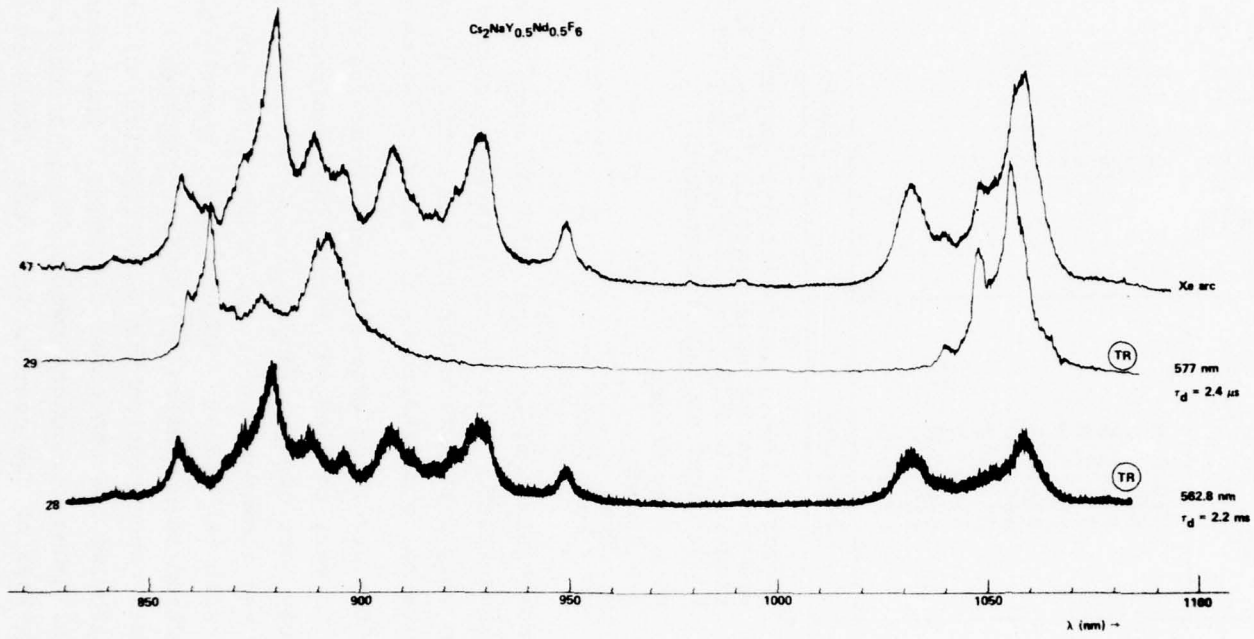

Figure 8. Emission Spectra of 50% Nd Perovskite Fluoride. The top trace was obtained with broadband excitation. Lower traces were time resolved (TR) and employed monochromatic excitation.

TABLE 3

LONG LIFETIME LINES (nm)*

$(Cs_2NaY_{0.75}Nd_{0.25}F_6)$

$^4F_{3/2} \rightarrow {}^4I_{9/2}$	$^4F_{3/2} \rightarrow {}^4I_{11/2}$
950.0 S	1058.0 S
930.5 S	1050.0 W
928.0 S	1046.0 W
918.5 W	1039.0 W
909.0 W	1032.0 S
896.0 S	1023.0 VW
888.0 S	1020.0 VW
879.0 VS	
876.0 W	
872.0 W	
867.0 W	
856.5 W	
12 Lines	7 Lines

*Obtained from liquid nitrogen temperature spectra, except some lines in $^4F_{3/2} \rightarrow {}^4I_{11/2}$ transitions which were too weak and had to be obtained at room temperature

VS - Very Strong
S - Strong
W - Weak
VW - Very Weak

When the concentration of Nd drops below 10 atom %, a significant change in the spectra is manifest. This is illustrated in Figure 9. The Xenon trace differs now very little from the monochromatically excited traces. The spectrum begins to be dominated by the short lifetime species.

By scanning the dye-laser excitation and observing the shape of the decay curves, it is easy to find the excitation wavelengths at which the fast and slow decay portions are respectively maximized. The intensity (specifically of the slow component) is, however, too small to obtain time-resolved spectra with the boxcar. In each case, therefore, the overall shape of the spectrum is dominated by the fast component. It should be noted that for this concentration the short lifetime has lengthened 12 μs while the long lifetime has shortened to 0.9 ms. This represents a truly intermediate case. When the concentration of Nd is dropped to 1% or below (Type C), any vestiges of two centers disappear. This is illustrated on Figure 10 where broadband and monochromatic excitation produce essentially the same spectrum. Moreover, only one lifetime is observed (90 μs for this case) and there is no detectable change of spectrum with varying excitation wavelength.

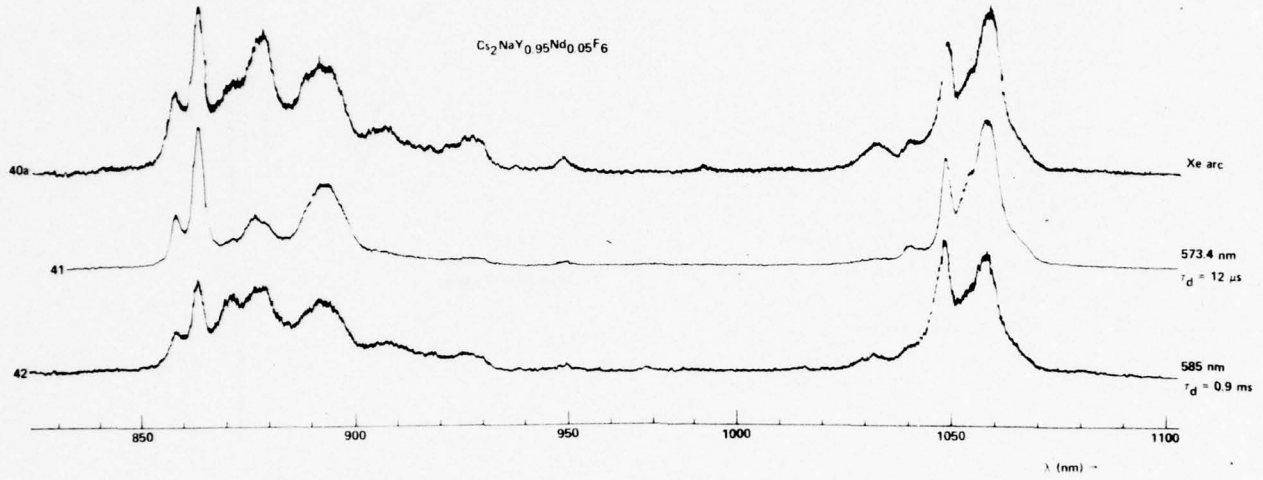

Figure 9. Emission Spectra of 5% Nd Perovskite Fluoride Under Broadband Excitation (Top Trace) and Two Monochromatic Excitations Chosen to Maximize Short and Long Lifetime Components

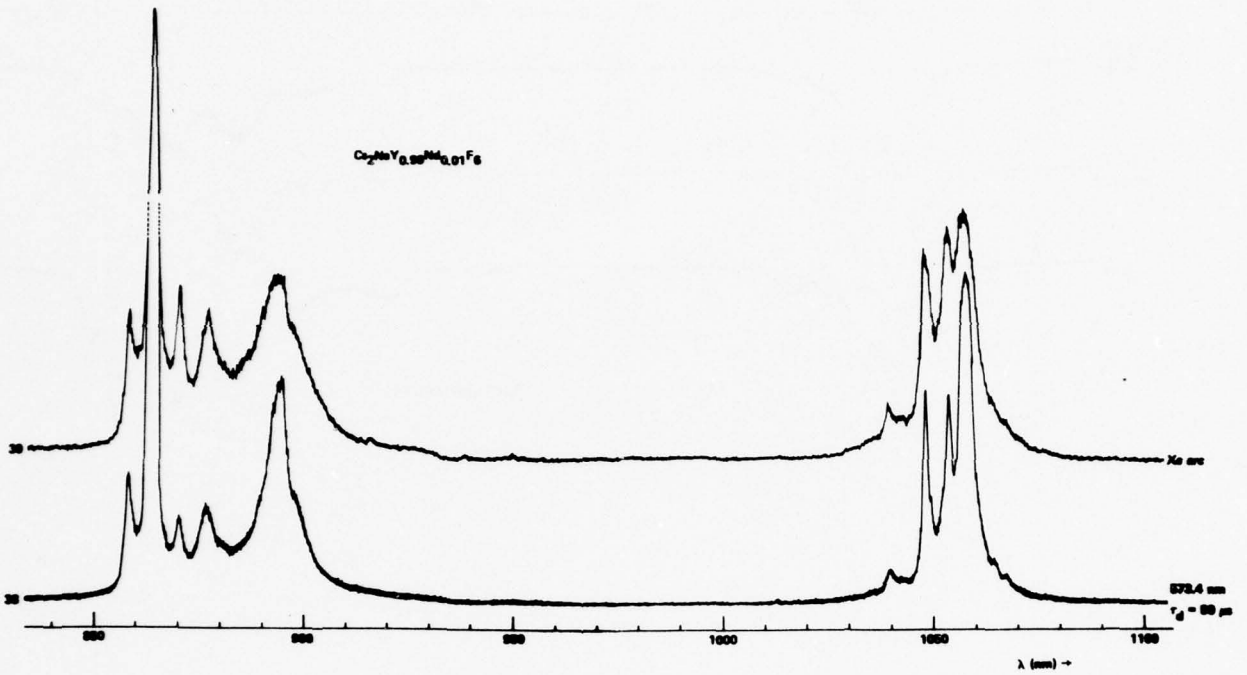

Figure 10. Emission Spectra of 1% Nd Perovskite Fluoride Under Broadband and Monochromatic Excitation

At a still lower concentration (0.1% Nd) the spectra remain essentially unchanged but the lifetime reaches 300 μs. The diluted samples are thus characterized by a single center.

Mixed Hexahalides $Cs_2NaNdCl_{6-y}H_y$

Many attempts were made to remove the center of inversion at the Nd site by substitution of mixed halides in the coordination sphere of Nd. These results were not successful as shown on Figure 11 which compares spectra of the pure chloride with that of mixed chloride-bromide. The effect of substitution is primarily a broadening of the spectrum without drastic effects on intensity distribution or lifetime. Mixed chloride-fluoride materials did not accomplish this goal either. Substitution of even one fluorine atom resulted in the immediate appearance of a very short lifetime site shown on Figure 12, whereas the bulk of the emission consisted of essentially the unchanged hexachloride spectrum (Figure 12, top trace).

$NaNd_xY_{1-x}F_4$

As explained in Section 2.2, this material is not expected to yield an efficient stoichiometric compound. Our interest in it results from a remarkable resemblance of its emission spectrum with the short lifetime emission spectrum of the $Cs_2NaNd_xY_{1-x}F_6$ compounds. A direct comparison of the two spectra is shown on Figure 13, the top trace being a reproduction of the middle trace (#29) of Figure 8.

At greater dilution the tetrafluoride spectrum sharpens and again becomes identical to the dilute hexafluoride spectrum shown on Figure 10. These results indicate that the origin of the short lifetime species in the hexafluoride is an inclusion of the tetrafluoride phase. This latter phase becomes dominant at low concentration. Moreover, since it is apparently more stable, it is the phase into which the hexafluoride is converted by exposure to moisture (see Figure 6). However, even $Cs_2NaNd_xY_{1-x}F_6$, which were carefully prepared and handled under inert conditions, exhibited the presence of the short lifetime species which is characteristic of $NaNdF_4$.

Eu^{3+} Compounds

To confirm the presence of a tetrafluoride phase in the fluoride elpasolites, a series of analogous compounds containing Eu^{3+} instead of Nd^{3+} were prepared. Since the level structure of the Eu^{3+} ion is considerably simpler than that of Nd^{3+}, the spectra are simpler to interpret. Samples

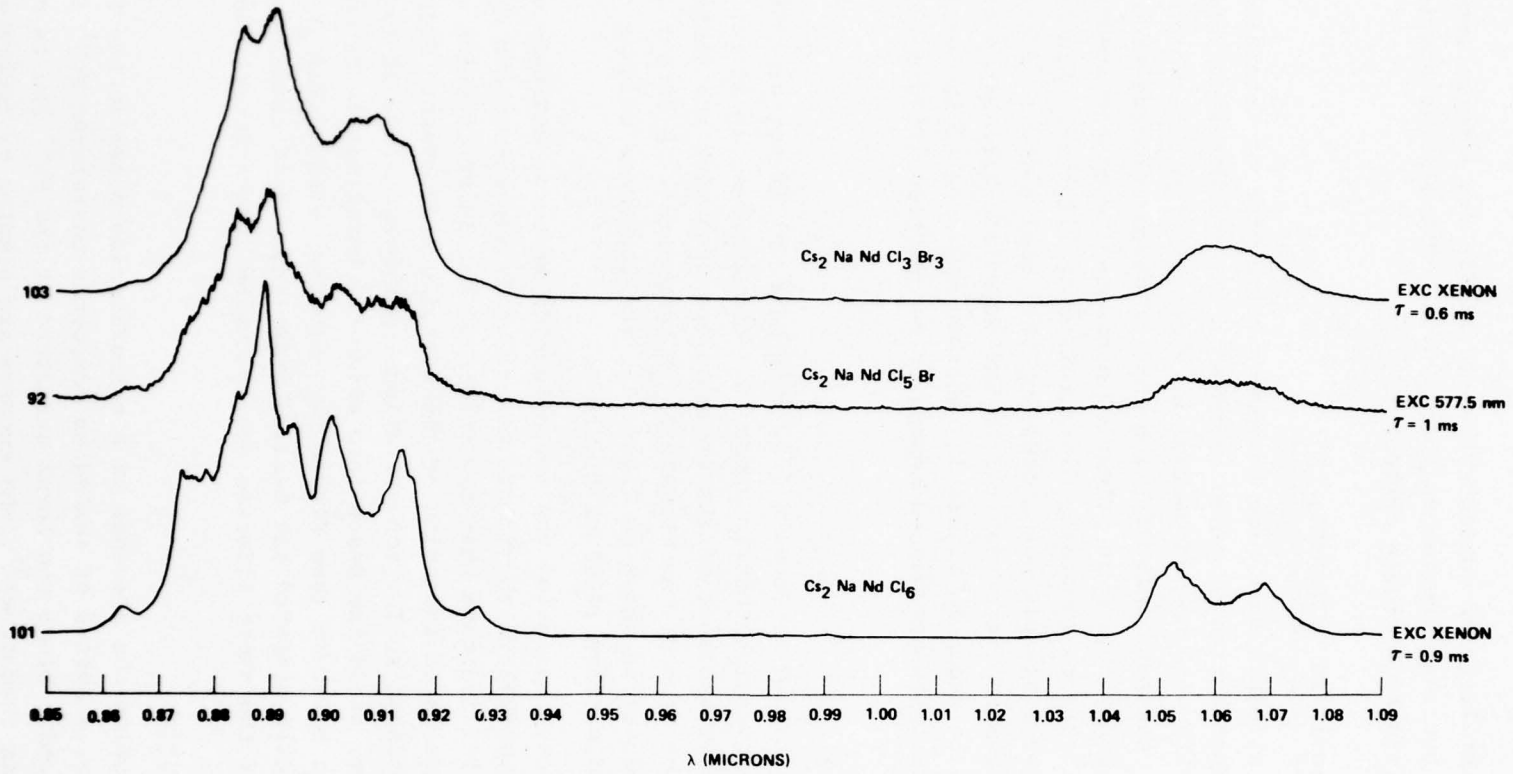

Figure 11. Comparison of the Emission Spectra of $Cs_2NaNdCl_6$ (Bottom Trace) with those of Mixed Chloride-Bromides. Note the long lifetimes but broadened nature of the latter.

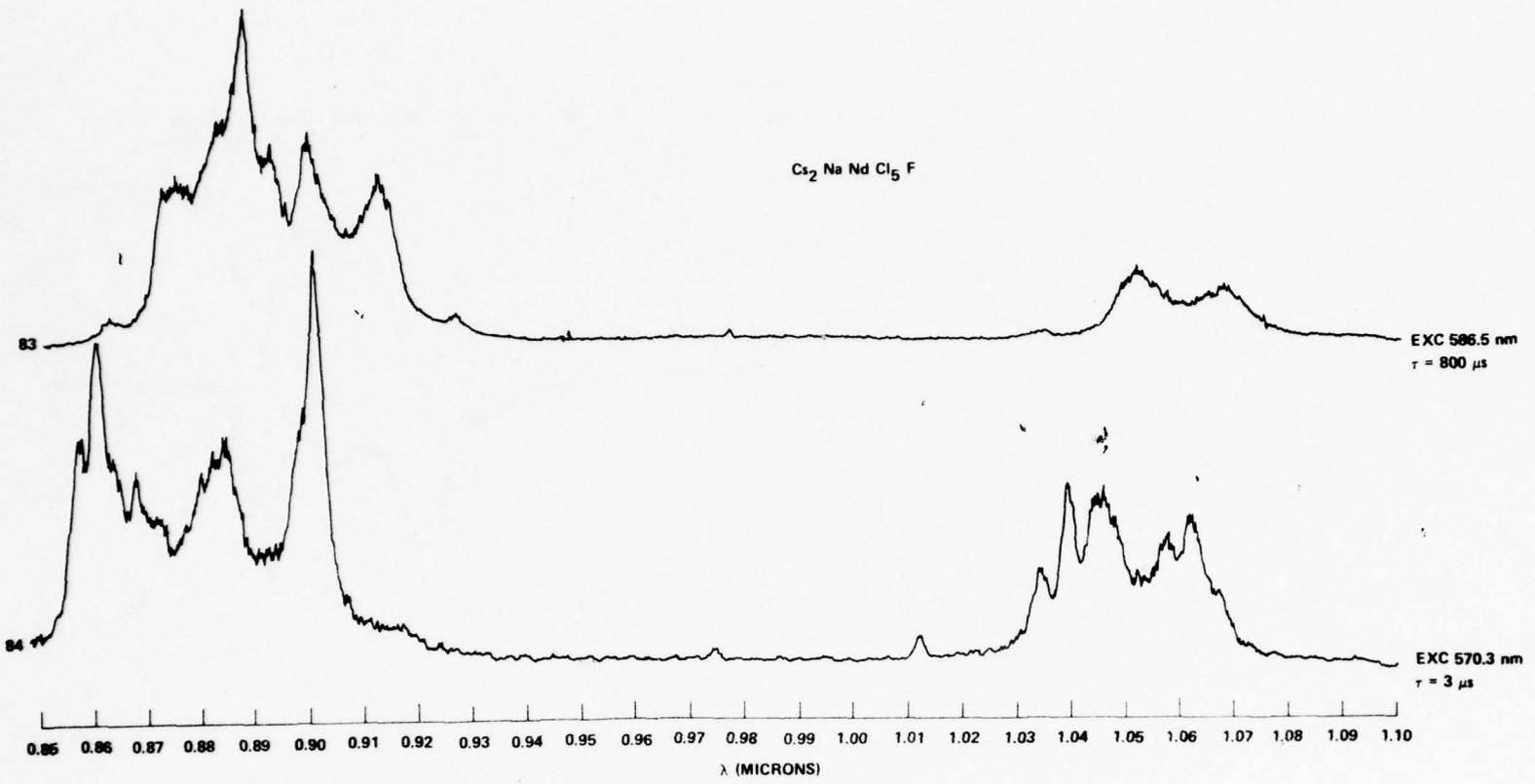

Figure 12. The Short and Long Lifetime Emission Spectra of Samples of the Nominal Composition $Cs_2NaNdCl_5F$

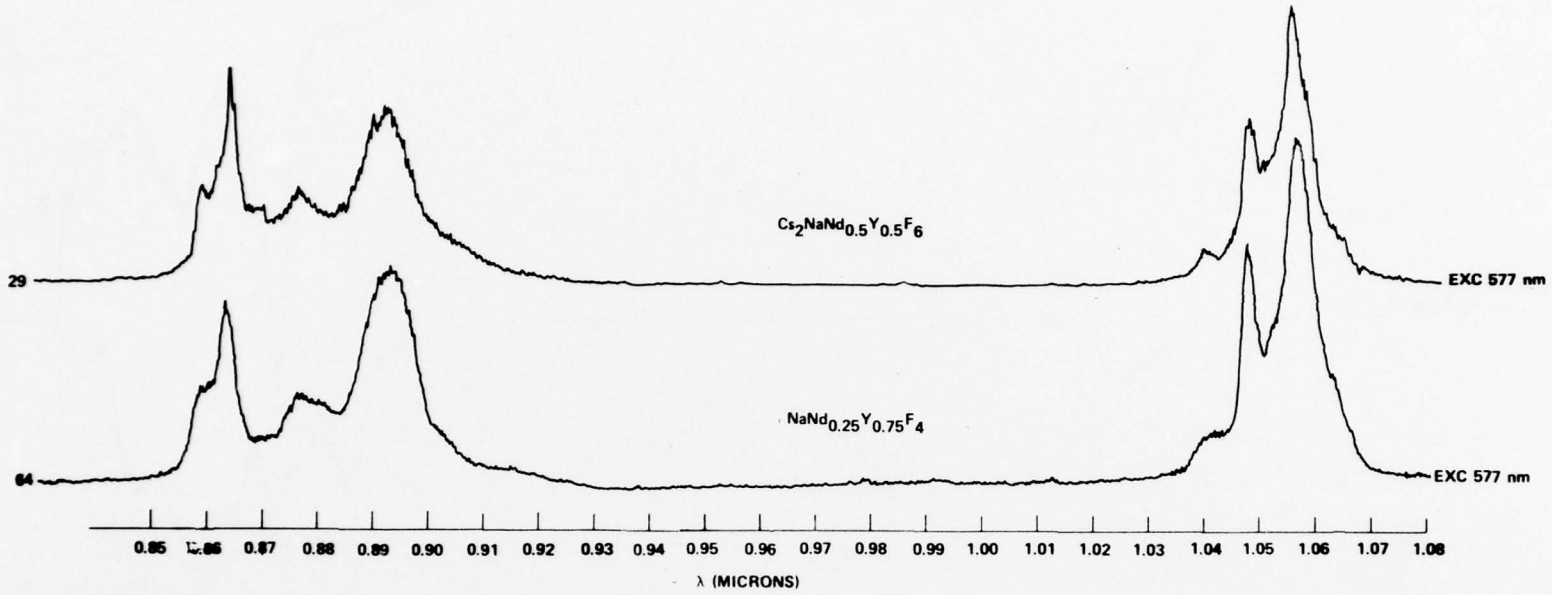

Figure 13. Direct Comparison of the Short Lifetime Spectra Found in Hexafluoride (Top Trace) with that of a Tetrafluoride (Bottom Trace)

were pumped with the dye laser tuned to the $^7F_0 - ^5D_1$ transition occurring in the vicinity of 525 nm and and emissions occurring from the $^5D_0$ or $^5D_1$ levels to the lower members of the ^7F manifold were recorded.

Figure 14 gives a comparison of three relevant spectra. The two upper traces obtained on the same sample, but differing only in the excitation wavelength, revealed the existence of two different sites in the elpasolite. The top spectrum is an excellent example of an octahedral site where the dominant transitions $^5D_0 - ^7F_1$ and $^5D_0 - ^7F_4$ are of magnetic character. Changing the excitation from 525.5 nm to 524.8 nm results in a complete change of the spectrum (middle trace) indicating a lowered symmetry. The bottom trace is obtained from a tetrafluoride ($NdEu_{0.25}Y_{0.75}F_4$) containing the same molar fraction of Eu as the hexafluoride. It is seen to be very nearly a replica of the middle trace. This suggests that here also the "distorted" site in the hexafluoride corresponds to a site characteristic of the tetrafluoride.

An interesting feature of the spectra corresponding to the tetrafluoride site (Figure 14, E8, E19) is the amost complete absence of lines originating from the $^5D_1$ state when time integrated detection is used. This indicates a fast $^5D_1 - ^5D_0$ relaxation. When the concentration of Eu is reduced to 1%, the lines originating from the $^5D_1$ state begin to appear. This is shown on Figure 15, which is analogous to Figure 14 except for greater dilution of the Eu ions. The $^5D_1 - ^5D_0$ relaxation is thus strongly concentration dependent. This suggests that it may occur via a $^5D_1 - ^5D_0$: $^7F_0 - ^7F_3$ cross relaxation, which would obviously depend upon the average distance between the ions. It is, we believe, quite significant (see Discussion section) that the appearance or disappearance of lines originating from $^5D_1$ levels is quite parallel in the pure tetrafluoride and tetrafluoride-like site in hexafluoride.

The dynamics of $^5D_1 - ^5D_0$ relaxation were studied in greater detail by using methods of time-resolved spectroscopy. As an example we show in Figure 16 time-resolved traces of the emission taken at two different times during the decay. At early times (delay 0.5 ms, trace E22) the $^5D_1$ emissions are clearly visible whereas at longer delays (trace E23) they are absent. The time integrated spectrum of the same material (Figure 13, trace E19) shows only a very weak trace of the $^5D_1$ emission. The relaxation rate for the $^5D_1 - ^5D_0$ process is thus relatively slow, of the order of a millisecond, at a 25 atom % concentration of Eu^{3+}.

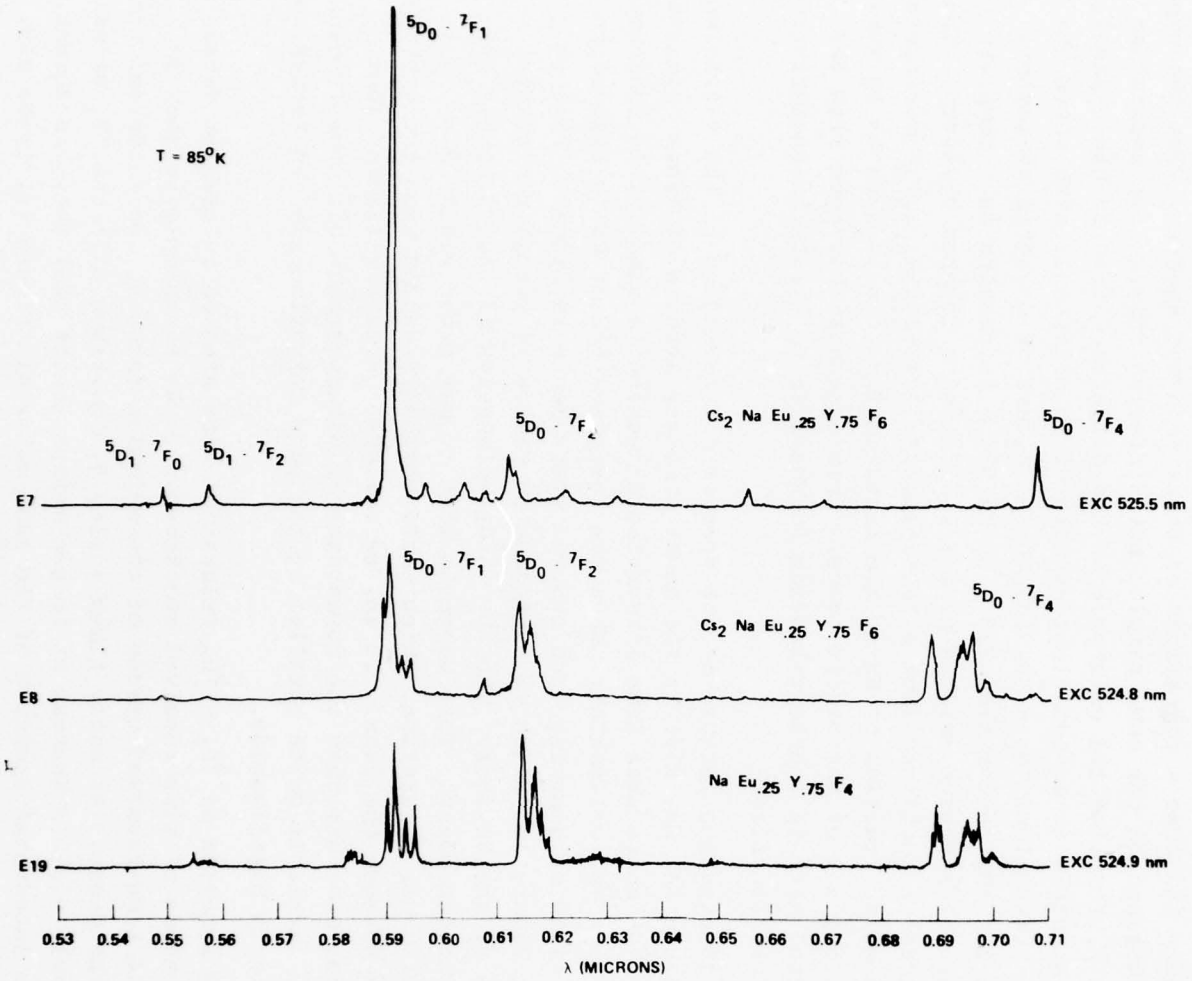

Figure 14. Eu^{3+} Emission Spectra for $Cs_2NaEu_{.25}Y_{.75}F_6$ Excited at two Different Wavelengths (Top and Middle Trace) Compared with Emission of $NaEu_{.25}Y_{.75}F_4$ (Bottom Trace). Note the similarity of middle and bottom traces indicating presence of a tetrafluoride site in the hexafluoride.

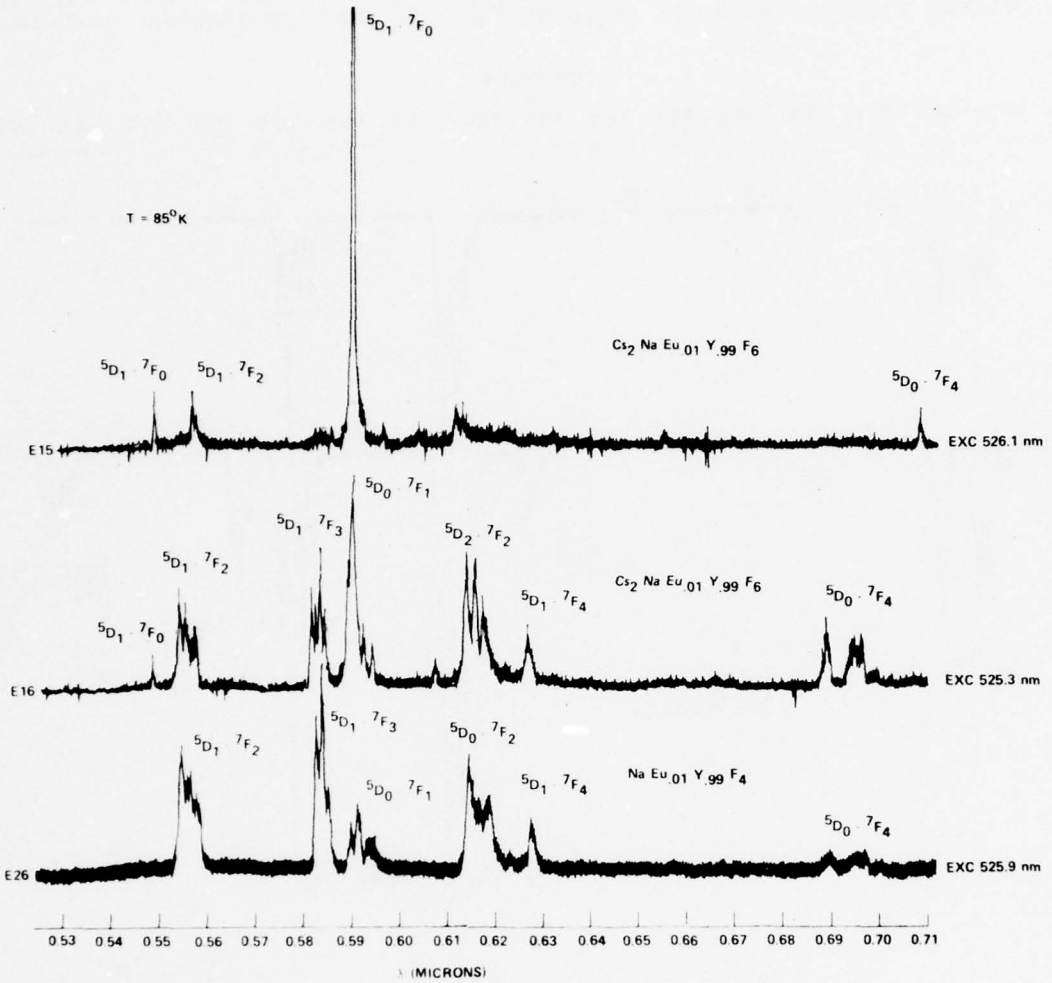

Figure 15. Emission Spectra at 85°K of the Two Eu^{3+} Sites in $Cs_2NaEu_{.01}Y_{.99}F_6$ (Top and Middle Trace) Compared with the Site in Tetrafluoride $NaEu_{.01}Y_{.99}F_4$ (Bottom Trace).

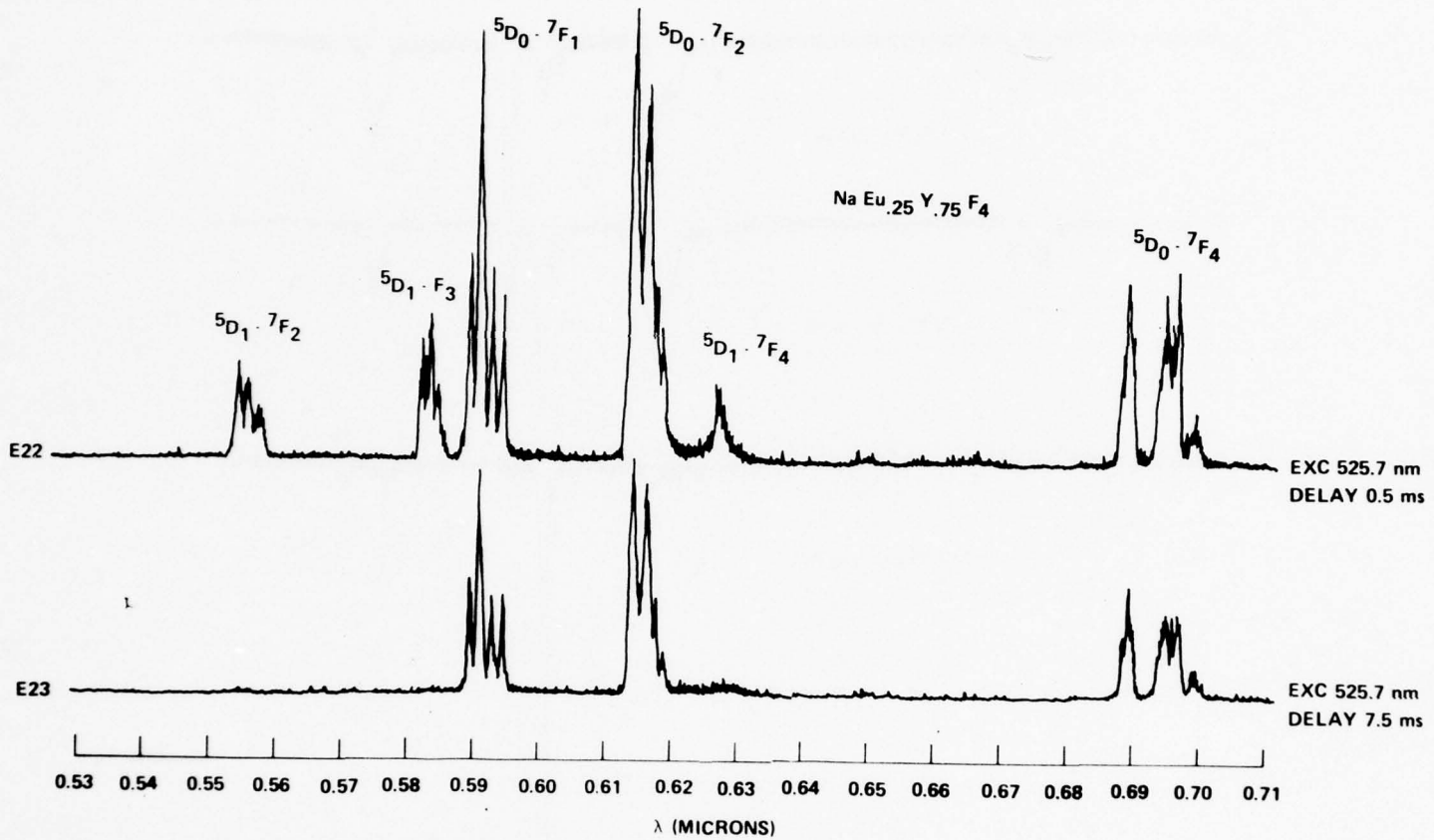

Figure 16. Emission Spectra of $NaEu_{.25}Y_{.75}F_4$ at 85°K, Monochromatically Excited at 525.7 nm and Detected at Different Times during the Decay. Note the absence of lines originating from $^5D_1$ level at longer delay times.

There is one further remark which has to be made concerning the tetrafluoride spectra. Invariably in the $^5D_0$ - $^7F_1$ region we observe four lines while only three should be present if maximum splitting occurs. The same is true in trace E8 of Figure 14 which corresponds to the "impurity" site in the hexafluoride. This is presumably caused by the presence of two different sites in the tetrafluoride structure.

Both $NaNd_xY_{1-x}F_4$ and $NaEu_xY_{1-x}F_4$ are isostructural with the hexagonal form of $NaCeF_4$ which has the β-Na_2ThF_6 structure.[11] In this structure 2/3 of the Ce atoms occupy nine coordinate sites and 1/3 of them are found in six coordination, which is consistent with our observation that Eu^{3+} occupies two sites in the tetrafluoride. We have not been able to resolve these two sites at liquid nitrogen temperature by fine tuning the dye laser. Presumably the splitting of the $^7F_0$ - $^5D_1$ transitions (corresponding to the 524.8 nm excitation) in these two sites are separated by less than the minimum bandwidth of our dye laser source.

Thus, to sum up, the results obtained with europium compounds support our conclusion that the short lifetime species always present in Nd hexafluorides is due to a contamination by the tetrafluoride phase.

Lifetimes

The decay times of the $Cs_2NaNd_xY_{1-x}F_6$ compounds show the existence of two vastly different values. The long lifetime is characteristic of the hexafluoride (cubic) spectrum while the short lifetime corresponds to the tetrafluoride impurity. Both of these change with the Nd concentration and have been plotted on the same (Figure 17) graph. Both lifetimes show an increase with dilution, the long lifetime reaching a remarkably large value of 5 ms at x = 0.1. The short lifetime increases monotonically from about 3 μs at x = 1 to 300 ms (point not included on the graph) at x = 0.01. Below x = 0.1 (roughly the demarcation between A and B type spectra) the intensity of the long lifetime emission becomes too weak to obtain reliable measurements of the decay.

We should point out here that the x-ray powder data show the dominant crystalline phase present to be the ordered perovskite; this is especially so for samples with a low Nd content. In fact, in many samples, it is difficult to ascertain the presence of the tetrafluoride phase from x-ray data. It seems reasonable to suppose the short lifetime Nd emission is more intense than that of the long lifetime site. The reduced long lifetime emission at concentrations below x = 0.1 probably reflects, in part, the reduced Nd

concentration. Below x = 0.1, the very weak octahedral site emission may simply reflect the preference of the ordered perovskite structure for the smaller Y^{3+} with the result that Nd^{3+} is preferentially found as $NaNdF_4$ impurity.

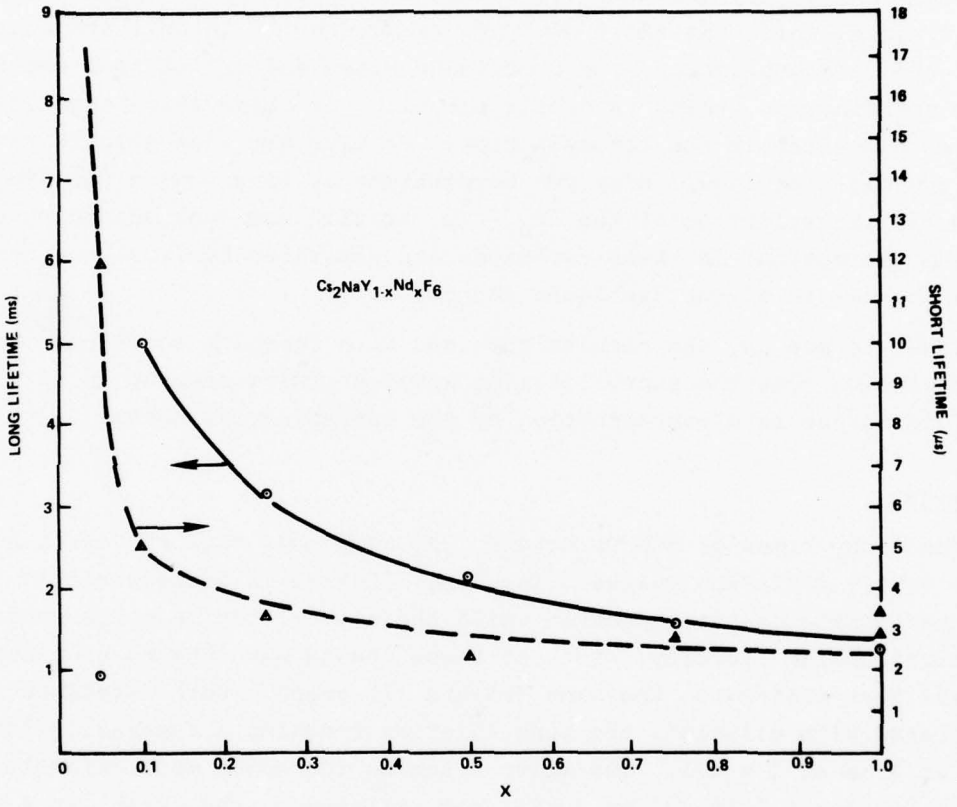

Figure 17. Lifetimes of Fluorescence as a Function of Nd Concentration (x)

3. DISCUSSION

3.1 MATERIALS

Very Little needs to be added to the description already given of $Cs_2NaNdCl_6$ and related materials. Both the x-ray and spectroscopic data agreed that the Nd ion is present in a single site of O_h symmetry.[5,7,10] One might only add that sections of sample rods were difficult to polish because of the softness and moisture sensitivity of the chloride material. This would seem to severely limit the utility of perovskite chlorides as potential laser materials.

Most of this work encompassed the investigation of the $Cs_2NaNd_xY_{1-x}F_6$ system. The obvious conclusion is that there is a strong tendency toward a partial decomposition to CsF and $NaNdF_4$. Several groups had reported the preparation of Cs_2NaYF_6 by reaction of pressed pellets of mixed components at 500° to 600°C.[9,12] No mention of decomposition was given at higher temperatures and it is presumed that the principal reasons for the use of such low temperatures were to avoid container attack and to minimize loss of the volatile CsF.

From our work, in which a number of samples were annealed overnight below 600°C, it seems unlikely that really pure phase material results even from low temperature preparations. It would be helpful to obtain detailed phase diagram data for this system, but this was beyond the scope of this project. Since CsF is both volatile and insensitive, it would be necessary to design closed containers suitable for thermal analyses. Of course, special care in handling the materials would be required whether the system were investigated as the ternary (CsF, NaF, NdF_3) or the pseudobinary (CsF, $NaNdF_4$).

As has been pointed out, attempts to distort the Nd site in ordered perovskites were unsuccessful. These primarily involved anion substitution such as the partial substitution of bromide for chloride. The chief result was a broadening of the emission spectra, presumably from the presence of multiple Nd sites from random substitution. The attempted substitution of fluoride for chloride failed to form a genuine mixed anion perovskite. It would seem that for a single site to result that ordering of the anions would be necessary. This would probably imply the necessity of a significant difference in anion size and/or a difference in anion charge. Perhaps oxyfluorides or oxychlorides might offer a better prospect for a reduction of Nd site symmetry.

Variation of M in the formula Cs_2MNdF_6 was also tried with M represented by Li and K, and mixtures of Mg and Na. The potassium substitution seemed superficially to give a cleaner x-ray powder pattern, but the superlattice lines were very much reduced in intensity and a short lifetime site present in the fluorescence spectra was assigned to that in $KNdF_4$. The Li substitution failed to result in a perovskite material and the attempted distortions with Md substitutions also were not useful.

3.2 SPECTROSCOPY

The spectra of all the materials studied by us depart significantly from the simple picture of a Nd^{3+} ion placed in a site of octahedral symmetry. The expected transitions allowed by symmetry selection rules are shown on Figure 18.[13] As shown, the magnetic dipole transitions would result in three lines in the resonance region $\left({}^4F_{3/2} \rightarrow {}^4I_{9/2}\right)$ and four lines in the laser transition region $\left({}^4F_{3/2} \rightarrow {}^4I_{11/2}\right)$. Any departure from cubic symmetry removes all the J + 1/2 degeneracy (except Kramer's degeneracy) from all the levels resulting in splitting of the ${}^4F_{3/2}$, ${}^4I_{11/2}$ and ${}^4I_{9/2}$ levels into respectively two, six and five Stark components. This should cause the appearance of 12 lines in the laser transition region and 10 lines in the resonance region as shown on Figure 19 for the case of D_{4h} symmetry (representing a tetragonal distortion of the octahedral Nd^{3+} site). The removal of all symmetry forbidden transitions in Nd^{3+} upon lowering the symmetry makes the interpretation of the spectra of that ion much more difficult than, say, Eu^{3+}. Serra and Thompson report,[10] for instance, a strict adherence to the O_h symmetry selection rules in the compounds $Cs_2NaEuCl_6$ and $Cs_2Na(Eu, Y)Cl_6$. The case of Nd compounds is evidently quite different since invariably more than a total of 7 lines (characteristic of O_h) and often more than 22 lines (symmetry less than O_h) are observed. This leaves open the possibilities of vibronic transitions and multiple sites or combinations of both.

The results presented in Section 2 indicate that in the majority of fluoride compounds at least two sites are present. Referring to Table 2, we see that the short lifetime site can be interpreted as due to a distortion (lower symmetry than O_h) without the need to invoke vibronic transitions. If the 896.0 and 888.0 nm lines are rejected, the total number of 10 and 12 lines is consistent with the 2(J + 1/2) of possible transitions. This is consistent with the interpretation of the short lifetime site as due to the tetrafluoride phase.

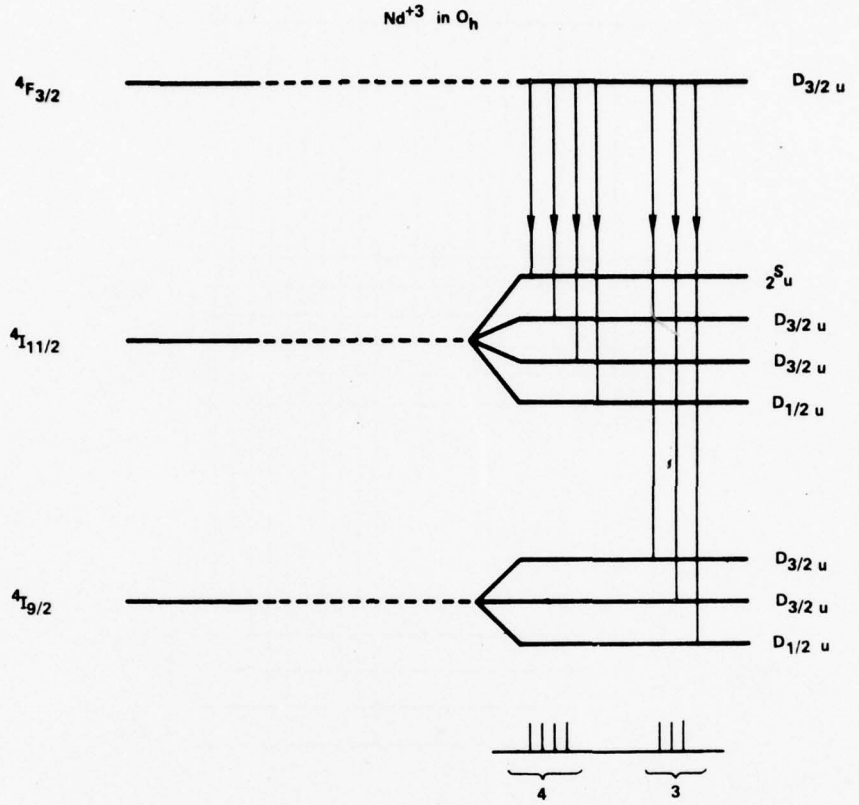

Figure 18. Level Splitting and Symmetry Allowed Transitions in Symmetry O_h

The situation is more complicated for the long lifetime spectrum (Table 2), since in this case, we observe more than the maximum possible number of lines (12 instead of 10) in the resonance region and 7 instead of the maximum of 12 in the laser transition region. This suggests that the long lifetime site may have nearly octahedral symmetry but that some of the lines have vibronic origins. This is the conclusion reached by Tofield and Weber in their work on $Cs_2NaNdCl_6$.[5]

The interpretation of vibronic spectra is usually quite a complicated matter (especially for an ion like Nd^{3+} showing a multitude of lines), requiring emission and absorption measurements often at helium temperatures. It is futile to base interpretation only on emission spectra taken on powder samples.

The dependence of lifetime upon concentration shown in Figure 17 indicates that throughout most of the composition range the luminescence of both the long and short lifetime sites is strongly concentration quenched. The laws of this quenching are, of course, of great importance if better stoichiometric materials are to be developed.

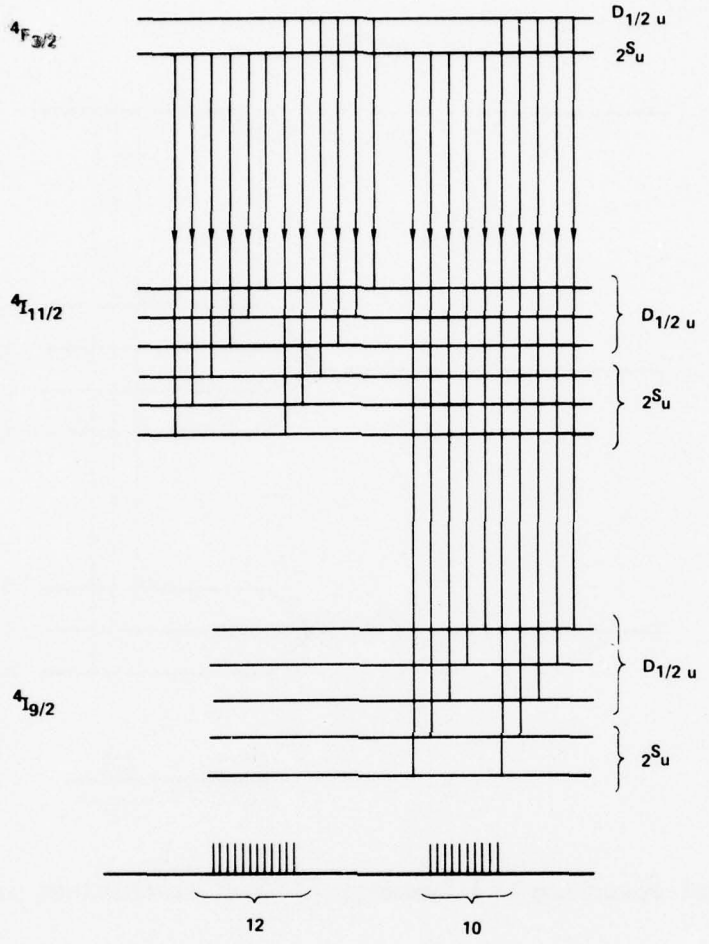

Figure 19. Level Splitting and Symmetry Allowed Transitions in D_{4h} Symmetry

It is customary to express the quenching process by the following expression:

$$\frac{1}{\tau_d} = \frac{1}{\tau_o} + k_c(x)$$

where τ_d is the observed decay of luminescence, τ_o the decay at infinite dilution and $k_c(x)$ a rate constant for the quenching process which is a function of x, the fraction of Nd^{3+} in the rare earth sites. A normalized (dimensionless) version of this constant is given by:

$$k_{cn}(x) = \frac{\tau_d - \tau_o}{\tau}$$

It has been noted recently by Singh, et al.,[14] that for Nd pentaphosphate the quenching constant varies linearly with the Nd^{3+} concentration. Chinn, Hong and Pierce[1] have confirmed this observation and have shown that the linear relationship is obeyed by several other stoichiometric materials studied by them. The same appears to be true of the $Cs_2NaNd_xY_{1-x}F_6$ system as shown on Figure 20. The upper curve corresponds to the short lifetime species (with τ_o taken as 300 μs corresponding to x = 0.01) and the bottom curve corresponds to the long lifetime component. In this case, the choice of τ_o is rendered difficult by the lack of data below x = 0.1 (see Figure 17). We have chosen τ_o to be 9 ms which is a rough extrapolation of the long lifetime curve to x = 0 in Figure 17. This behavior is in marked contrast to doped materials such as Nd:YAG, $Nd:LaF_3$; $Nd:La_2O_2S$ in which the quenching rate varies as the square of the concentration. It is interesting to note that the linear quenching rate applies also to a material like $Cs_2NaNd_xY_{1-x}F_6$ and thus to situations where electric dipole transitions (at least for the long lifetime site) may be forbidden.

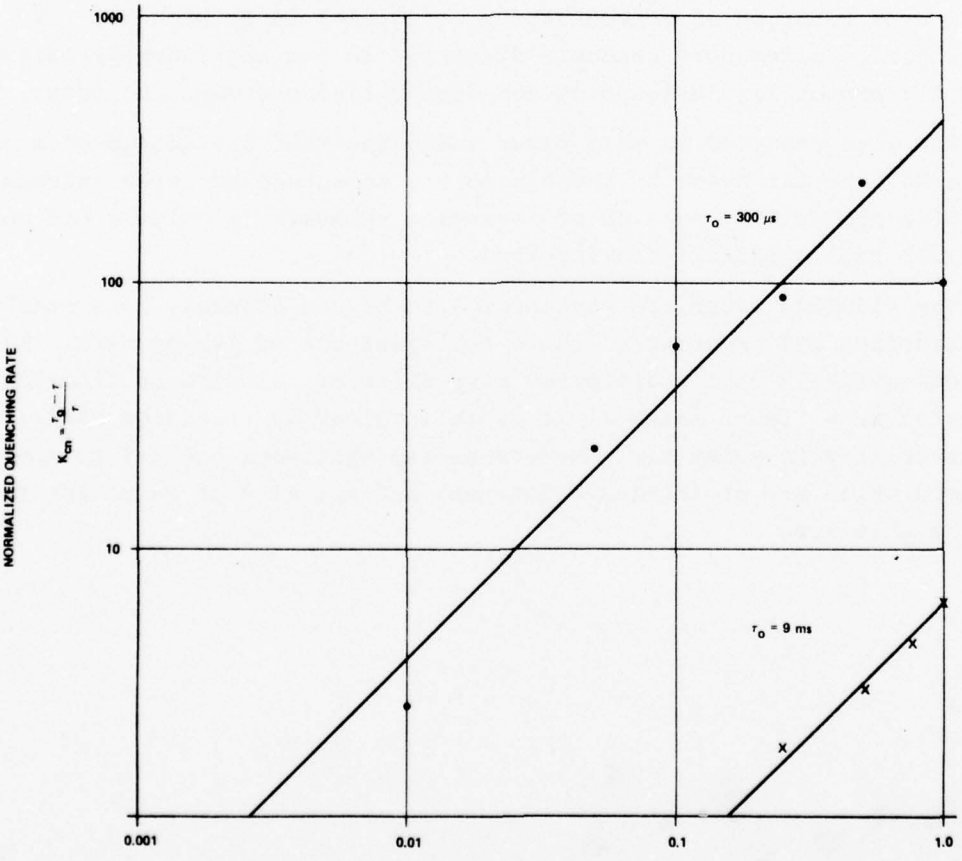

Figure 20. Normalized Rate Constant for Concentration Quenching in $Cs_2NaY_{1-x}Nd_xF_6$: • - Short Lifetime Luminescence; x - Long Lifetime Luminescence. Data from Figure 16.

The short lifetime center occurring in $Cs_2NaNd_xY_{1-x}F_6$ has been ascribed to the presence of a luminescence center similar to that occurring in tetrafluoride. There is at present no definite evidence whether the tetrafluoride appears as a separate phase or as a localized distortion of the lattice. The short lifetime center is much more strongly quenched than the long lifetime center. The absolute values of k_{cn} for the short lifetime centers are more than two orders of magnitude larger than those reported for other stoichiometric materials. For the long lifetime centers, the disparity is much less - only about a factor of 3 or 4. The meaning of this is not entirely clear in the absence of better structural information and better understanding how quenching occurs in the first place. It is significant, however, that we have not been able to detect any energy transfer between the two systems of centers. Each can be excited individually by choosing the right excitation wavelength. This lack of communication between centers is a strong argument for the existence of a separate tetrafluoride phase spatially separated from the elpasolite phase. This conclusion is also supported by the sensitivity of the $^5D_1$ - $^5D_0$ relaxation in Eu^{3+} compounds as a function of concentration, mentioned in Section 2.3. If, the tetrafluoride sites were randomly dispersed in the hexafluoride lattice one would expect little tendency for cooperative phenomena to occur.

The work reported in this paper indicates that the design of a stoichiometric Nd material based on the elpasolite structure but with increased radiative probability (center of inversion removed) is quite a bit more difficult than originally anticipated.

The fluoride materials have proved to be, in general, less stable than the chlorides and invariably led to the existence of two centers. Also, it seems unlikely that a distorted perovskite of chloride or fluoride would be useful as a laser material if Cs is involved as the large cation because of instability in moist air. Nevertheless, this work has led to some conclusions which are of intrinsic interest and are also of value for future work in this area.

4. REFERENCES

1. S.R. Chinn, H.Y.P. Hong and J.W. Pierce, "Laser Focus," 64 (May 1976).
2. H.G. Danielmayer, J. Lumin. 12/13, 179 (1976).
3. A. Lentz, J. Phys. Chem. Solids 35, 827 (1974).
4. C. Brecher and L.A. Riseberg, Phys. Rev. 13B, 81 (1976).
5. B.C. Tofield and H.P. Weber, Phys. Rev. 10B, 4560 (1974).
6. F.S. Galasso, Structure, Properties and Preparation of Perovskite-Type Compounds, Pergamon Press, Oxford (1969).
7. L.R. Morss, M. Siegal, L. Stenger and N. Edelstein, Inorg. Chem. 9, 1771 (1970).
8. C. Brecher, GTE Laboratories, Waltham, MA, Private Communication.
9. S. Aleonard and C. Pouget, J. Appl. Cryst. 1, 113 (1968).
10. O.A. Serra and L.C. Thompson, Inorg. Chem. 15, 504 (1976).
11. W.H. Zachariasen, Acta. Cryst. 1, 265 (1948).
12. A. Vechine, J. Besse, G. Baud and M. Capestan, Rev. Chim. Minerale 7, 593 (1970)
13. See for instance, J.L. Prather, "Atomic Energy Levels in Crystals," NBS Monograph 19 (1961).
14. S. Singh, D.C. Miller, J.R. Potopowicz, and L.K. Shick, J. Appl. Phys. 46, 1191 (1975).

SECTION II

POTASSIUM LITHIUM NEODYMIUM FLUORIDES

1. INTRODUCTION

This work is primarily comprised of the investigation of a particular Nd containing phase in the KF-LiF-NdF_3 system, which from spectroscopic studies, shows promise as a mini-laser material. The investigation of various compositions in the KF-LiF-NdF_3 ternary system was an outgrowth of our investigation of neodymium ordered perovskite halides as potential mini-laser candidate materials. As discussed in the report on these latter materials,* a principal problem was the removal of the center of inversion at the octahedral neodymium site. A number of attempts were made at this which primarily involved anion and cation substitutions. A third approach was to exceed the limits of cubic perovskite stability as dictated by the relative size of the ions of the $A_2BB'X_6$ composition. Among oxides of the perovskite type, the tolerance factor, t, represents the situation where all the component ions are in contact and is equal to one when the A and X ions are the same size in the general ABX_3 cubic perovskite. In the following expression,

$$t = \frac{R_A + R_B}{\sqrt{2}\,(R_B + R_X)}$$

R_A, R_B and R_X refer to the ionic radii.[1] For cubic perovskite oxides, t falls between 0.8 and 0.9. A number of oxides are known in which the unit cell has been distorted to tetragonal, hexagonal, orthorhombic or monoclinic types. This does not necessarily mean that the nearest neighbor B ion symmetry has been changed very much, if at all.

Perovskite halides of less than cubic symmetry are somewhat rarer.[1-3] Hexagonal and tetragonal distortion have been observed for fluorides as t becomes less than $\sim$0.8 or greater than $\sim$0.9. Monoclinic structures have been reported for $KMgF_3$ (t = 0.94), $RbMgF_3$ (t = 1.03) and $KCaF_3$ (t = 0.93). The expression for the tolerance factor becomes less useful for ordered perovskite halides containing rare earth ions because of the larger size differential (e.g., for Cs_2NaNdF_6) between the A and X ions and the complicating factor that R_B represents two ions of different size and charge. This is probably less true for a compound like $Cs_2NaNdCl_6$ in which Cs^+ and Cl^- are about the same size and Na^+ and Nd^{3+} are not too different in size.

*See Section I

The calculated t for this material is 0.87 to 0.89, depending on the value of R_B chosen, which is well within the range for perovskites.

Certain ions tend toward nonsymmetric octahedral coordination, such as Cu^{2+} in $CsCuCl_3$, in which two of the Cl^- are more remote than the other four.[3] Octahedral coordination is not very common for trivalent rare earth ions which are mostly found in seven to nine coordinate sites. Neodymium is certainly found in a regular octahedral site in $Cs_2NaNdCl_6$.[4,5] In general, similar fluorides might be expected to show less tendency toward regular octahedral rare earth sites because the fluoride ion is much smaller than the chloride ion.

Preparations of a number of $A_2BB'X_6$ ordered cubic perovskites were made in the course of this project (see Section I). None showed x-ray evidence of any distortion of the cubic unit cell. These were mostly fluorides with A ions represented by the larger group I cations (Cs, Rb, K), the smaller B ions by Li through Rb, and B' ions were various trivalent rare earths (especially Nd). Among fluorides, the rather large Nd ion was found to lead to a partial decomposition of the perovskite phase to the tetrafluoride ($NaNdF_4$, $KNdF_4$) and an alkali fluoride. The composition $K_2LiNd_{0.25}Y_{0.75}F_6$ was among those prepared and examined spectroscopically. Interestingly, although the composition contained several phases, one of them gave spectroscopic indications of a long lifetime component, which in turn implied a large separation of the Nd ions in the responsible phase. This report, then, describes our investigation of the $KF-LiF-NdF_3$ system and the search for a new mini-laser material.

2. MATERIALS PREPARATION

Polycrystalline samples for the potassium lithium neodymium fluoride system were routinely prepared by heating the anhydrous component fluorides in a flow of argon and HF at about 900°C for two or three hours. The samples were located in a small platinum foil boat, which was placed in a larger alumina combustion boat for support. The Monel apparatus and the general procedure which was used was that described elsewhere (see Section I - 2.2) for the preparation of ordered perovskite samples. The reactants were stored in an argon-filled glove box, although only KF is particularly moisture sensitive. Starting materials (Kf, LiF, NdF_3) were dried under dynamic vacuum at 100° to 150°C. However, no moisture was collected in a cold (-195°C) trap and no differences were found in reaction products made from reactants which were not dried prior to use. The KF and LiF were five 9'2 pure from United Mineral and NdF_3 was supplied in four 9's purity by Research Chemical. Weight losses in a typical preparation were generally less than 0.1g from 2.0g samples made in a few hours under flow conditions. In colosed graphite boats, 7g samples were exposed to temperatures over 800°C for several days with weight losses of 0.1g to 0.2g. As a precautionary measure, reaction products were handled under argon in a glove box.

Samples of the following compositions were prepared for studies in this program: K_2LiNdF_6, K_3LiNdF_7, K_4LiNdF_8, $KLiNdF_5$, $KNdF_4$ and K_3NdF_6. These were examined by x-ray powder diffraction techniques as well as the special methods of Section 3 of this Report.

As more became known of the phase of inderest, several series of diluted samples were synthesized. These included $K_2LiNd_xY_{1-x}F_6$, $K_2LiNd_xGd_{1-x}F_6$, $K_2LiNd_xLa_{1-x}F_6$ and $K_2LiNd_xCe_{1-x}F_6$. Of these, the most useful was the $K_2LiNd_xCe_{1-x}F_6$ because it provided a wider isostructural composition range.

A number of attempts have been made to grow single cyrstals of the Nd phase of interest. The gradient freeze method has been employed using the closed horizontal and vertical graphite containers sketched in Figure 1. These were constructed from a special high density, high purity graphite (Poco DFP-3-2*). Since the melting point is uncertain, samples of K_2LiNdF_6 and K_3LiNdF_6 have been cooled slowly (2° to 5°C/hr) from about 850°C with gradients of 25° to 100°C along the 4-in. boat. The graphite containers were maintained in an argon environment during the crystal growth process. In early experiments severe carbon contamination was

*Union Poco Graphite, Inc., Decater, Texas.

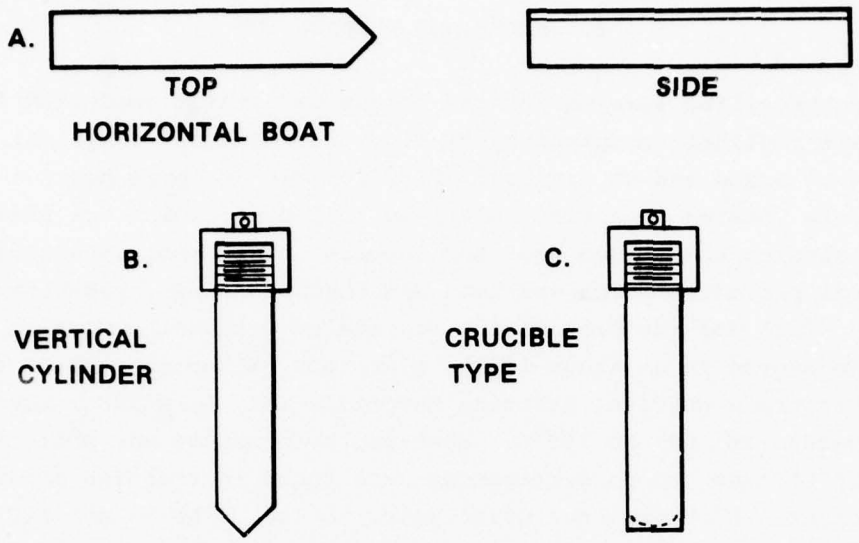

Figure 1. Closed Graphite Containers Used for Crystal Growth

obvious even though precautions were taken to dry the samples prior to growth under dynamic vacuum. On occasion, the starting materials were pretreated by heating in Pt containers up to 800°C in an HF-Ar gas flow. The situation was finally improved markedly by pretreating the graphite containers in a flow of HCl at 950°C, then transferring them under Ar to an inert atmosphere glove box where sample loading took place. Even this was not entirely satisfactory with respect to graphite contamination.

Later when a flux growth method (KF·2LiF) was employed and the container shape was not considered important, the graphite boats were lined with one mil platinum foil so as to further reduce container attack. This sample was cooled at 2½°C/hr from about 800° to 500°C.

3. RESULTS

The equipment and methods employed in the spectroscopic investigation of the $KF-LiF-NdF_3$ system has been described in detail (Section I - 2.1) and will not be repeated here. The emission spectra of three different fluorides of Nd are given in Figure 2. All of these were taken with a broadband Xenon arc excitation. The top trace is that of the tetrafluoride $KNdF_4$, a compound in which nine coordinate Nd^{3+} ions exist, and having an orthorhombic structure with the space group Pnma.[6] As an efficient material, the tetrafluoride is of little interest since its lifetime ($\sim$5 μs) is strongly quenched at stoichiometric composition. The spectrum associated with the tetrafluoride phase is designated as Type I. The middle trace (Type II) belongs to the composition K_3LiNdF_7 and is of considerably greater importance because of a much longer decay time (280 μs) indicating significantly reduced quenching. The bottom trace (Type III) belongs to the composition K_3NdF_6. Although the emission spectrum has an attractive simplicity and apparently favorable branching ratio (ratio of integrated emission in the 1.05 nm region to that at 0.89 nm), the decay time is again short - of the order of a few microseconds.

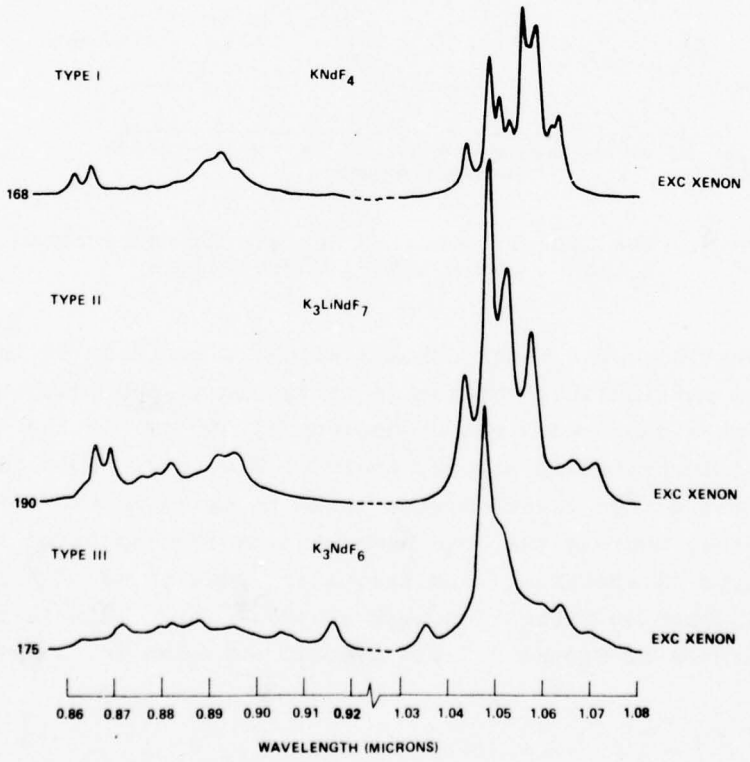

Figure 2. The Emission Spectra of Three Different Nd Fluorides

Clearly the fluoride of composition K_3LiNdF_7 with its characteristic Type II spectrum is of greatest interest. In fact, the decay time of 280 μs is the longest known for any noncentrosymmetric stoichiometric Nd compound. The lack of sensitivity to the exact proportion of potassium to fluorine is illustrated in Figure 3, which shows two identical (Type II) spectra for materials of nominal composition K_3LiNdF_7 and K_2LiNdF_6.

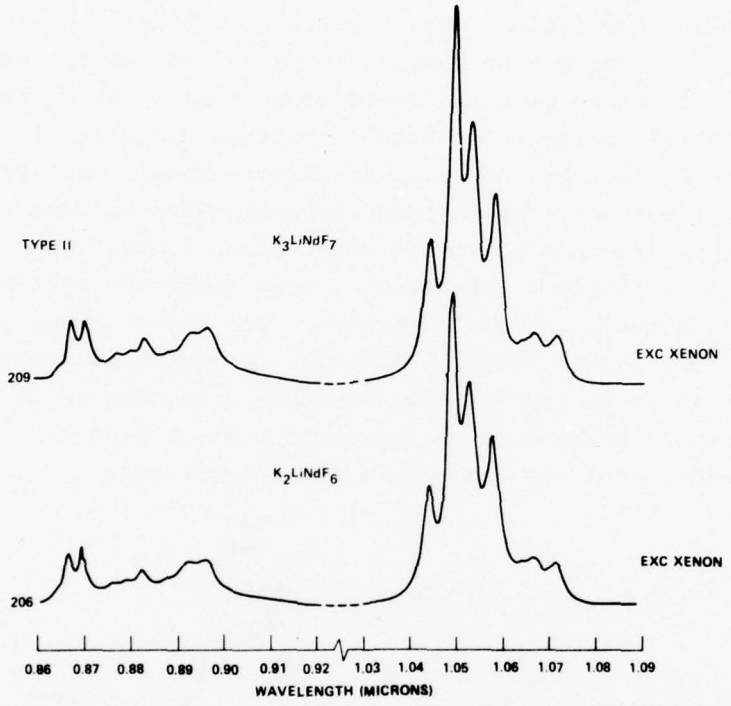

Figure 3. The Type II Emission Spectra Characteristic of K_3LiNdF_7 and K_2LiNdF_6 Compositions

Some preparations of K_2LiNdF_6 show a slight distortion of the Xenon excited spectrum particularly noticeable in the long wavelength tail (1.063 nm) and as a short wavelength shoulder (1.056 nm) in the 1.058 nm line. This is illustrated in the top trace of Figure 4. Upon excitation with a monochromatic (dye laser) source tuned to maximize the emission, it becomes immediately obvious that the broadband excited spectrum is a superposition of a Type II spectrum (with excitation peak at 428.4 nm) and a Type I spectrum (with an excitation peak at 427.4 nm). This is shown on the two lower traces of Figure 4. The overall emission is, however,

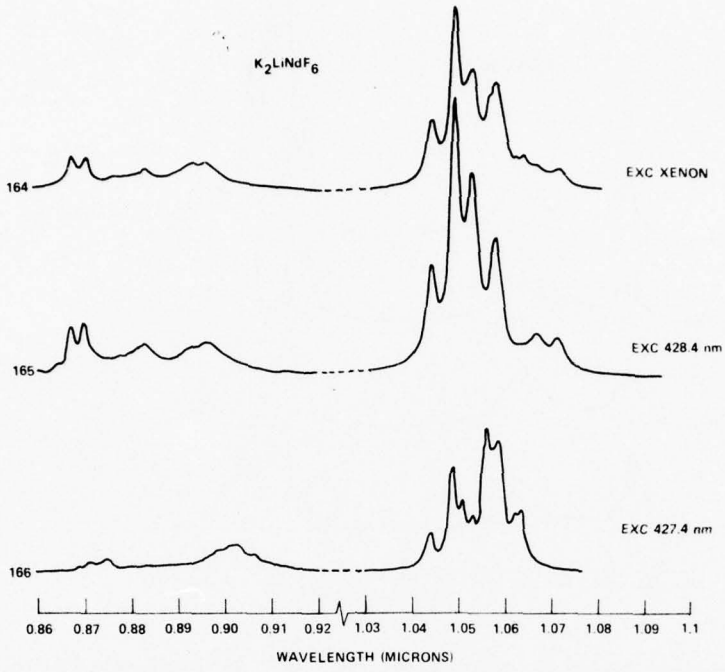

Figure 4. Emission Spectra of K_2LiNdF_6 with Xenon Arc and Selected Dye Laser Excitation

dominated by the Type II spectrum, the Type I (tetrafluoride) being present only as a small component. The dominance of the Type II spectrum is even more pronounced in the Xenon spectra of K_3LiNdF_7 and K_2LiNdF_6 samples shown in Figure 3.

The effect of dilution (in this case with Ce^{3+}) on the spectra of $K_2LiNd_xCe_{1-x}F_6$ is shown on Figure 5. Here all the traces were taken with broadband Xenon excitation. The clearly visible, overall effect is that, as the Nd content is reduced, the spectrum shows a definite transformation from Type II to Type I. At 1% composition ($x = 0.01$), the emission spectrum is virtually indistinguishable from that of the tetrafluoride phase. Thus at the high concentration end ($x \sim 1$), the emission is dominated by the Type II spectrum, the tetrafluoride component (Type I) being relatively very weak. Exactly the opposite is true at the other end of the composition scale ($x \sim 0.01$) where the Type II spectrum is the much weaker component. Figure 6 shows the Type II spectrum still present in this diluted material. Note that the ratio of the peak intensities

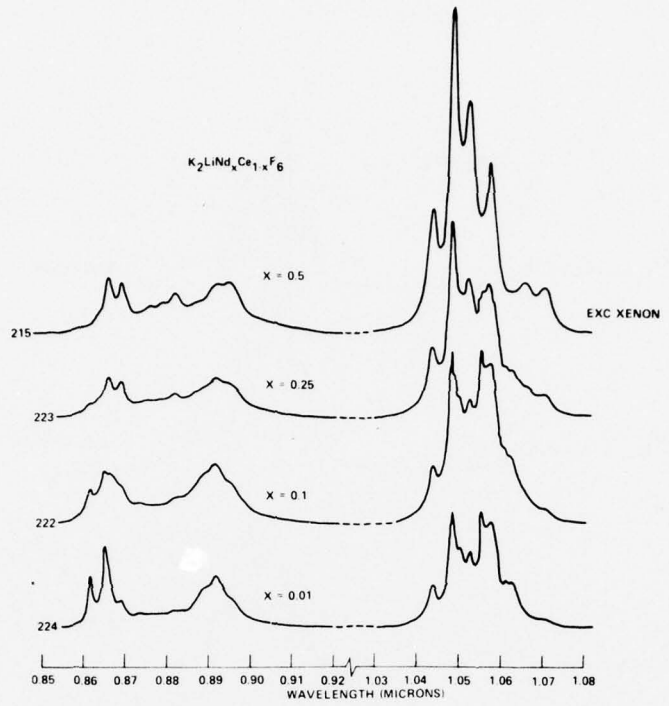

Figure 5. Emission Spectra of $K_2LiNd_xCe_{1-x}F_6$ at Several Nd Concentrations

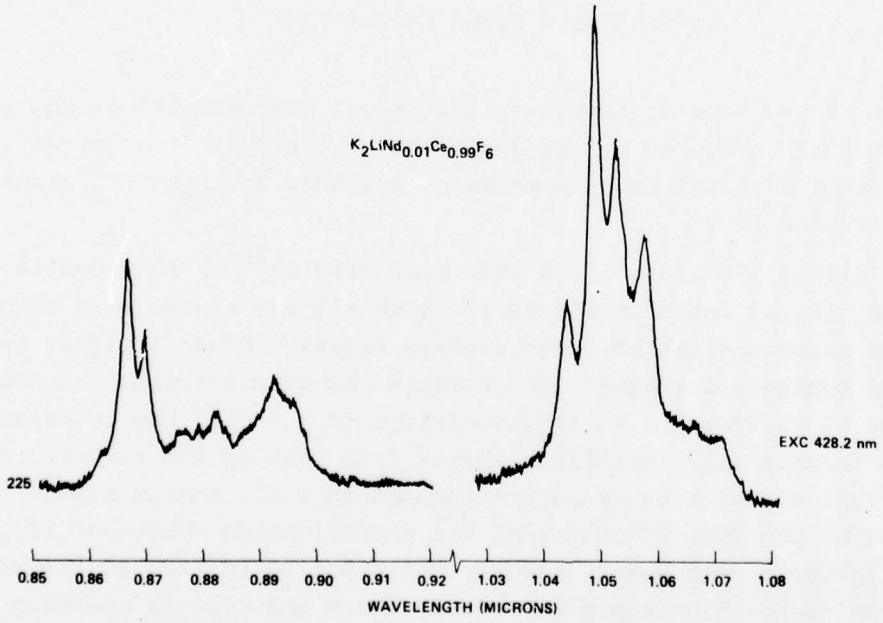

Figure 6. The Type II Emission Spectrum of $K_2LiNd_{0.01}Ce_{0.99}F_6$

of the long and short wavelengths components has decreased considerably from the case of the undiluted compound (Figure 3). We shall use this fact in Section 4, Discussion, to present a qualitative picture of the composition of the material.

Lifetimes

In order to measure decay times, the dye laser was tuned to the main excitation peaks of the two types of spectra (427.4 nm for Type I, 428.4 nm for Type II). The decay was followed for approximately two orders of magnitude with the boxcar operating in the logarithmic output mode.

The dependence of the decay times on composition, for the two types of spectra, are given in Figure 7. Both curves show a decrease of lifetime with concentration, the major portion of the decrease being confined to rather low concentration. In discussing the significance of these curves, one should note that the variable x is defined only by the nominal composition of the compound $K_2LiNd_xCe_{1-x}F_6$. Since there is no guarantee that the ratio of this compound to the tetrafluoride phase $KNdF_4$ is constant throughout the range of x, the abscissa of each of the experimental points may be in error. Because of this uncertainty, we prefer to represent the lifetime quenching of the important Type II emission as made of segments rather than a monotonic function.

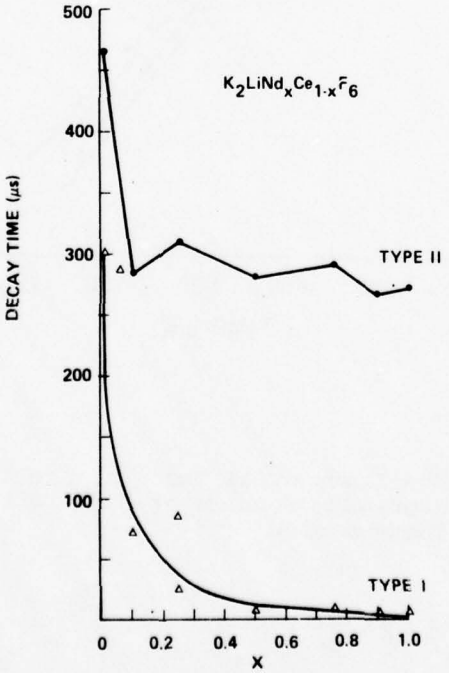

Figure 7. The Composition Dependence of the Fluorescence Lifetimes of Types I and II Nd Sites

For the Type II emission, the decay is strictly exponential over the whole range of x as shown in Figure 8. This is not true of the decay of the Type I emission which shows departure from exponential behavior as illustrated on Figure 9. Nonexponential decay is encountered often in luminescence but since in the present case, Type I emission is an unwanted impurity component, we have not investigated this aspect in any detail.

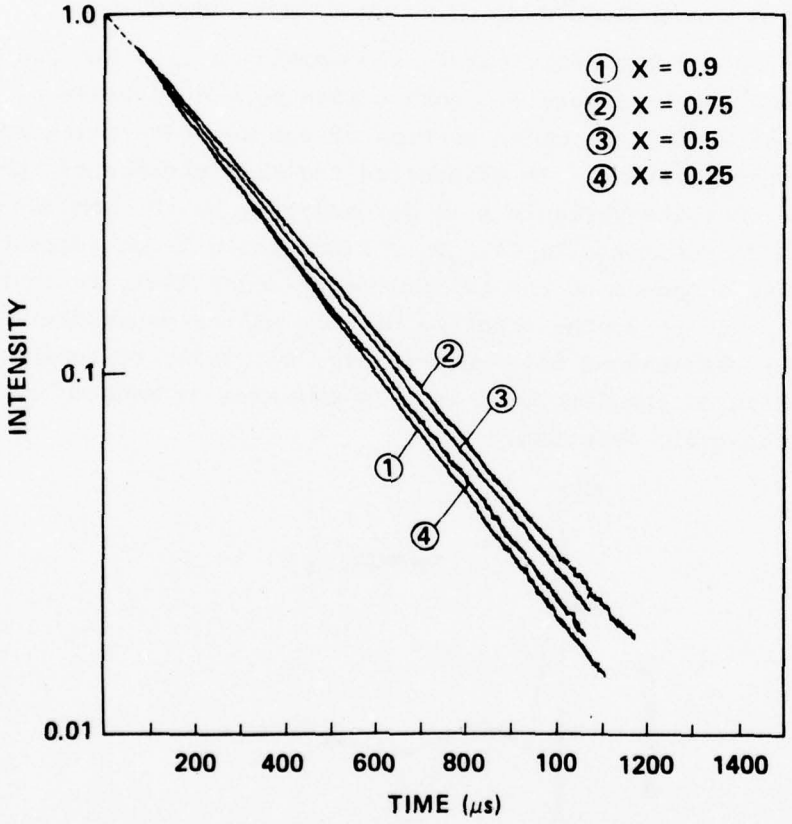

Figure 8. The Exponential Decay of the Type II Neodymium Species at Different Temperatures

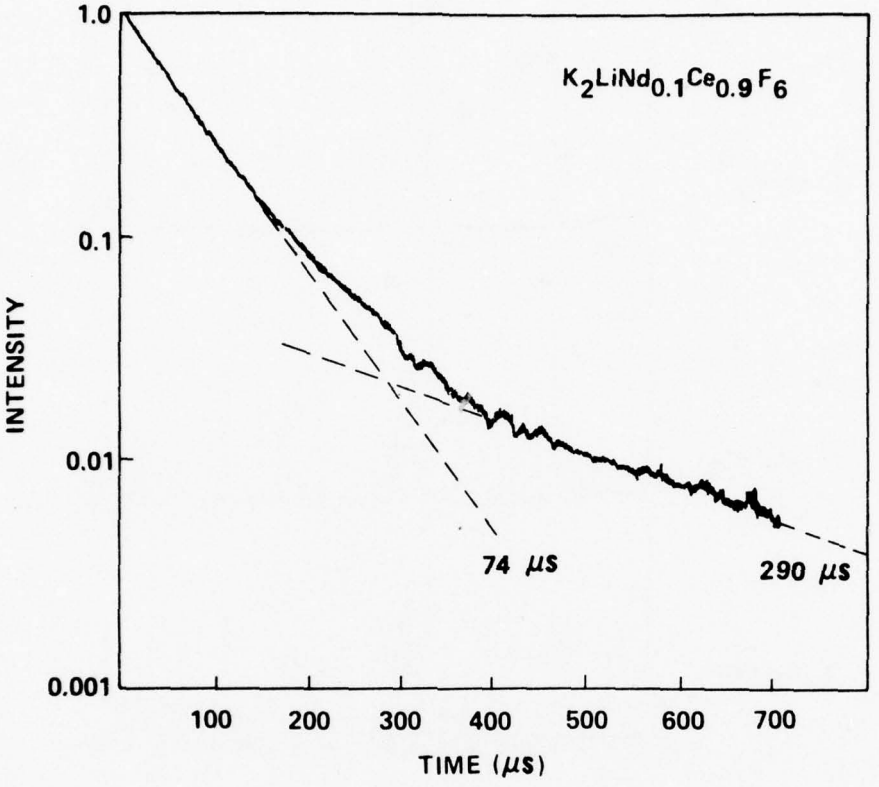

Figure 9. The Fluorescence Decay Curve for a Typical Type I Neodymium Site. Note nonexponential behavior.

X-ray powder diffraction patterns of the various samples, as well as spectroscopic data, were obtained as the materials became available. A comparison of the x-ray powder data for $KNdF_4$, K_2LiNdF_6 and K_3LiNdF_7 are shown in Figure 10. It is obvious that lines are in common in all three samples. Those lines corresponding to tetrafluoride lines became progressively weaker as the "extra" lines became stronger in going to the K_3LiNdF_7 composition. Neither $K_2Li_2NdF_7$ or K_4LiNdF_8 show further development of intermediate x-ray lines, and if anything, produce x-ray patterns which are more like $KNdF_4$. Ordinarily one would assume the patterns of K_2LiNdF_6 and K_3LiNdF_7 to represent $KNdF_4$ plus one or more additional phases in lesser amounts. The materials, as routinely prepared in a single day, are not particularly crystalline in appearance and it was not possible to pick out individual crystals for separate examination. However, the spectroscopic evidence (Spectroscopic Results section) clearly

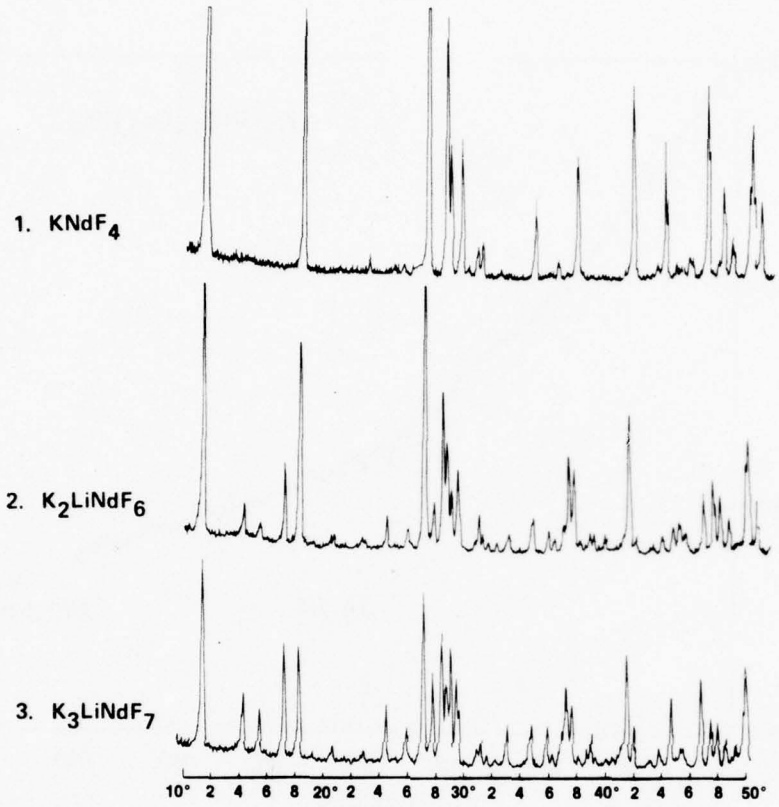

Figure 10. Comparison of the X-Ray Powder Diffraction Patterns of $KNdF_4$, K_2LiNdF_6 and K_3LiNdF_7. Relative intensity is plotted vs. 2θ.

indicated the long lifetime phase to be predominant. This, plus the fact that not very much difference was seen in either x-ray or spectroscopic data as KF was added to the compositions, lead us to believe that the increased isolation of Nd^{3+} was achieved by an expansion of the orthorhombic $KNdF_4$ unit cell[6] and that the extra lines were possibly superlattice lines. Accordingly, an effort was made to index these patterns by using an available program capable of indexing cubic, hexagonal, tetragonal or orthorhombic structures. This effort was not successful, indicating that if the unit cell were expanded that this might well be monoclinic rather than orthorhombic. Of course, lines from an impurity phase could have interfered in the indexing procedure.

The crystal growth experiments with K_2LiNdF_6 and K_3LiNdF_7 compositions have been somewhat disappointing. The later experiments gave samples which are considerably more crystalline in appearance than single day preparations, but obviously are not single crystals as a whole. Some material from these samples has been ground lightly and attempts have been made to pick out single crystal pieces under a microscope at low magnification. Thus far, most of the better-looking pieces were found to exhibit short lifetime Nd sites only. Some small pieces were found which have regions which indicate only long lifetime sites, but these require excitation at selected surface locations. One might conclude that either the sample compositions are not quite correct or that some other means of crystal growth must be tried.

In order to gain further information, DTA data were obtained for several compositions and the thermal transitions in heating curves run at $10^{\circ}C$/min are shown in Figure 11. The major transition in each of the compositions K_2LiNdF_6, K_3LiNdF_7, K_4LiNdF_8 and $K_2Li_2NdF_7$ occurs between 550° and $575^{\circ}C$. In the samples of the most interest, K_2LiNdF_6 and K_3LiNdF_7, additional transitions are found at 760° and $782^{\circ}C$, respectively. Surprisingly, the larger of the thermal effects occurs at the lower temperature. One would have expected a melting point to be more pronounced than, say, a phase transition. If the lower effect represents the decomposition of a phase, this would suggest crystallization of this phase from a solvent as the most reasonable route to crystal growth. Certainly, the DTA data do not suggest any of the compositions to be congruently melting.

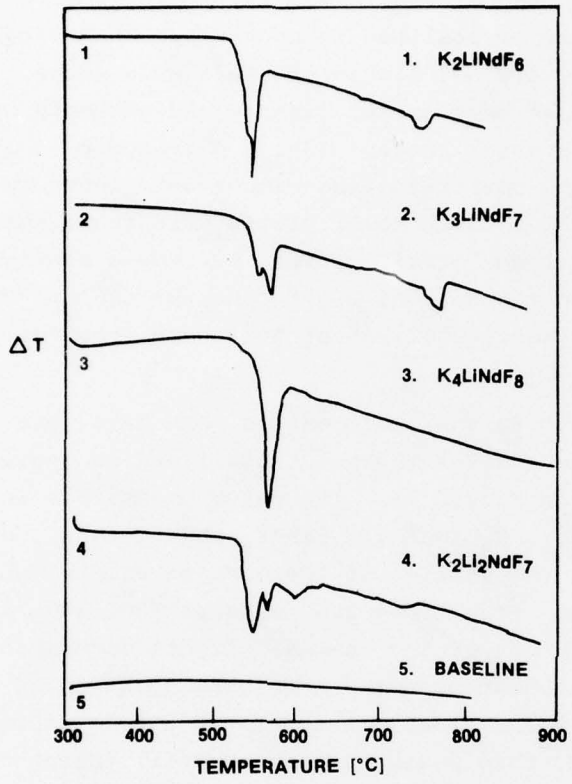

Figure 11. DTA Heating Curves for Several Compositions

4. DISCUSSION

The fact that an unexpectedly interesting phase can be made in the $KF-LiF-NdF_3$ system is well established. This is important because, with a lifetime of 280 μs, it is certainly a member of the small family of stoichiometric Nd materials in which the active ion separation is large enough that quenching is much reduced compared to glasses and conventional laser host crystals.

A comparison of the emission spectra of highly crystalline NdP_5O_{14} and a sample of K_2LiNdF_6 powder is shown in Figure 12. The data are taken under essentially identical experimental conditions and the two materials are seen to be very similar, with the pentaphosphate 1.05μ emission somewhat more intense. The branching ratio (simply defined as the relative intensity of the highest peak in the emission region divided by that of the highest peak in the resonance region) of the fluoride is about 9, compared to about 4.5 for the pentaphosphate. When one considers that the fluorescence lifetime of the fluoride is more than twice that of the pentaphosphate (280 μs vs. 130 μs), it is found to compare very well as a potential mini-laser material.

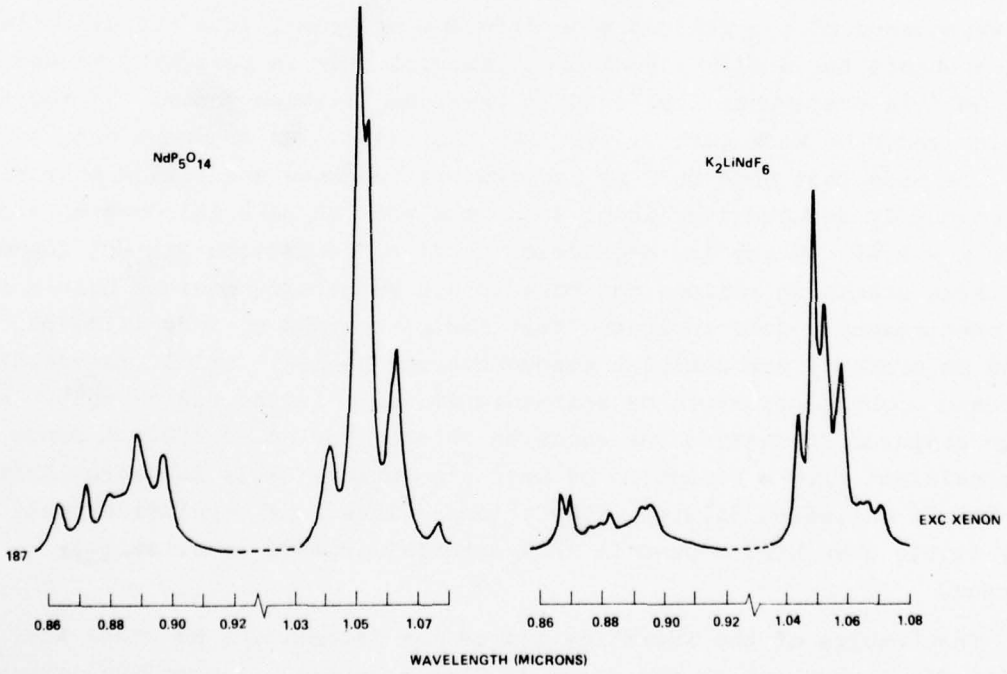

Figure 12. A Comparison of the Emission Spectra of NdP_5O_{14} and a Powder Sample of the K_2LiNdF_6 Composition. These represent essentially identical experimental conditions.

Further structural and quenching experiments were somewhat frustrated by the fact that when dilution experiments were performed, it was found that the desired Nd phase is very restrictive in the rare earth ions it will accept. For example, $K_2LiNd_xLa_{1-x}F_6$ powder diffraction data were essentially those of the tetrafluoride material, and this conclusion was supported by spectroscopic data. Gadolinium and yttrium were tried as diluent ions but the x-ray data showed obvious departures from the desired phase with very little substitution for neodymium. Finally, cerium was found to be much better and samples diluted with Ce^{3+} ($K_2LiNd_xCe_{1-x}F_6$) appeared viable spectroscopically down to about x = 0.1. Of course, some care must be exercised to prepare materials under conditions in which Ce^{4+} contamination does not occur.

The most interesting feature of Figure 7 in Section 3, Results, which shows the dependence of fluorescence lifetime on concentration, is the apparent lack of variation of fluorescence lifetime from x = 0.1 to x = 1. The material would therefore be very interesting to study in more detail when single crystals and a crystal structure are obtained. Of course, as pointed out earlier, the compositions probably represent a mixture of $KNdF_4$ and the long lifetime phase. If only two Nd-containing phases are present, the data are probably fairly reliable since the curve representing the dependence of the fluorescence lifetime of Type I (the tetrafluoride) is reasonable for a dilution of that material. It is possible, however, that Nd^{3+} is preferentially found in the long lifetime phase. If so, the samples could be much less dilute than indicated. An argument can, however, be made that some Ce^{3+} is incorporated because the branching ratios are gradually reduced from about 9 for the pure Nd material down to about 2 for x = 0.01. A regular dependence on Nd concentration was not found for these branching ratios, but this is not surprising because both x-ray and spectroscopic data indicated that the percentage of long lifetime phase is probably not constant throughout the series. Still, the relative increase upon dilution of the resonance emission in the 850 nm to 900 nm range compared to that of the emission in the 1030 nm to 1080 nm range is consistent with a reduction of self absorption. This indicates that the sample is indeed diluted with Ce ions. Thus, the conclusion that very little quenching occurs in this material appears qualitatively correct.

The results of the investigation of the interesting Nd phase are admittedly incomplete at the close of this contract. A continued investigation should be made until some of the questions presented here are

cleared up. If a route to good quality single crystals can be found, this phase could be especially valuable for elucidating quenching mechanisms. Its behavior is apparently quite different from other stoichiometric Nd compounds[7,8] and may provide valuable insight for the development of improved materials.

5. REFERENCES

1. F.S. Galasso, Structure, Properties and Preparation of Perovskite-Type Compounds, Pergamon Press, Oxford (1969).

2. A. Vedrine, J. Besse, G. Baud and M. Capestan, Rev. Chim Minerale 7, 593 (1970).

3. A.F. Wells, Structural Inorganic Chemistry, Oxford University Press, Oxford (1962).

4. B.C. Tofield and H.P. Weber, Phys. Rev. 10B, 4560 (1974).

5. L.R. Morss, M. Siegal, L. Stenger and N. Edelstein, Inorg. Chem. 9, 1771 (1970).

6. G. Brunton, Acta Cryst. B25, 600 (1969).

7. S.R. Chinn, H.Y.P. Hong and J.W. Pierce, Laser Focus, 64 (May 1976).

8. H.G. Danielmayer, J. Lumin. 12/13, 179 (1976).

SECTION III

CONCENTRATION QUENCHING IN Nd^{3+} STOICHIOMETRIC MATERIALS*

*Reprinted from Optics Communications, Vol. 23, No. 3 (December 1977).

CONCENTRATION QUENCHING IN Nd^{3+} STOICHIOMETRIC MATERIALS *

A. LEMPICKI
GTE Laboratories Inc., 40 Sylvan Road, Waltham, Massachusetts 01254, USA

Received 5 September 1977

Basic experimental facts concerning the luminescence of $Nd_xLa_{1-x}P_5O_{14}$ are reviewed. Interpretation of the data by a diffusion model leads to the possible presence of $\sim 10^{17}$ cm^{-3} energy sinks in this material. Consequences and weaknesses of this model are discussed.

The discovery that some materials containing Nd^{3+} in stoichiometric proportion (at concentrations exceeding 10^{21} ions per cm^3) retain their luminescence efficiency has given rise to a new technology of miniaturized, optically pumped lasers [1,2]. At the same time, these developments have revived interest in the mechanisms of concentration quenching or the relative lack of it in materials such as NdP_5O_{14}.

It is the purpose of the present note to examine which particular features of the luminescence require an explanation, to explore the possibility of providing such an explanation in terms of *established* models of concentration quenching, and in general to point out the unsatisfactory state of affairs concerning the understanding of this phenomenon.

Since most data reported in the literature and obtained by us pertain to $Nd_xLa_{x-1}P_5O_{14}$, we shall consider primarily this material. The following are experimental facts which appear to dominate the luminescence behavior of Nd ultraphosphate (NdUP); otherwise also known as pentaphosphate:

1) Concentration quenching in NdUP is unusually weak. For $x = 0.1$ the measured decay time does not deviate from the radiative lifetime by more than 20 percent and at half this concentration is essentially completely radiative [3].

2) The quenching constant varies linearly with the molar fraction x. This fact has been noted by Singh et al. [4] and by Chinn, Hong and Pierce [1]. If we denote by $\tau(x)$ the observed decay constant at the composition x and by τ_0 the decay constant at infinite dilution ($x \to 0$), we can define a quenching rate by

$$q(x) = 1/\tau(x) - 1/\tau_0 .$$

A *normalized* quenching constant is then defined as

$$q_n(x) = (\tau_0 - \tau(x))/\tau(x) .$$

Chinn et al. [1] have noted that for a whole family of stoichiometric materials $q_n(x)$ varies linearly with x. Our own data obtained for just three Nd pentaphosphate compositions confirm this and are shown on fig. 1. The linear quenching appears to be a fundamental and distinguishing feature of these materials, yet some very recent publications [5] do not acknowledge its existence and attempt to explain quenching in terms of a $q_n \sim x^2$ law, characteristic of Nd:YAG [6].

3) The decay is logarithmic over most if not all of the time accessible to measurement. Decay curves taken at the three values of x and extending over more than two decades are shown in fig. 2. These we obtained by using a 5 ns dye laser pulse exciting the samples in the $^4I_{9/2} \to {}^2P_{1/2}$ transition and observing the decay of the $^4F_{3/2} \to {}^4I_{11/12}$ luminescence using a PAR 162 boxcar integrator with a logarithmic output. The decays were followed to times of the order of 1 ms after the exciting pulse. Visual observation of oscilloscope traces indicated no anomalies at shorter times. According to ref. [7] the decay at $x = 0.05$ is also exponential.

* Work partly supported by Army Research Office, Durham, N.C.

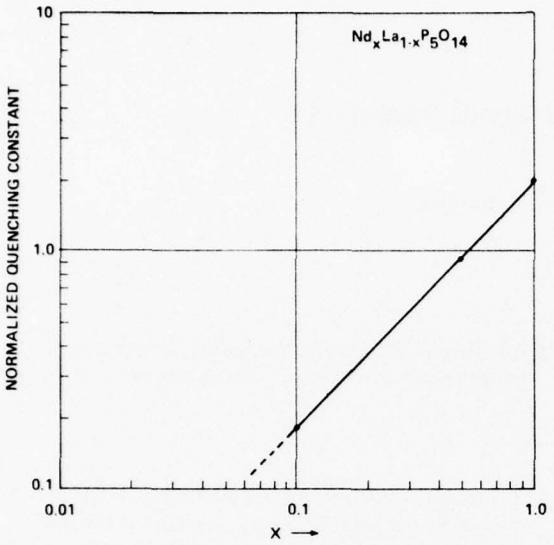

Fig. 1. Normalized quenching constant versus molar fraction x in $Nd_xLa_{1-x}P_5O_{14}$. (τ_0 = 320 μs; ref. [1]).

4) The decay time at any concentration of Nd is independent of temperature.

Any model of concentration dependence of luminescence has to account for all these facts simultaneously. We shall first inquire how this can be accomplished by using established models of concentration quenching.

Exponential decay at low concentration ($x \to 0$) may be due to single, noninteracting ions. The persistence of exponential decay at larger values of x implies, however, a mechanism of energy redistribution which maintains the equivalence of every excited ion in the lattice. It is customary then to treat such cases by assuming that the probability of excitation $\phi(r, t)$ is governed by a diffusion equation [8,9]

$$\partial\phi(r, t)/\partial t = D\nabla^2\phi(r, t) - C\phi(r, t)\sum_n \frac{1}{|r - r_n|^6} - \frac{1}{\tau_0}\phi(r, t). \quad (1)$$

In this equation D is the diffusion constant for energy migration among the Nd ions, C is the dipole-dipole transfer constant to some unspecified energy sinks located at points r_n. A solution of eq. (1) assumes a simple exponential form if the diffusion is large. We have then

$$1/\tau = 1/\tau_0 + 1/\tau_D, \quad (2)$$

where

$$1/\tau_D = 8.5\, n\, C^{1/4} D^{3/4}, \quad (3)$$

n is the sink (acceptor) concentration. An expression for the diffusion constant in terms of the Nd^{3+} con-

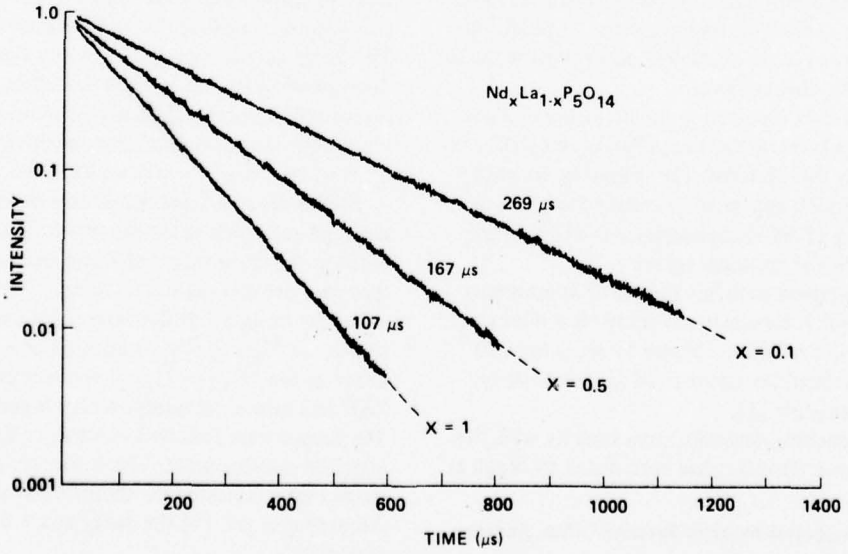

Fig. 2. Luminescence decay curves for three compositions of $Nd_xLa_{1-x}P_5O_{14}$.

centration N is, following Förster [10]

$$D = (s/\tau_0) R_0^6 N^{4/3}, \quad (4)$$

where s is a lattice sum (of the order of 2.8) and R_0 is the Förster critical radius for Nd^{3+}–Nd^{3+} transfer. Combining eqs. (3) and (4) we obtain:

$$\frac{1}{\tau_D} = 8.5\, C^{1/4} \left(\frac{s}{\tau_0} R_0^6\right)^{3/4} nN. \quad (5)$$

If the origin of quenching is an interaction between *identical* ions, eq. (5) explains the quadratic dependence of q_n on N by simply assuming $n \sim N$. This may very well apply to the case of Nd:YAG in which cross relaxation via the $^4I_{15/2}$ level is supposed to be fast [6]. At some small level of doping when eq. (2) breaks down, one should then expect a departure from strict exponentiality. We are not aware of any measurements on Nd:YAG either supporting or contradicting this possibility.

If interaction between identical ions is weak, as it appears to be, the case in Nd pentaphosphate (cross relaxation via $^4I_{15/2}$ does not occur) [11], eq. (5) can formally account for experimental facts 1–4 listed above. We must, however, consider n as a constant, independent of x, and C as temperature independent.

Leaving for the moment the reasonableness of such a model, we can estimate the required concentration of sinks n by the following approximate arguments. R_0 can be estimated from its definition which expresses the Nd–Nd dipole–dipole transfer rate W as [10]

$$W = (1/\tau_0)(R_0/R)^6, \quad (6)$$

where R is the distance between neighbors taken here as 0.6 nm [12]. From the value of $W = 2.4 \times 10^7\ s^{-1}$ estimated by Liao, Weber and Tofield [13], we obtain $R_0 = 2.6$ nm. It further follows from ref. [13] that the diffusion constant $D \approx 8 \times 10^{-8}\ cm^2/s$ (this, incidentally, is almost ten times smaller than the diffusion in Nd:YAG obtained from laser experiments [14] and casts some suspicion on either or both of these numbers).

To estimate the Nd sink transfer constant C, we shall assume (see below) that the same rate applies, namely $W = C/R^6$, which would yield $C = 1.1 \times 10^{-36}\ cm^6/s$. Finally, we have $\tau_D = \tau_0/q_n(x = 1) = 0.006$. With these values we find from eq. (5) $n \sim 10^{17}$ sinks/cm^3. Thus, even at low Nd content ($x = 0.01$), the sink concentration amounts to no more than one in some few hundred Nd ions.

The model would tend to identify the sinks with some crystal defect determined perhaps by the method of preparation and constant over the whole range of Nd/La proportions. It is conceivable that a Nd ion located at or near such a defect could have its energy levels sufficiently shifted as to allow for rapid pair relaxation, normally ruled out for this material [11]. If this were the case, the rate of the final transfer step could be essentially the same as all of the previous transfer steps between "normal" Nd ions. This would justify our way of estimating C.

Another possibility would be the presence of hydroxyl groups which are known to be effective quenchers of Nd^{3+} luminescence and whose concentration may be determined by the method of preparation and be common to all of the crystals [15]. Although the value of C may be different, the dependence on its actual value is rather weak (see eq. (5)). It is a rather remarkable fact that as the method of crystal growth improves, the decay time at $x = 1$ tends to steadily increase (chronologically $\tau = 60\ \mu s$, 115 μs, and 135 μs – see refs. [16], [7] and [17], respectively). Aside from the possibility that the defects are being gradually eliminated, it raises the question whether the dependence of the normalized quenching constant on x for *different* stoichiometric materials is universal as suggested in ref. [1], or is a family of close-lying parallel curves. The diffusion model would favor a family of curves. Very careful measurements would be required to settle this point.

Again, a consequence of the model is that at some low value of x, eqs. (2) and (3) should break down because D cannot be considered as large any more. In this case, deviations from exponential decay are expected to occur, and the initial portion of the decay should show the $t^{1/2}$ Förster dependence [9, 18]. This has not been reported in Nd pentaphosphate and, although precise data may be lacking, it is not likely to be observed because at low values of x the decay is radiative anyway. It would appear, therefore, that at some intermediate concentration the radiative decay of individual ions merges directly with a regime where fast migration occurs, the exponential decay being maintained throughout. An analytic treatment of the qualitative picture is yet to be developed.

The main drawback of the diffusion model as applied to the pentaphosphate is the arbitrary nature of the defects and the postulated independence of n on x. What are the alternatives?

To obtain a linear quenching rate and an exponential decay over the whole range of x without introducing defects, a major departure from the formulation of the problem via eq. (1) is indicated. At the same time, a fast migration rate has to be maintained in order to retain the equivalence of all ions. This appears to be the main theoretical problem.

Without claiming rigor consider the following possibility. According to ref. [4], a quenching interaction in the pentaphosphate is possible via the $^4F_{3/2} \rightarrow {}^4I_{13/2}$; $^4I_{9/2} \rightarrow {}^4I_{15/2}$ pair relaxation. This should be considerably weaker than the cross relaxation in YAG. The proability of deactivation by dipole–dipole interaction can be written in the form of eq. (7):

$$\bar{w} = (1/\tau_0)\overline{(r_0/r)^6}\,, \tag{7}$$

where the average is over the spatial distribution of ions, r_0 is the Förster critical radius [18] and r the separation of Nd ions. As long as $\bar{w}$ depends only on the average quantity $\overline{1/r^6}$, it is immaterial whether the distribution is random or uniform; we have:

$$\overline{1/r^6} = N \int_R^\infty \frac{4\pi r^2 \mathrm{d}r}{r^6} = \frac{4\pi}{3R^3} N \tag{8}$$

and

$$\bar{w} = \frac{4\pi}{3\tau_0} \frac{r_0^6}{R^3} N. \tag{9}$$

We thus obtain a quenching rate linear in N, without the introduction of any defects.

From experiments (fig. 1) we knew that $\bar{w} = q_n(x = 1)/\tau_0 = 6 \times 10^3\ \mathrm{s}^{-1}$; this leads to a critical radius of $r_0 = 0.54$ nm, which is just about equal to the nearest Nd–Nd separation. The statistical fraction of single ions as a function of x and the number of contacts Z to other Nd sites is given by [19]

$$S = x(1 - x)^Z\,.$$

For $Z = 8$, roughly characteristic of NdUP, and $x = 0.05$, we obtain $S = 0.33$. Hence at this concentration, 66 percent of all Nd ions are singles and not likely to undergo pair quenching. At $x = 0.01$, 92 percent are singles and hence decay radiatively.

This simplistic model requires an energy migration which is either fast over the entire range of x or varies as a considerably higher power of N than indicated by eq. (5). In the latter case, we can almost think of a fast diffusion to be rapidly turned on when x approaches and exceeds ~0.01, i.e., when single ions decaying radiatively begin to disappear from the scene [10]. It is possible that such long range migration may be supplied by a recently proposed hopping mechanism [20] or coherent transfer [21].

In conclusion, we believe that the ordinary diffusion – defect model cannot be conclusively proved or disproved at the present time. In addition, it requires an explanation why the Förster decay ($t^{1/2}$-law) is not observed at some value of x. Measurement of the decay for very dilute samples, and possible ways of detecting or eliminating defects would shed light on its validity. The defectless model, being very incomplete, requires much further elaboration. Direct measurements of the diffusion length and high resolution, line narrowing experiments similar to those recently performed on ruby [21], could shed light on energy migration rates and mechanisms.

Numerous discussions with Drs. E.J. Johnson, S.J. Nettel, B. McCollum, L. Andrews and S.R. Chinn are gratefully acknowledged.

References

[1] S.R. Chinn, H.Y.P. Hong and J.W. Pierce, Laser Focus 64 (May 1976).
[2] H.G. Danielmeyer, Festkörperprobleme XV (1975) 253.
[3] H.P. Weber, P.F. Liao and B.C. Tofield, IEEE J. Quant. Electr. QE-10 (1974) 563.
[4] S. Singh, D.C. Miller, J.R. Potopowicz and L.K. Shick, J. Appl. Phys. 46 (1975) 1191.
[5] W. Strek, C. Szafranski, E. Lukowiak, Z. Mazurak and B. Jeżowska-Trzebiatowska, Phys. Stat. Sol. (a) 41 (1977) 547.
[6] H.G. Danielmeyer and M. Blatte, Appl. Phys. 1 (1973) 269.
[7] I.A. Bondar, T.G. Mamedov, L.P. Mezentseva, I.A. Shcherbakov and A.I. Domanskii, Sov. J. Quant. Electr. 4 (1975) 1463.
[8] M. Yokota and O. Tanimoto, J. Phys. Soc. Japan 22 (1967) 779.
[9] M.J. Weber, Phys. Rev. B 4 (1971) 2932.
[10] Th. Förster, Ann. Phys. 6 Folge 2 (1948) 55.
[11] M. Blätte, H.G. Danielmeyer and R. Ulrich, Appl. Phys. 1 (1973) 275.
[12] Y.H.P. Hong, Acta Cryst. B30 (1974) 468.
[13] P.F. Liao, H.P. Weber and B.C. Tofield, Sol. State Comm. 16 (1975) 881.

[14] H.G. Danielmeyer, J. Appl. Phys. 42 (1971) 3125.
[15] W.K. Zwicker, T. Kovats and S.R. Chinn, Intern. Conf. on Crystal Growth, MIT (July 1977). OH groups are known quenchers of Nd^{3+} luminescence in liquid media; see, for instance, C. Brecher and K.W. French, J. Phys. Chem. 77 (1973) 1370.
[16] H.G. Danielmeyer and H.P. Weber, IEEE J. Quant. Electr. QE-8 (1972) 805.
[17] S.R. Chinn and W.K. Zwicker, Appl. Phys. Lett. 31 (1971) 178.
[18] Th. Förster, Z. Naturforsch. 4a (1949).
[19] L.G. van Uitert and S. Iida, J. Chem. Phys. 37 (1962) 486.
[20] I.A. Bondar et al., Sov. J. Quant. Electr. 7 (1977) 167, and reference listed therein.
[21] P.M. Seltzer, D.S. Hamilton and W.M. Yen, Phys. Rev. Lett. 38 (1977) 858.

SECTION IV

APPROXIMATE ANALYTICAL APPROACH TO LASER PULSE PHENOMENA

1. INTRODUCTION

Pulse phenomena in lasers, such as Q-switching, transient spiking and cavity dumping are usually treated using the rate equations.[1] In most regions of interest, these equations form a set of coupled monlinear differential equations and solutions are usually obtained using computer numerical integration. Unfortunately, in such calculations, the physical details become obscured; and it is difficult to answer basic questions and compare different phenomena without large catalogs of numerical data. We have examined in detail the rate equations for a four-level system and have found that by sacrificing rigor and piecing together solutions with approximations appropriate to different levels of excitation we can provide detailed insight into laser pulse phenomena. The approximations are such that the resulting expressions can be trusted to give the qualitative behavior. In most cases the resulting expressions agree well with numerical integration. However, for rigorous practical solutions one should resort to computer numerical integration with the guidance provided by the approximate analytic expressions.

We compare various pulse modes such as Q-switching, cavity dumping and transient spiking. We consider pulse narrowing and extend the equations to include a system consisting of two types of centers with the same energy level scheme but with different lifetimes. Preliminary considerations appeared to indicate that such a two center laser system might have enhanced pulse behavior and in earlier work we came to suspect such centers occured in certain stoichiometric rare-earth compounds. The two center analysis has implications to glasses where many different lifetimes exist.

2. DETAILS OF PHYSICAL MODEL

Let us consider a lasing center that can be characterized by a four-level system.

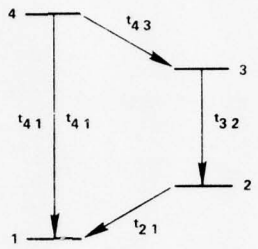

Figure 1. Energy Level Diagram for a Four-Level Center

The principal transitions are shown by arrows and appropriate lifetimes. If favorable relations occur between the magnitudes of the respective lifetimes, the absorption constant involving the pumping transition 41 is independent of pumping intensity, and the population of level 2 can be neglected. Under these circumstances, only t_{41} and t_{32} enter quantitatively into the dynamics of the laser output transition 32. The lifetime t_{41} is implicit in the absorption coefficient, α; and t_{32}, if it is limited by radiative transitions to level 2, corresponds to a lifetime for spontaneous emission τ. The transition 32 is also characterized by an Einstein coefficient, per quantum, per mode for spontaneous emission:

$$B = \frac{c^3}{8\pi\nu^2\Delta\nu\tau} \tag{1}$$

From this one can define a quantity q_o:

$$\tau B = \frac{c^3}{8\pi\nu^2\Delta\nu} \equiv \frac{V}{q_o} \tag{2}$$

where V is the volume of the radiation field contained by the resonator. The quantity q_o is the number of modes contained within the line width, $\Delta\nu$, and will be found to be useful in describing the laser dynamics. In our numerical examples we will assume a typical value of $q_o = 1.25 \times 10^{12}$, corresponding to a volume of 1 cm^3.

The lasing centers are postulated to occur in a solid host where they can be characterized by an absorption coefficient. The laser medium is in a resonator which is characterized by a cavity loss rate given by:

$$r_c = r_R + r_\ell \tag{3}$$

where r_R corresponds to the coupled output:

$$r_R = \frac{c}{2\ell} (1 - R)$$

Here ℓ is the resonator length and R is the reflectivity of the output mirror. The second term in Eq. (3), r_ℓ, is the equivalent rate of any additional losses.

$$r_\ell = \frac{c}{2\ell} \left(e^{-\alpha_x \ell} + f_s \right) \tag{4}$$

where α_x is an absorption coefficient that accounts for absorption and scattering in the cavity and f_s is the fraction of light scattered or diffracted at each incidence on the two end mirrors.

Note that all losses are taken as continuous. This is generally not the case in practice. For events of duration on the order of the transit time, $2\ell/c$ or less, the concept of a cavity loss rate can be expected to breakdown.

A useful unit of time is given by the cavity lifetime, t_c, given by:

$$t_c = \frac{1}{r_c} \tag{5}$$

It should be pointed out that, in general, the cavity lifetime for spontaneous emission is much shorter than that for stimulated emission. In what follows we will neglect this complication.

3. LASER RATE EQUATIONS AND STEADY STATE SOLUTIONS

The number of excited centers in the cavity, n, under optical pumping, will be governed by:

$$\frac{dn}{dt} = w - VBnq - \frac{n}{\tau} \tag{6}$$

where we neglect nonradiative transitions and w is the pumping rate which is dependent upon the absorption coefficient and the incident light flux, q is the number of photons of a given mode present in the cavity. The third term is the spontaneous emission over the line width and the second term is the stimulated emission per mode. Using Eq. (2), Eq. (6) becomes:

$$\frac{dn}{dt} = w - \frac{n}{\tau}\left(\frac{q}{q_o} + 1\right) \tag{7}$$

The time dependence of the number of photons in the laser cavity is given by:

$$\frac{dq}{dt} = BnVq + BnV - \frac{q}{t_c} \tag{8}$$

where the first two terms are, respectively, the stimulated and the spontaneous emission per mode of the radiation field, and the last term is the rate at which photons leave the resonator* as laser output and internal losses. Using Eq. (2), Eq. (8) can be written:

$$\frac{dq}{dt} = \frac{n}{\tau}\left(\frac{q}{q_o} + \frac{1}{q_o}\right) - \frac{q}{t_c} \tag{9}$$

$$\frac{dn}{dt} = w - \frac{n}{\tau}\left(\frac{q}{q_o} + 1\right)$$

$$\frac{dq}{dt} = \frac{n}{\tau}\left(\frac{q}{q_o} + \frac{1}{q_o}\right) - \frac{q}{t_c} \tag{10}$$

We define two quantities whose significance will become obvious below:

$$w_o = r_c\, q_o \quad ; \quad \rho = \frac{n}{q_o \tau} \tag{11}$$

With these definitions Eq. (10) can be written in the convenient form:

$$\frac{d\rho}{dt} = \frac{r_c}{\tau}\left[\frac{w}{w_o} - \frac{\rho}{r_c}\left(\frac{q}{q_o} + 1\right)\right]$$

$$\frac{dq}{dt} = \rho\,(q + q_o) - r_c\, q \tag{12}$$

For cw laser operation one can easily obtain the steady state solutions:

$$\rho = r_c \frac{q}{q + q_o} \tag{13}$$

$$n = w\tau/(q/q_o + 1) \tag{14}$$

$$q/q_o = \frac{1}{2}\left(\frac{w}{w_o} - 1\right) + \frac{1}{2}\left[\left(\frac{w}{w_o} - 1\right)^2 + 4\,\frac{1}{q_o}\,\frac{w}{w_o}\right]^{\frac{1}{2}} \tag{15}$$

In Figure 2 we plot q/q_o versus w as given by Eq. (15). For $w = w_o$ the photon number shows the virtual discontinuity characteristic of the threshold for laser action.

As is confirmed in Figure 3, Eq. (15) can be simplified to considerable accuracy except in the immediate neighborhood of threshold by:

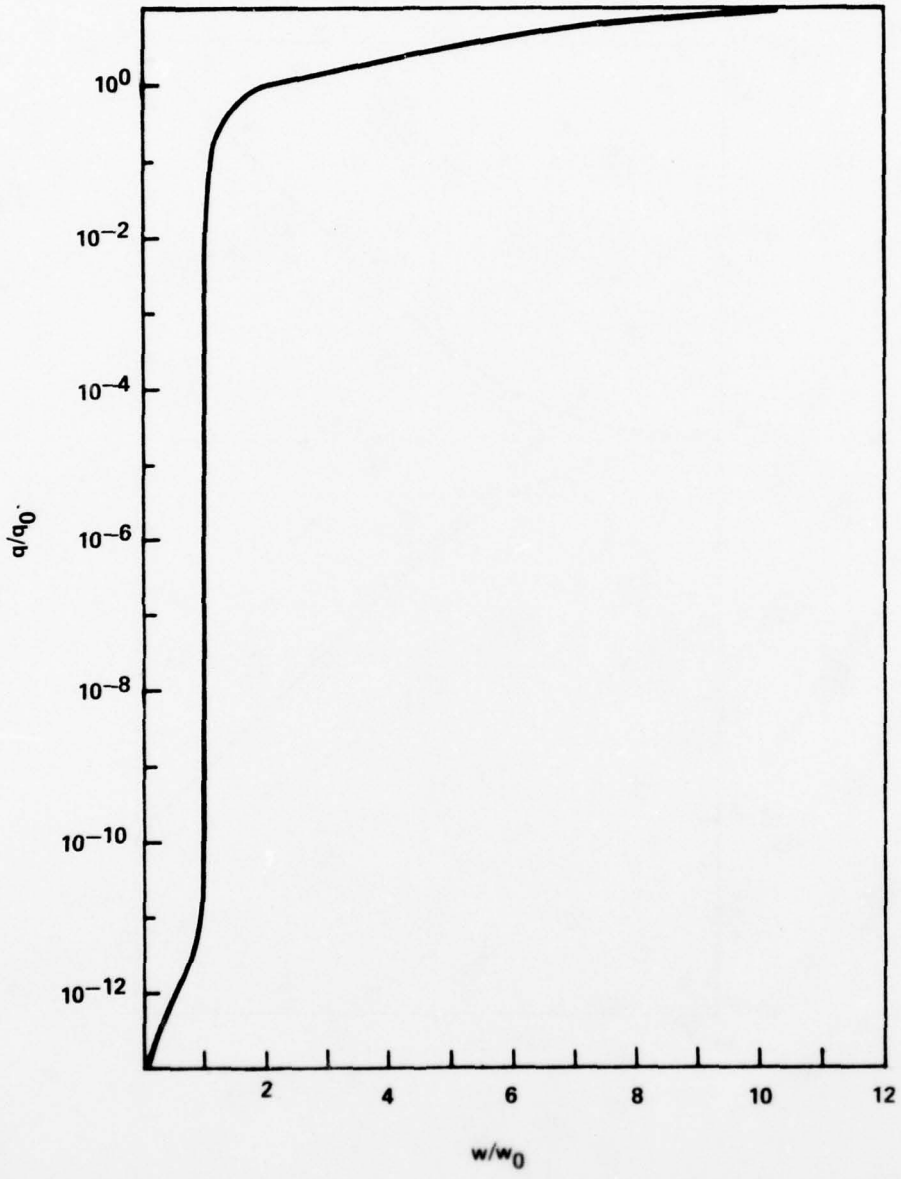

Figure 2. Steady State Photon Number vs. Pumping Level

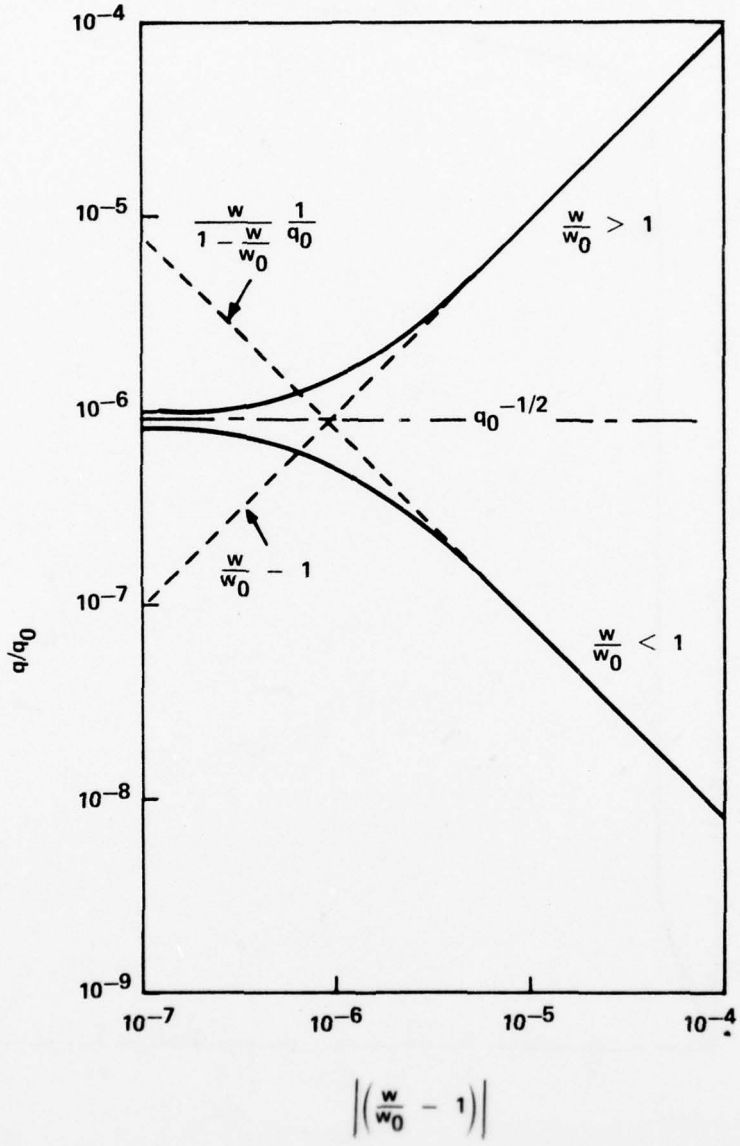

Figure 3. Steady State Photon Number for Pumping Levels Near Threshold

The laser output intensity can be written:

$$r_R q = (w - w_o)\left(1 - \sqrt{\frac{r_\ell\, q_o}{w}}\right) \tag{17}$$

if the output coupling r_R is optimized:

$$r_R q = w\left(1 - 2\sqrt{\frac{q_o\, r_\ell}{w}}\right) \tag{18}$$

For laser operation these steady-state solutions with optimized output coupling represent the maximum intensities available for a given pumping rate. This limitation results from the fact that in cw operation the round trip gain cannot exceed the round trip loss. In pulsed operation, this constraint does not exist and possibilities exist for obtaining much larger intensities than result from Eq. (18). Other applications require narrow pulses and transient effects can give an output pulse narrower than the pumping pulse. To understand these phenomena we examine approximate analytic solutions to the rate equations in detail in the following sections.

4. BUILDUP OF ELECTRONIC EXCITATION

The buildup of electronic excitation initially occurs independent of the number of photons in the cavity. In this situation Eq. (7) can be written:

$$\frac{dn}{dt} = w - \frac{n}{\tau} \tag{19}$$

This has the general solution:

$$n = e^{-\frac{t}{\tau}}\left(\int e^{\frac{t}{\tau}} w dt + C\right) \tag{20}$$

where C is a constant of integration.

As long as the turn-on time is fast compared to τ and w is reasonably flat during the pulse, little generality is lost in taking w in the form of a step function. In this situation, the electronic excitation is given by:

$$n(t) = n(o)\ e^{-\frac{t}{\tau}} + w\tau\left(1 - e^{-\frac{t}{\tau}}\right) \tag{21}$$

where n(o) is the electronic excitation at t = o.

There are two aspects of the electronic excitation that are of interest for the laser dynamics. There is the total electronic excitation itself, i.e., n, which, when multiplied by the photon energy, represents the total electronic energy available for optical output. In addition, there is the quantity ρ defined above which when multiplied by q gives the stimulated emission. Therefore, ρ is the stimulated emission rate and, as such, plays a central role in the buildup of photons in the cavity. As we will see later $\rho = r_c$ is the threshold condition for exponential growth in the photon population which is required if a laser pulse is to take place.

5. PHOTON BUILDUP

The presence of electronic excitation induces photons to build up in the cavity. At low levels the presence of photons has virtually no effect on the electronic excitation. At higher levels, coupling occurs and the problem becomes more complicated. In this section we assume a variety of time dependences for the electronic excitation and examine how the photons build up in the cavity.

For these purposes we take the second of Eq. (12):

$$\frac{dq}{dt} \approx (\rho - r_c)\, q + \rho \tag{22}$$

where ρ for present purposes is considered to be a given function of time independent of the photon number, q. The general solution to Eq. (22) is given by:

$$q = e^{\beta} \left(\int e^{-\beta} \rho dt + C \right) \tag{23}$$

where:

$$\beta = \int (\rho - r_c)\, dt$$

and C is a constant of integration.

Solutions will differ depending upon the form taken by ρ. We consider separately ρ a constant, and ρ linear with time.

As a first example consider ρ = constant and $q = q(o)$ at $t = 0$. Under these conditions Eq. (23) becomes:

$$q = q(o)\, e^{(\rho - r_c)\, t} + \frac{\rho}{\rho - r_c} \left[e^{(\rho - r_c)\, t} - 1 \right] \tag{24}$$

This behavior is shown in Figure 4 where the threshold character of $\rho = r_c$ is illustrated. For a stimulated emission rate above this value, q builds up exponentially, whereas q saturates for lower values of ρ.

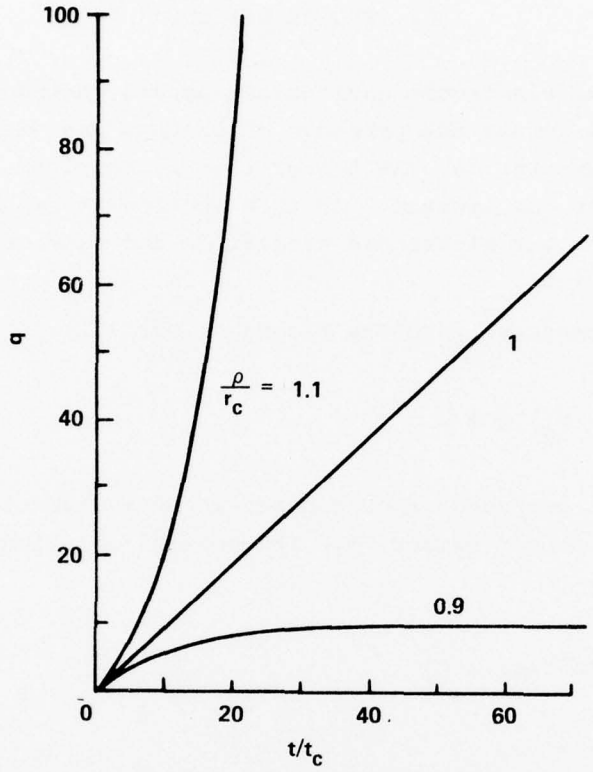

Figure 4. Photon Buildup Assuming Constant Electronic Excitation

For our second example we set:

$$\rho = at \tag{25}$$

where a is a constant. We define another constant t_o:

$$at_o = r_c \tag{26}$$

where it is seen that t_o is the time when the stimulated emission rate is equal to the cavity loss rate.

We then obtain for δ:

$$\delta = \frac{a}{2}(t - t_o)^2 \tag{27}$$

Substituting Eq. (27) into Eq. (23) we obtain:

$$q + 1 = e^{\frac{a}{2}(t - t_o)^2}\left[\frac{1}{t_c}\int e^{-\frac{a}{2}(t - t_o)^2} dt + C\right] \tag{28}$$

The integral in Eq. (28) can be handled using the error function. However, to provide deeper physical insight, we consider simple approximations suitable for separate regions. Schematically we show the form the integral takes in Figure 5.

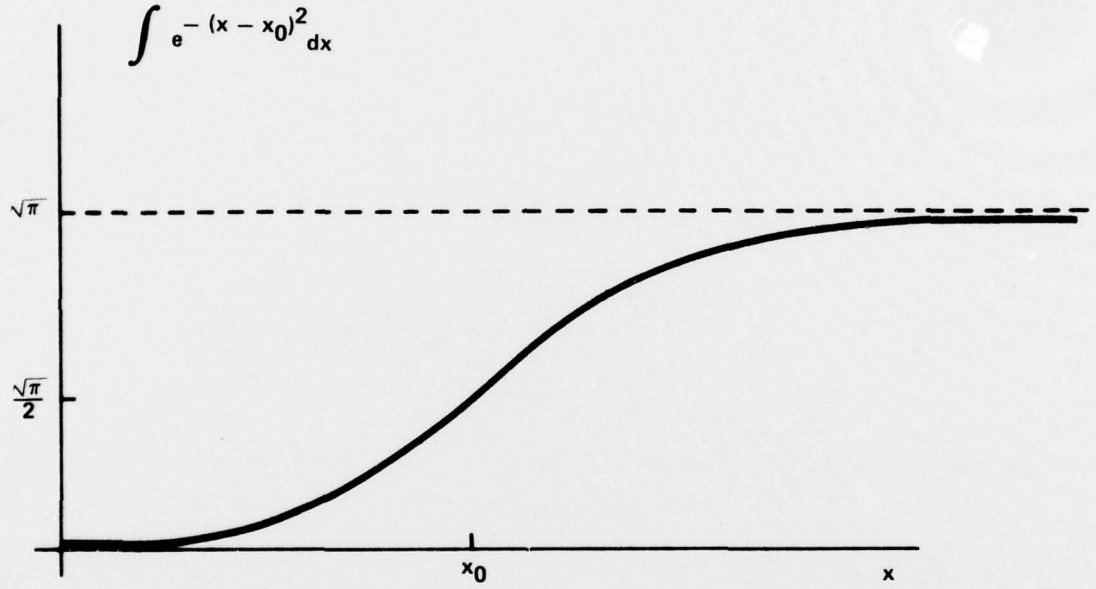

Figure 5. Schematic Form of the Integral in Eq. (28).

For $t << \left(t_o - \sqrt{\frac{t_o t_c}{2}}\right)$, the integral can be approximated by:

$$\int e^{-\beta} dt = t_c\, e^{-\frac{a}{2}t_o^2 + at_o t}\left(1 - \frac{t_c}{t_o} + \frac{t}{t_o} - \frac{at^2}{2}\right) \tag{29}$$

if $q = o$ at $t = o$, the integrating constant becomes:

$$c = \frac{t_c}{2} e^{-\frac{a}{2}t_o^2} \tag{30}$$

and the solution appropriate for $t << \left(t_o - \sqrt{\frac{t_o t_c}{2}} \right)$ becomes:

$$q = \frac{t_c}{t_o} \left(e^{-\frac{t}{t_c}} - 1 \right) + \frac{t}{t_o} \tag{31}$$

which is quadratic for $t << t_c$ and linear for $t >> t_c$.

For $\left(t_o - \sqrt{\frac{t_o t_c}{2}} \right) < t < \left(t_o + \sqrt{\frac{t_o t_c}{2}} \right)$ a suitable approximation to the integral is:

$$\int e^{-\beta} \, dt \approx \frac{\pi}{2a} + (t - t_o) - \frac{a}{6} (t - t_o)^3 \tag{32}$$

and the solution for q in this region is:

$$q \approx \sqrt{\frac{\pi}{2} \frac{t_o}{t_c}} - 1 + \frac{t_c}{t_o} e^{-\frac{a}{2} t_o^2} + \frac{t - t_o}{t_c} + \frac{1}{2} \sqrt{\frac{\pi}{2} \frac{t_c}{t_o}} \frac{(t - t_o)^2}{t_c^2} \tag{33}$$

Finally for $\left(t_o + \sqrt{\frac{t_o t_c}{2}} \right) << t$

$$\int e^{-\beta} \, dt \approx \sqrt{\frac{2\pi}{a}} \tag{34}$$

giving

$$q + 1 = \left(\sqrt{2\pi \frac{t_o}{t_c}} + \frac{t_c}{t_o} e^{-\frac{1}{2} \frac{t_o}{t_c}} \right) e^{\frac{1}{2} a (t - t_o)^2} \tag{35}$$

To help interpolate between the regions where good approximations occur, we consider the following. An upper limit to q at a time when the stimulated emission rate is at a level γ is given by the asymptotic value of Eq. (24). That is:

$$q < \frac{\gamma}{t_o} - 1 \tag{36}$$

where ρ can be a function of time. In addition, for $t >> t_c$ one could expect the right side of Eq. (36) to approach a good approximation to q. Indeed, one can obtain such a solution by setting the derivative equal to zero in Eq. (22). We assume that in some range of t, Eq. (35) is a valid solution. If $\rho = at$, Eq. (36) becomes:

$$q \lesssim \frac{\frac{t}{t_o}}{1 - \frac{t}{t_o}} \tag{37}$$

This agrees well with Eq. (31) for $t_c << t << t_o$, and can be expected to be a good approximation at higher values of t until dq/dt increases too rapidly as t approaches t_o.

Now we consider how these solutions might be applied to the results of the last section. There we found that if we apply a step function pumping pulse, the electronic excitation can be expected to follow Eq. (21) which can be written:

$$\rho = \frac{w}{q_o} (1 - e^{-t/\tau}) \tag{38}$$

The straightforward approach to obtain the time dependence of q would be to substitute Eq. (38) into Eq. (23). Unfortunately, in doing so we obtain integrals which are not easily solved. One way to overcome this difficutly is to write Eq. (38) in terms of a series giving:

$$\rho = \frac{w}{q_o} \sum_{n=1}^{\infty} (-1)^{n+1} \frac{1}{(n)!} \left(\frac{t}{\tau}\right)^n \tag{39}$$

or if $t >> \tau$

$$\rho \simeq \frac{w}{q_o} \tag{40}$$

To illustrate the physics of the pulse phenomena one can avoid detailed consideration of the infinite series in Eq. (39). The appropriate approximation depends upon relations between the magnitudes of t, t_c, t_o and τ.

If $t_o << \tau$ only the first term of the series in Eq. (39) need be considered, and all of the expressions based upon a linear behavior of ρ can be taken over by setting $t_o = \frac{w_o}{w} \tau$.

The case where $w < w_o$ is also a simple situation. Here t_o does not exist since ρ does not reach the level of r_c. Eq. (31) holds for $t < \tau$, nevertheless, if t_o is replaced by $\frac{w_o}{w} \tau$ giving:

$$q = \frac{w}{w_o} \frac{t_c}{\tau} \left(e^{-\frac{t}{t_c}} - 1 \right) + \frac{w}{w_o} \frac{t}{\tau} \tag{41}$$

At longer times this connects smoothly with an expression obtained from Eq. (36) with substitution of Eq. (38):

$$q = \frac{\frac{w}{w_o} (1 - e^{-t/\tau})}{1 - \frac{w}{w_o} (1 - e^{-t/\tau})} \tag{42}$$

In the case where $w \gtrsim w_o$ the situation is more complicated; but, as it turns out, not much. Eqs. (41) and (42) are still valid, except that the behavior given by Eq. (42) is terminated abruptly when the stimulated emission rate reaches the cavity loss rate at $t = t_o$. To obtain t_o one needs the more general expression:

$$t_o = -\tau \ln \left(1 - \frac{w_o}{w} \right) \tag{43}$$

Things happen so rapidly in the neighborhood of t_o that we can still use a linear approximation for the stimulated emission rate where a is given by:

$$a = \left(\frac{w}{w_o} - 1 \right) \frac{1}{\tau t_c} \tag{44}$$

We can then write for t somewhat greater than t_o:

$$q = 1 + a^{\frac{1}{2}} a (t - t_o)^2 \tag{45}$$

This expression is qualitatively no different than Eq. (35). However, the constants a and t_o have the special definitions given above and the constant B cannot in general be obtained in a simple manner from the behavior at earlier times. If $w >> w_o$, B can be estimated from Eq. (35):

$$B \approx \sqrt{2\pi \frac{w_o}{w} \frac{\tau}{t_c}} \tag{46}$$

6. NUMERICAL INTEGRATION RESULTS FOR PHOTON BUILDUP

Computer numerical integration was used to obtain the time dependence of q and these results were compared with the approximate analytic expressions obtained in Section 5. The numerical integration employed similar techniques to those reported in several papers.[1]

In Figure 6 numerical results for w/w_o = 0.1, 1.0 and 10 are shown. At levels well below $q \approx 10^{-21}\ q_o$, the characteristics of Eq. (31) are displayed. Below $t = t_c$, q varies quadratically passing over to a linear dependence. In fact, the numerical results are in exact agreement with the analytic expression.

At high levels of q there is a region where the cavity photon number saturates for $w < w_o$. For $w = w_o$, q takes on a superlinear dependence in

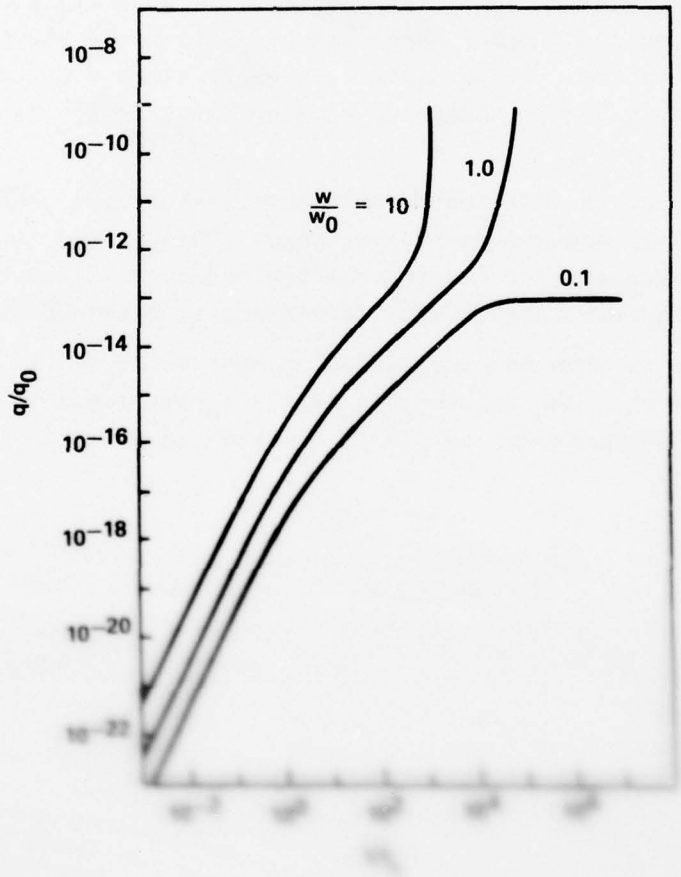

AD-A054 434 GTE LABS INC WALTHAM MASS F/G 20/5
ND MINI LASER BASED ON STOICHIOMETRIC RARE EARTHS COMPOUNDS.(U)
APR 78 A LEMPICKI, E JOHNSON, B MCCOLLUM DAAC29-75-C-0028
UNCLASSIFIED ARO-13299.3-P NL

2 OF 2
AD
A054434

END
DATE
FILMED
6 -78
DDC

this region in accordance with that expected when $\rho \approx r_c$. An even greater superlinear region occurs for $w > w_o$, which is apparently related to the onset of exponential behavior expected when the stimulated emission rate exceeds the cavity loss rate.

The region above $q = 10^{-14}$ is shown in a larger scale in Figure 7. Comparison is made between the numerical integration and points calculated according to Eq. (31), which is exact at lower levels, and calculations based upon the asymptotic Eq. (36).

For $w/w_o = 0.1$ departures from Eq. (31) are observed even at $q = 10^{-14}\ q_o$. However, good agreement is obtained between Eq. (36) and the numerical integration. This agreement with the asymptotic expression should continue indefinitely since ρ cannot exceed $0.1\ r_c$.

A similar situation occurs for $w/w_o = 1.0$. However, since ρ approaches r_c the denominator in Eq. (36) makes itself felt and $\frac{dq}{dt}$ becomes too large to permit q to keep up with Eq. (36). However, since ρ cannot exceed the cavity loss rate, q does saturate at a value equal to $\sqrt{q_o}$ (not shown in Figure 7).

For $w/w_o = 10$, in addition to the above features, q shows a region where its variation appears nearly vertical. This is the region where the stimulated emission rate exceeds r_c, giving exponential growth. This region is of principle interest for lasers and is examined in detail below.

In Figure 8 we show numerical results near $t \approx t_o$, i.e., for the region where $\rho \approx r_c$. The values of q at $t = t_o$ are found to agree quite well with those predicted by Eq. (33), as shown in Table 1.

TABLE 1

COMPARISON OF TYPICAL VALUES OF PHOTON NUMBER AT THRESHOLD

w/w_o	$q(t_o)$ FROM EQ. (33)	$q(t_o)$ FROM NUMERICAL INTEGRATION
10	39.6	44
5	58.2	64
2	103.3	123

In Figure 9 the various curves of Figure 8 have been shifted vertically to facilitate comparison of their slopes at $t = t_o$. As shown in the figure the slopes are all close to a value equal to r_c as predicted by Eq. (33).

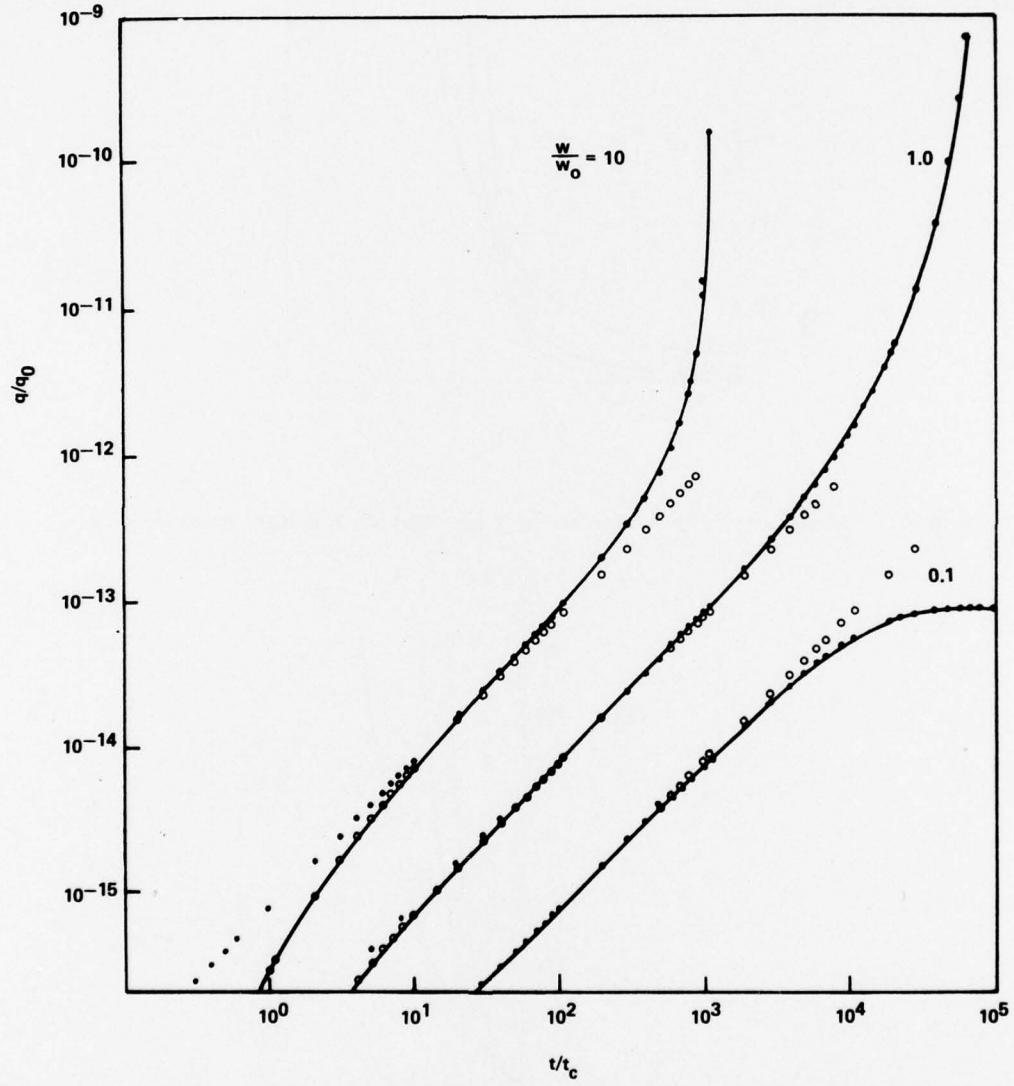

Figure 7. Comparison of Analytic Expressions and Numerical Integration Calculations of Time Dependence of Photon Number

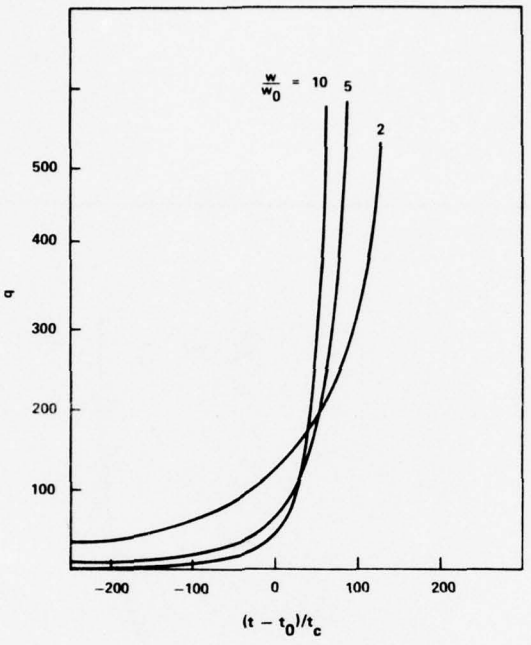

Figure 8. Numerical Calculations for Photon Number Near $t = t_o$

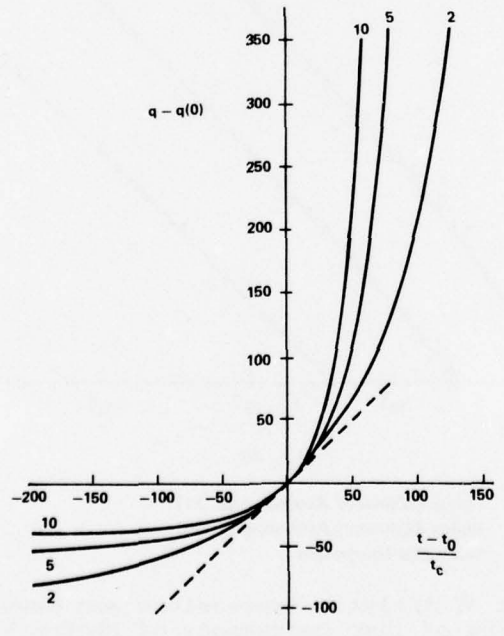

Figure 9. Curves of Figure 8 Shifted to Compare Slopes at $t = t_o$

In Figure 10, the numerical integration shows clearly the transition to exponential growth in the range $t \approx t_o$. Above the transition q grows as exp $(t - t_o)^2$ in agreement with Eq. (35) and has an intercept at $t = t_o$ of 70, compared to 79 calculated according to Eq. (35).

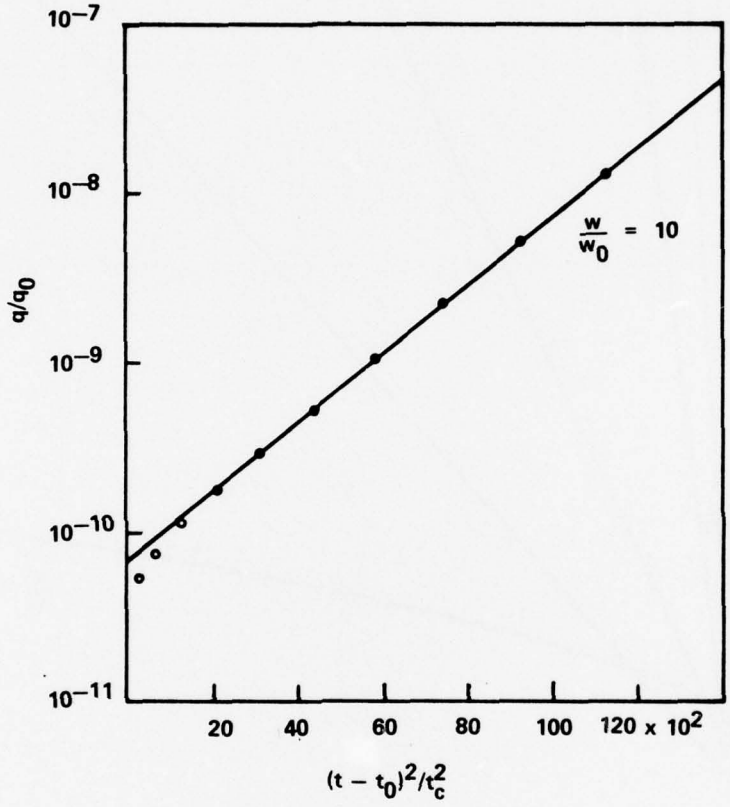

Figure 10. Transition to Exponential Growth in Photon Number

In Figure 11 we show the exponential growth for a variety of examples in the range from $w/w_o = 1.1$ to $w/w_o = 10$. It is seen that Eq. (45) is a good approximation to the behavior with the constant B varying from 350 for $w = 1.1\ w_o$ to 44 for $w = 10\ w_o$.

The numerical integration shows that the approximate analytic expressions developed in Section 5 are valid analytic approximations for the growth of q during a step function pumping pulse and therefore should provide a good foundation for analyzing pulsed lasers.

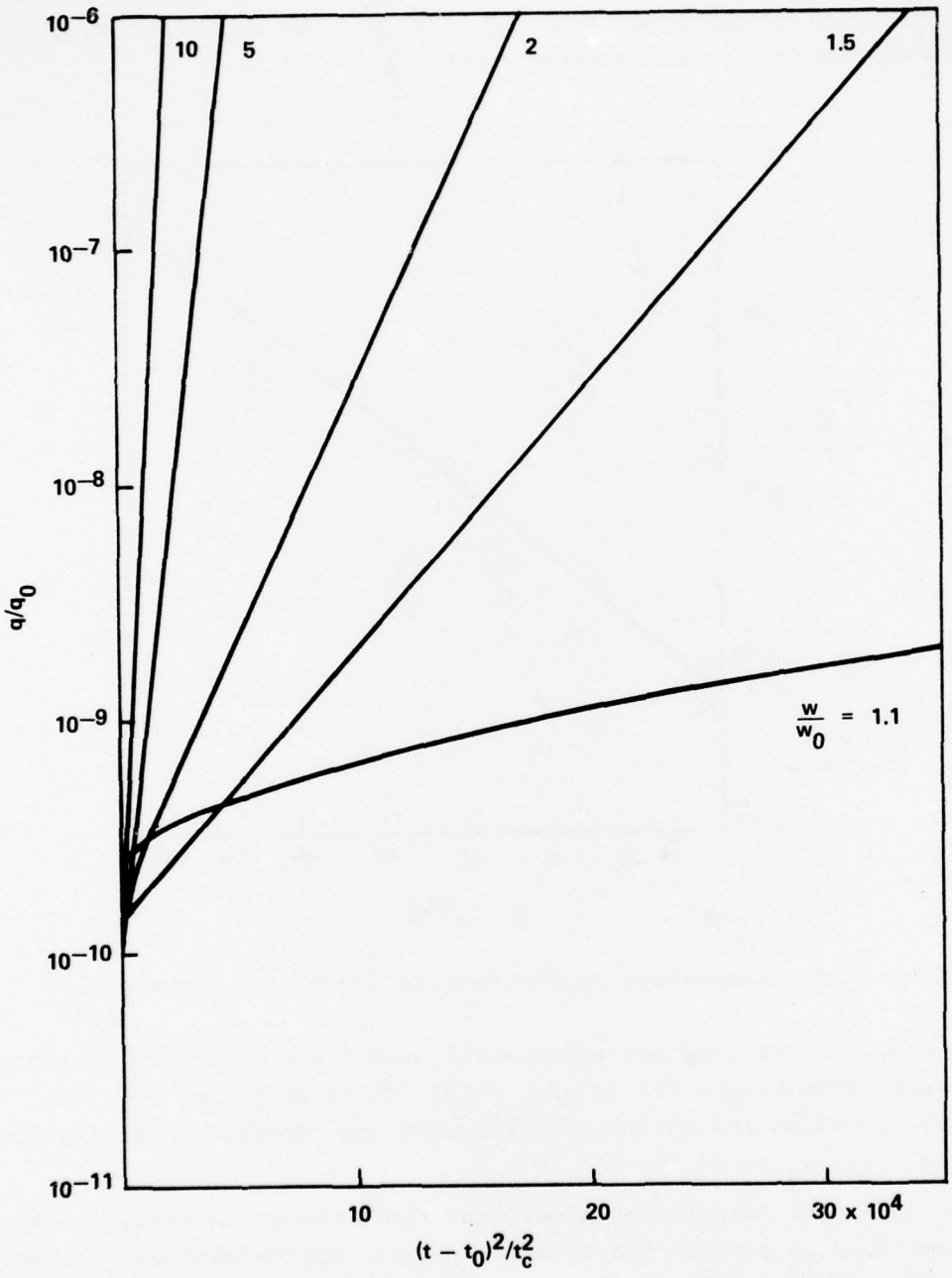

Figure 11. Exponential Growth in q for a Variety of Pumping Levels

7. COUPLING BETWEEN THE PHOTON FIELD AND THE ELECTRONIC EXCITATION

We have seen that the first requirement for the initiation of a pulse is that the spontaneous emission rate rises to equal the cavity loss rate. Under these conditions one gets exponential growth in q. But how high does q go before it reaches a peak value? From the equations it is apparent that q will rise until the stimulated emission rate falls back to again equal the cavity loss rate. Therefore, the second condition for a laser pulse is that the stimulated emission rate spend some time where it is greater than the cavity loss rate. Further, one might expect that the peak intensity of the laser pulse might depend upon the peak level attained by the stimulated emission rate.

Let us assume that by some process the stimulated emission rate has risen and leveled off at some maximum value, ρ_{max}. Further assume that q, though greater than q_o, is at a level small compared to what it will attain in the pulse.

In this situation Eq. (12) can be approximated by:

$$\frac{d\rho}{dt} = -\frac{1}{\tau}\,\rho\,\frac{q}{q_o}$$

$$\frac{dq}{dt} = q\,(\rho - r_c) \tag{47}$$

where, since exponential growth in q is occurring, we neglect the pumping term. We can eliminate time from these equations giving:

$$\frac{dq}{d\rho} = -\tau\, q_o\,\frac{\rho - r_c}{\rho} \tag{48}$$

The solution to this equation is given by:

$$q = q_o\,\tau\left(\rho_{max} - \rho - r_c\,\ln\frac{\rho_{max}}{\rho}\right) \tag{49}$$

We can immediately write for the maximum value attained by q:

$$q_{max} = q_o\,\tau\left[\rho_{max} - r_c\left(1 + \ln\frac{\rho_{max}}{r_c}\right)\right] \tag{50}$$

where we neglect the value of q at the beginning of the exponential growth.

To obtain the time dependence of q we could substitute Eq. (49) into Eq. (47). Since this gives difficult integration, we make use of the approximation:

$$q \approx q_{max} - \frac{1}{2} \frac{q_o \tau}{r_c} (\rho - r_c)^2 \tag{51}$$

This approximation is valid for $\rho \approx r_c$ and therefore near the peak value of q.

Substituting Eq. (51) in Eq. (47) gives:

$$\frac{d(\rho - r_c)}{\frac{\rho}{r_c}\left[\frac{2r_c}{\tau}\frac{q_{max}}{q_o} - (\rho - r_c)^2\right]} = \frac{1}{2} dt \tag{52}$$

Near the peak the variation in $(\rho - r_c)$ affects the integral much greater than the variation in ρ. We set the ratio $\rho/r_c \approx 1$. Integration and substitution in Eq. (49) then yields:

$$q \approx q_{max} \operatorname{sech}^2 \left(\frac{t}{\gamma}\right) \tag{53}$$

where γ corresponds to the pulse half-width and is given by:

$$\frac{1}{\gamma} = \frac{1}{2} \sqrt{\frac{2r_c}{\tau}\frac{q_{max}}{q_o}} \tag{54}$$

Substituting from Eq. (50):

$$\frac{1}{\gamma} = \sqrt{\frac{r_c}{2}\left[\rho_{max} - r_c\left(1 + \ln\frac{\rho_{max}}{r_c}\right)\right]} \tag{55}$$

If ρ_{max} is too large, one can expect errors in Eq. (53) near the half power points. These errors will tend to compensate, making the rise time sharper and the decay time slower.

In the case where $\rho_{max} < 2r_c$, Eq. (55) becomes simplified to:

$$\gamma = 2t_c \frac{r_c}{\rho_{max} - r_c} \tag{56}$$

8. CAVITY DUMPING

The first pulsed laser phenomena we consider is cavity dumping. This technique can produce peak powers enhanced over the optimum cw powers and provides a means of modulating the laser output in the megahertz range.

In cavity dumping the output mirror is replaced by a 100% reflecting mirror. The circulating power is allowed to build up and means are provided to quickly deviate all or part of the circulating beam out of the cavity. In terms of the rate equations, this amounts to modulating the output coupling.

The number of photons in the cavity corresponds to the cw stored energy and is given by Eq. (16). Well above threshold and with the output coupling reduced to zero, q is limited by scattering losses and is given by:

$$q = (wt_\ell - q_o) \tag{57}$$

The electronic excitation is given by:

$$n = q_o \frac{\tau}{t_\ell} \tag{58}$$

The corresponding stimulated emission rate is:

$$\rho = \frac{1}{t_\ell} \tag{59}$$

We have a situation where there can be much energy stored in the photon field in the cavity (if t_ℓ is long), and little stored in the electronic excitation if ($t_\ell \gtrsim \tau$). If now the output coupling is abruptly switched to give a short cavity lifetime, t_c, a peak output intensity results, given by:

$$r_R q = \frac{wt_\ell - q_o}{t_R} \tag{60}$$

The output can result in enhanced intensity in two respects. First, the circulating power is higher than cw; and second, the output coupling can be much smaller than the optimum coupling in the cw case.

The decay is given by:

$$\frac{dq}{dt} = \rho \left(\frac{q}{q_o} + \frac{1}{q_o} \right) - r_c q \tag{61}$$

Since $r_c >> \rho \approx \frac{1}{t_\ell}$, the decay of the output is exponential and given by:

$$r_R q = \frac{wt_\ell - q_o}{t_c} e^{-\frac{t}{t_c}} \tag{62}$$

Once the output coupling is switched back to zero, the circulating power recovers in a time t_o, given by Eq. (43):

$$t_o = \tau \ln \frac{wt_\ell}{wt_\ell - q_o} \tag{63}$$

Had the laser been operating cw at some optimum output coupling, τ_c, it would have had an output given by Eq. (18). The optimized cavity dumped output is given by:

$$r_R q = \frac{c}{4\ell} (wt_\ell - q_o) \tag{64}$$

Therefore, cavity dumping increases the peak power by the factor:

$$F = \frac{c}{4\ell} \frac{wt_\ell - q_o}{1 - 2\sqrt{\frac{q_o r_\ell}{w}}} \approx \frac{c}{4\ell} \frac{t_\ell}{1 - 2\sqrt{\frac{q_o r_\ell}{w}}} \tag{65}$$

In principle, an output coupling of 100% would be possible giving t_c equal to the round-trip time of the cavity. However, practical considerations in real systems limit the maximum output coupling to 50% as used in Eq. (62). With high output coupling the decay departs from simple exponential behavior showing the effect of discrete passes in the resonator.

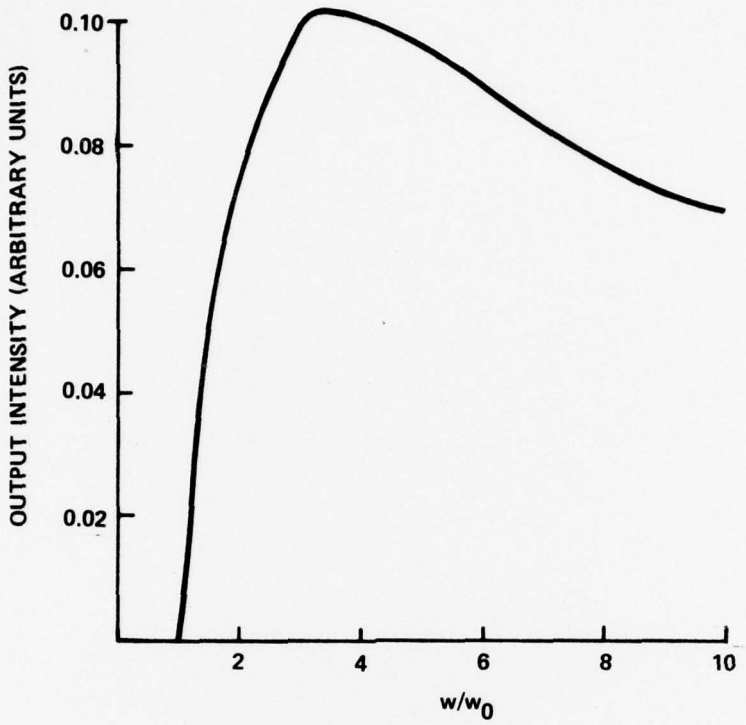

Figure 12. Variation of Q-Switch Output According to Eq. (68)

9. Q-SWITCHING

Q-switching is another pulsed laser phenomenon where one modulates the cavity loss rate. In this case one initially makes the cavity loss rate very large by introducing losses. This permits the stimulated emission rate to rise to high levels without lasing. However, since the losses are high the number of photons in the cavity are low. This situation is exactly the opposite of that in the cavity-dumping situation. If we now switch the cavity loss rate to a value much less than the stimulated emission rate, exponential growth in q occurs resulting in an intense output pulse.

To analyze this process we suppose a step function pumping pulse is applied to the laser. Since initially the losses are high, the laser does not reach threshold. The stimulated emission rate rises according to Eq. (38), therefore reaching a maximum of w/q_o in times comparable to a radiative lifetime τ. Since ρ never exceeds the cavity loss rate, the photon number saturates at the value $\frac{w}{q_o} t_c$. To the extent to which t_c can be considered to approach zero, q can be considered zero. The electronic excitation saturates at a value of $w\tau$.

If now r_c is switched to a value much less than w/q_o, the photon number rises exponentially according to Eq. (24):

$$q = \frac{\rho}{\rho - r_c} \left[e^{(\rho - r_c)t} - 1 \right] \tag{66}$$

This exponential rise in q will continue until q becomes comparable to the saturated electronic excitation, and ρ starts to become depleted. Although q may be less than q_o it quickly exceeds q_o, so that we can take over the results of Section 7. From Eq. (50) we can calculate the maximum value attained by q:

$$q_{max} = w\tau \left[1 - \frac{w_o}{w} \left(1 + \ln \frac{w}{w_o} \right) \right] \tag{67}$$

The peak output is:

$$r_R \, q_{max} = \frac{w^2 \tau}{q_o} \frac{w_o}{w} \left[1 - \frac{w_o}{w} \left(1 + \ln \frac{w}{w_o} \right) \right] \tag{68}$$

As is seen in Figure 12, this function has a broad maximum at $w/w_o = 4$, giving for optimized coupling:

$$r_R \, q_{max} = \frac{1}{10} \frac{w^2 \tau}{q_o} \tag{69}$$

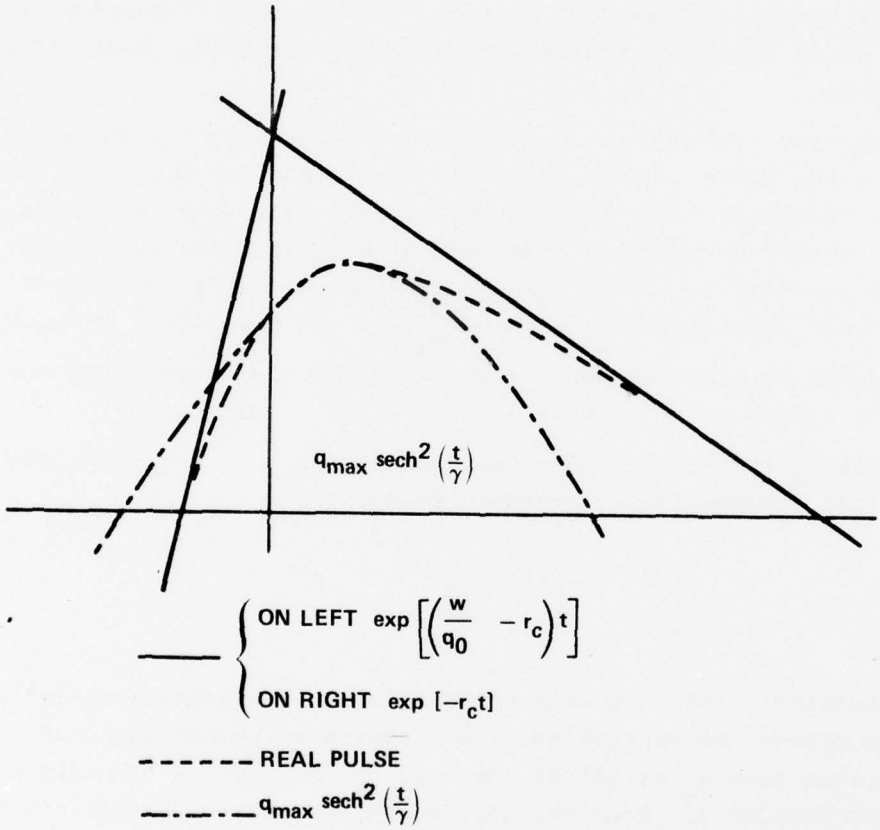

Figure 13. Schematic Diagram of Q-Switch Pulse

The q-switched peak intensity is enhanced over the cw level by the factor F, given by:

$$F = \frac{1}{10} \frac{w\tau/q_o}{1 - 2\sqrt{\frac{q_o r_\ell}{w}}} \tag{70}$$

A lower limit to the pulse width is obtained from Eq. (54):

$$\gamma = t_c \sqrt{2 \frac{w_o}{w}} \tag{71}$$

As pointed out previously, the pulse half-width given by Eq. (54) is based on a symmetric pulse which is a good approximation only for low values of excitation. The situation for Q-switching is likely to be more like that shown schematically in Figure 13, with a steep rise and a slow decay eventually going as $e^{-r_c t}$. This consideration would suggest that the pulse width would be larger than given by Eq. (54) with an upper limit:

$$\gamma \approx t_c \tag{72}$$

This value of half-width is consistent with a pulse energy given by:

$$E = w\tau \tag{73}$$

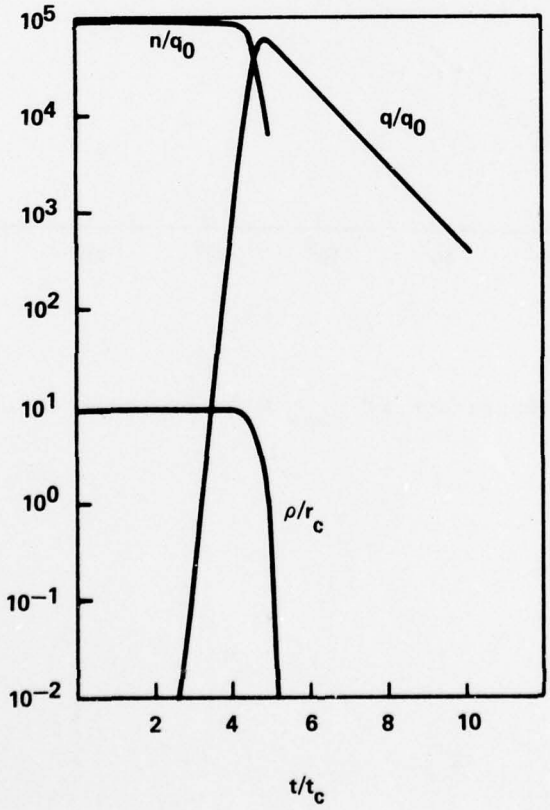

Figure 14. Numerical Integration Results for Q-Switch Pulse

In Figure 14 we show the results of numerical integration for the q-switch situation. The general conclusions obtained above are confirmed. The pulse is asymmetric, as expected, with a half-width $\approx t_c$. The photon number, q, rises to a value comparable to the electronic excitation. A calculation of q_{max} using Eq. (67) gives $q_{max} = 5.92 \times 10^4 \, q_c$ which agrees well with the numerical integration.

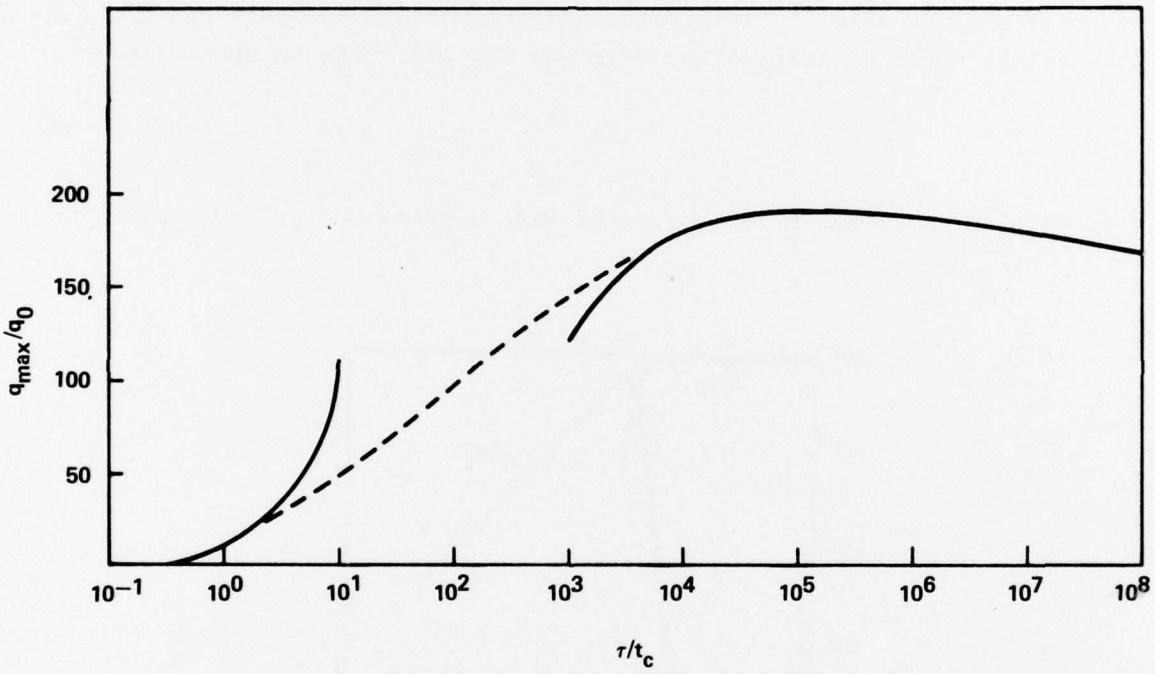

Figure 15. Variation of q_{max} with Spontaneous Lifetime

10. TRANSIENT SPIKE LASER OPERATION

We now consider the transient spike that occurs at the initiation of optical pumping. In this form of pulsed operation we modulate the pumping rate, w. Our discussion will be limited to the application of a step function pumping pulse. Such a situation applies to the practical situation where the pumping pulse is reasonably flat and where the turn on time is short relative to the spontaneous lifetime.

As in other forms of laser pulses, a pulse is initiated when the stimulated emission rate rises to the order of the cavity loss rate. There are three events during the optical pulse that have particular significance. First, there is the point in time where ρ first exceeds r_c. This situation permits exponential growth in q. However, since q starts from a very low level, the stimulated emission rate is permitted to rise significantly above r_c. There is little laser output during this period. Second, there is the point where ρ reaches its maximum. The photon number is still at a relatively low level, but the maximum value achieved by the stimulated emission rate determines the ultimate strength of the pulse. Third, there is the point at which ρ begins to drop below r_c. Coincident with this, q reaches its peak and the output pulse begins to decay in intensity.

The stimulated emission rate during the initial period is given by Eq. (38). However, in general, the pulse is so short that one can use the linear approximation with the constant a given by Eq. (44).

$$\rho = r_c + \frac{1}{\tau}\left(\frac{w}{w_o} - 1\right)\frac{t - t_o}{t_c} \tag{74}$$

and q during the initial period is given by Eq. (45):

$$q + 1 = B \exp\left[\frac{1}{2}\frac{t_c}{\tau}\left(\frac{w}{w_o} - 1\right)\left(\frac{t - t_o}{t_c}\right)^2\right] \tag{75}$$

where B depends upon w/w_o and can be determined as discussed in Section 5.

The condition that ρ reaches a maximum is that $\frac{d\rho}{dt} = 0$ in Eq. (12) which is satisfied by:

$$\rho = r_c \frac{w/w_o}{\left(\frac{q}{q_o} + 1\right)} \tag{76}$$

The maximum stimulated emission rate is given by the simultaneous solution of Eqs. (74), (75) and (76). This solution is given approximately by:

$$(\rho_{max} - r_c)^2 = \frac{2\, r_c \left(\frac{w}{w_o} - 1\right)}{\tau} \ln \left[\frac{q_o \left(\frac{r_c}{\rho_{max}} \frac{w}{w_o} - 1\right)}{B}\right] \tag{77}$$

If $w >> w_o$, in accordance with Eq. (46) the log function can be replaced in this and subsequent expressions by:

$$\ln \left[\frac{q_o \left(\frac{w}{w_o} - 1\right)}{B}\right] \approx \ln \left[\frac{q_o \left(\frac{w}{w_o}\right)^{\frac{3}{2}}}{\sqrt{2\pi \frac{\tau}{t_c}}}\right] \tag{78}$$

To obtain high stimulated emission rates one should use a high pumping rate and select material with a low spontaneous lifetime. However, as τ tends to zero the stimulated emission rate has a limit given by:

$$\lim_{\tau \to 0} \rho_{max} = \frac{w}{w_o} r_c = \frac{w}{q_o} \tag{79}$$

This limit is approached closely for

$$\tau \lesssim \frac{2}{\frac{w}{w_o} - 1} \ln \frac{q_o \left(\frac{w}{w_o} - 1\right)}{\sqrt{2\pi \frac{w_o}{w}}} \tag{80}$$

For higher values of τ where $\rho_{max} \approx r_c$, Eq. (77) can be approximated by:

$$\rho_{max} = r_c + r_c \left\{2 \frac{t_c}{\tau} \left(\frac{w}{w_o} - 1\right) \ln \left[\frac{q_o \left(\frac{w}{w_o} - 1\right)}{B}\right]\right\}^{\frac{1}{2}} \tag{81}$$

In the range of low spontaneous lifetimes specified by Eq. (80), the peak value of q is obtained by substitution in Eq. (50) is given by:

$$q_{\substack{max \\ \tau \to 0}} = q_o \frac{\tau}{t_c} \left(\frac{w}{w_o} - 1 + \ln \frac{w}{w_o} \right) \tag{82}$$

In this range we see that q_{max} increases linearly with lifetime. At longer lifetimes ρ_{max} approaches r_c, and Eq. (50) can be approximated by:

$$q_{max} = \frac{q_o \tau t_c}{2} \left(\rho_{max} - r_c \right)^2 \left(1 - \frac{2}{3} \frac{\rho_{max} - r_c}{r_c} \right) \tag{83}$$

Substitution of Eq. (81) gives:

$$q_{max} = q_o \left(\frac{w}{w_o} - 1 \right) \ln \left[\frac{q_o \left(\frac{w}{w_o} - 1 \right)}{B} \right] (1 - \phi) \tag{84}$$

where:

$$\phi = \frac{2}{3} \left[2 \frac{t_c}{\tau} \left(\frac{w}{w_o} - 1 \right) \ln \frac{q_o \left(\frac{w}{w_o} - 1 \right)}{B} \right] \tag{85}$$

If $w >> w_o$ we have from Eq. (46):

$$B \approx \sqrt{2\pi \frac{w_o}{w} \frac{\tau}{t_c}} \tag{86}$$

Expressions (85) and (86) provide the principal dependence of q_{max} on lifetime in the range where Eq. (84) is valid. In this range the dependence is very weak relative to the linear dependence at lower values of τ. At intermediate values of τ Eq. (85) dominates the behavior, continuing the trend toward greater values of q_{max}. Eventually this trend is reversed by the variation of B with lifetime, which dominates the behavior at high values of lifetime. This behavior is shown graphically in Figure 15.

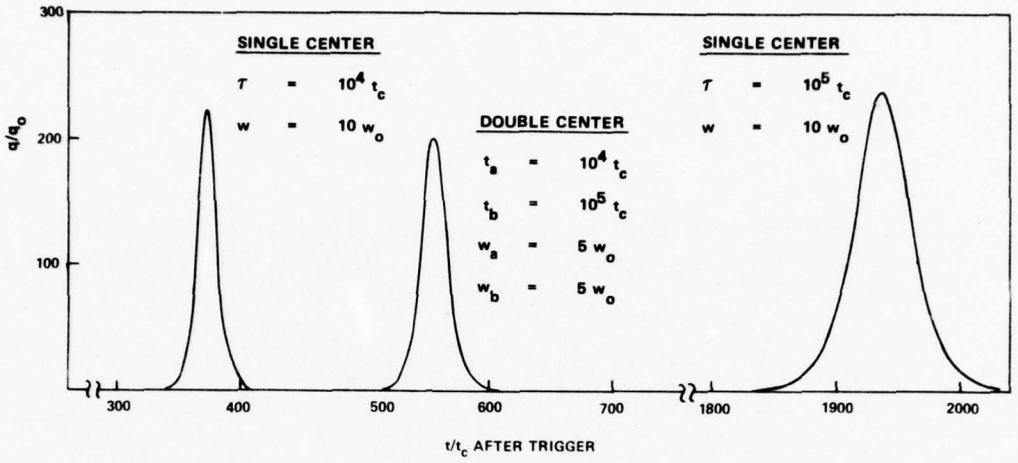

Figure 16. Numerical Integration for Optical Spiking

We now consider other aspects of the pulses in the range of the maximum in Figure 15 where we can assume $\rho_{max} \approx r_c$. The maximum laser output intensity becomes:

$$r_c\, q_{max} = r_c\, q_o \left(\frac{w}{w_o} - 1\right) \ln\left[\frac{q_o \left(\frac{w}{w_o} - 1\right)}{B}\right] \tag{87}$$

With optimized coupling this becomes:

$$r_c\, q_{max} \approx w\left[1 - 2\sqrt{\frac{q_o r_\ell}{w}}\right] \ln\left[\frac{q_o \left(\frac{w}{w_o} - 1\right)}{B}\right] \tag{88}$$

The enhancement factor of the peak intensity over cw is:

$$F = \ln\left[\frac{q_o \left(\frac{w}{w_o} - 1\right)}{B}\right] \tag{89}$$

From Eq. (53) the time dependence of the pulse is given by:

$$q \approx q_{max}\ \mathrm{sech}^2\left(\frac{t}{\gamma}\right) \tag{90}$$

where the pulse half-width is given by:

$$\gamma = 2.5 \frac{\sqrt{\tau t_c}}{\sqrt{\left(\frac{w}{w_o} - 1\right) \ln \left[\frac{q_o \left(\frac{w}{w_o} - 1\right)}{B}\right]}} \tag{91}$$

and a pulse energy given by:

$$E = 2.5 \sqrt{q_o^2 r_c \tau} \sqrt{\left(\frac{w}{w_o} - 1\right) \ln \left[\frac{q_o \left(\frac{w}{w_o} - 1\right)}{B}\right]} \tag{92}$$

We can check these conclusions in another way by integrating Eq. (47) term by term. From the first of Eq. (47) we obtain:

$$\tau q_o \int d\rho = \int w dt - \int q\rho dt - q_o \int \rho dt \tag{93}$$

We take as the initial limit of integration the point at which $\rho = \rho_{max}$ and the second limit at $\rho = r_c$. The term on the left becomes:

$$\tau q_o \int d\rho = \tau q_o (\rho_{max} - r_c) \tag{94}$$

For a short pulse the first term on the right of Eq. (93) is negligible. We assume that during the pulse ρ does not deviate much from r_c. The second term becomes:

$$\int r_c q dt = \frac{E}{2} \tag{95}$$

where E is the energy in the pulse and we assume for simplicity that the pulse is symmetrical. We further neglect the last term, assuming q becomes somewhat larger than q_o during the pulse. Therefore, we have:

$$E = 2\tau q_o (\rho_{max} - r_c) \tag{96}$$

Substituting from Eq. (81):

$$E = 2q_o \sqrt{2 \frac{\tau}{t_c} \left(\frac{w}{w_o} - 1\right) \ln \left[\frac{q_o \left(\frac{w}{w_o} - 1\right)}{B}\right]} \qquad (97)$$

This is in substantial agreement with Eq. (92).

The analysis in this section made liberal use of the results obtained in Section 7 which were based upon the assumption that at the time the stimulated emission rate reached its maximum, q was somewhat greater than q_o but at a smaller level compared to what it would attain in the pulse. To test the self-consistency of these assumptions, we calculate the values of these quantities for several examples in Table 2.

TABLE 2

TYPICAL VALUES OF VARIOUS QUANTITIES DURING TRANSIENT SPIKE OPERATION FOR $\tau = 10^4 t_c$

w/w_o	B	$r_c \rho_{max}$	q/q_o at $\rho = \rho_{max}$	q_{max}/q_o	F
10	70	1.22	7.2	484	25.8
5	120	1.14	3.38	196	24.5
2	190	1.07	0.87	49	22.6
1.5	200	1.05	0.42	25	21.8
1.1	450	1.04	0.06	16	19.4

For the assumptions to be satisfied, the numbers that appear in Column 4 should be greater than unity and small relative to those in Column 5. The first condition is satisfied for $w > 2w_o$ and the second in all cases. Therefore, the analytic expressions obtained should be good approximations except for w too close to w_o.

In Figure 16 we show numerical integration results for transient spikes for two values of spontaneous lifetime differing by an order of magnitude. The pulses are reasonably symmetrical as expected for a $\text{sech}^2 \gamma t$ and the peaks are nearly independent of lifetime, as shown in Table 3. Values of q_{max} and half-width agree quite well with the corresponding values calculated from the approximate analytic expressions. In Table 3 comparison is made of

values of q_{max} and γ calculated from analytic expressions and values obtained through numerical integration. Reasonable agreement occurs.

TABLE 3

COMPARISON OF ANALYTIC EXPRESSIONS AND NUMERICAL INTEGRATION FOR OPTICAL SPIKE OPERATION

		$\tau = 10^4\ t_c$	$\tau = 10^5\ t_c$
q_{max}/q_o	• Calculated	182	192
	• Numerical Integration	213	238
γ/t_c	• Calculated	16.4	51.9
	• Numerical Integration	16	52

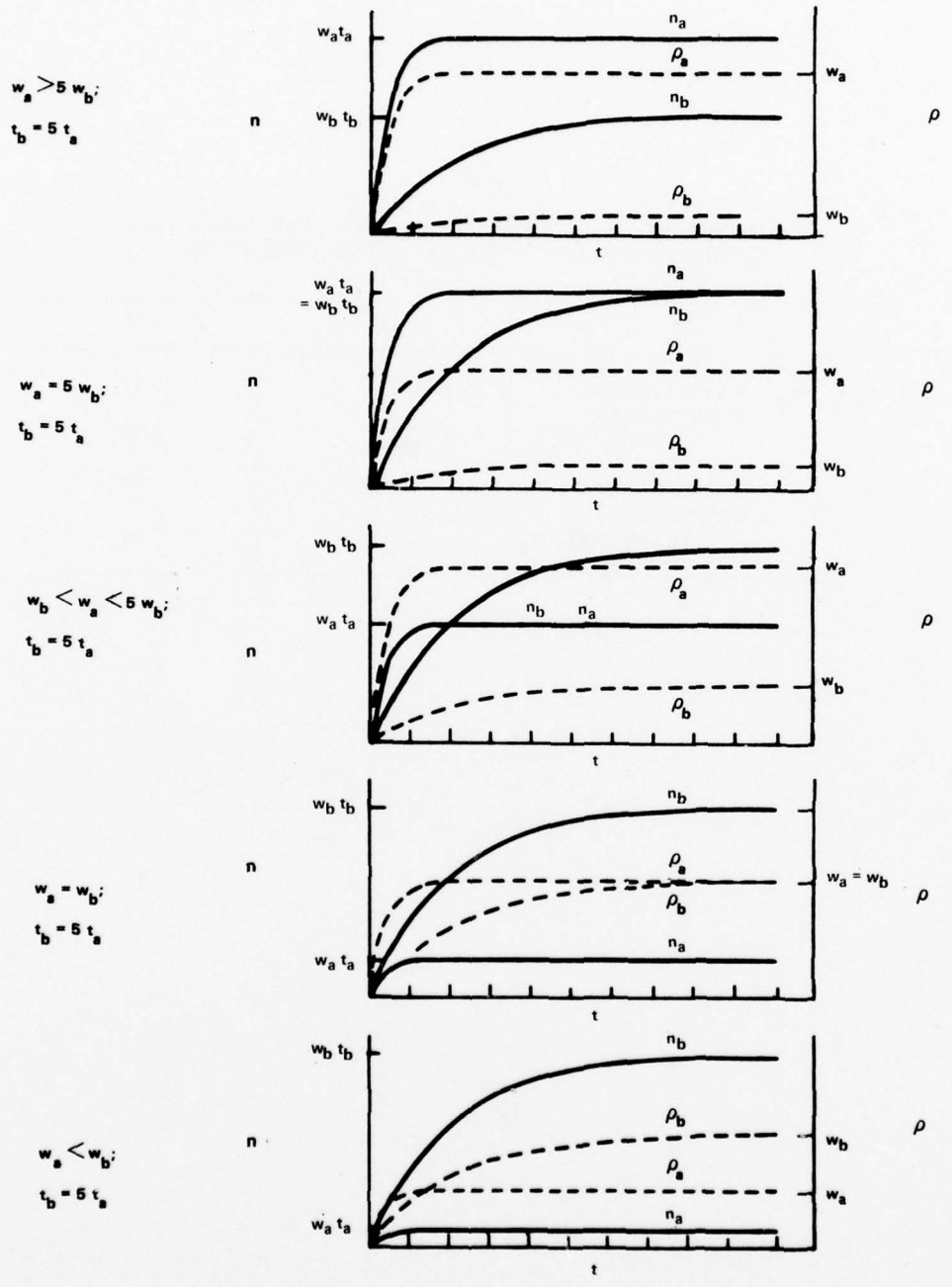

Figure 17. Time Dependence of Electronic Excitation Neglecting Coupling to Photons

11. PULSE NARROWING

Frequently the situation arises where one has a laser output that has more than enough intensity for the application. However, it may not be the right wavelength and the pulse width may be excessive for the application. Such may be the case with a Q-switched glass or ruby laser, or with a molecular nitrogen laser. One can use such a laser to pump a second laser whose output occurs at a longer wavelength and where interesting pulse narrowing phenomena may occur.

Of course, any of the pulse phenomena we have talked about is capable of pulse narrowing, since for any laser pulse that exists there is a pumping pulse that is longer. As we have seen, cavity dumping and Q-switching gives pulse widths on the order of a cavity lifetime. However, the spontaneous lifetime may be too short for Q-switching or for some other reason one can not or would prefer not to use such techniques. In this case, one can exploit the properties of transient spike operation.

The use of the transient spike approach to pulse narrowing was first suggested by Roess[2] who demonstrated the effect by numerical integration of the rate equations. The technique was further developed, largely in an emperical manner, by others.[3-7]

In our treatment of transient spike operation for long spontaneous lifetimes, we obtained the pulse width given by Eq. (91).

$$\gamma = 2.5 \sqrt{\frac{\tau t_c}{\left(\frac{w}{w_o} - 1\right) \ln\left[\frac{q_o\ (w/w_o - 1)}{B}\right]}} \tag{98}$$

Therefore, for narrow pulses one should use short cavities with high output coupling and pump as high above threshold as possible.

If this pulse width is to be isolated from additional oscillations or significant cw output, the pumping pulse must be turned off in a time slightly longer than the delay that occurs between the initiation of pumping and the transient spike. This delay is given by Eq. (43):

$$t_o = -\tau \ln\left(1 - \frac{w_o}{w}\right) \tag{99}$$

Returning to Eq. (98) we note that for narrow pulses it is helpful if the spontaneous lifetime is short as in dye lasers. However, if the lifetime approaches the cavity lifetime the assumptions that led to Eq. (98)

are no longer valid, and we need to derive a new expression to replace it. For short cavity lifetimes the maximum stimulated emission rate attained in a transient qulse is given by Eq. (79). This leads to a maximum photon number given by:

$$q_{max} = \tau \left[w - w_o - w_o \ln \frac{w}{w_o} \right] \tag{100}$$

From Eq. (54) we obtain the pulse width for short spontaneous lifetimes:

$$\gamma = \sqrt{2}\, t_c \left[\frac{w}{w_o} - 1 - \ln \frac{w}{w_o} \right]^{-\frac{1}{2}} \tag{101}$$

For pumping 3X threshold, this gives a pulse width approximately equal to the cavity lifetime. This is precisely what has been observed in dye lasers where pulse widths less than a nanosecond have been observed.[4-7]

12. TWO CENTER LASER

It is interesting to speculate whether a pulsed laser might profit from two types of lasing centers with the same energy level structure but with greatly different lifetimes. One would attempt to store large amounts of energy in long lifetime centers and to utilize the properties of the fast centers to dump this energy quickly in a sharp pulse. Perhaps in this way one could obtain transient spike operation to rival Q-switch operation without the complications of extra intracavity elements. The feasibility of this approach is not obvious and it is interesting to go through the arguments, which are at first encouraging, but eventually show that there is no advantage to such a two-center approach.

First we consider how to modify the rate equations to take into account two sets of centers of spontaneous lifetimes t_a and t_b, respectively. We assume t_b is something like a factor of five or ten greater than t_a.

If the line width is independent of the spontaneous lifetime (as in the case of the Doppler limited situation) and is the same for both types of centers, then:

$$t_a B_a = t_b B_b = \frac{c^3}{8\pi\nu^2\Delta\nu} \equiv \frac{V}{q_o} \tag{102}$$

Therefore, q_o is the same for both types of centers. The set of coupled Equations (12) become:

$$\begin{aligned}
\frac{d\rho_a}{dt} &= \frac{r_c}{t_a}\left[\frac{w_a}{w_o} - \frac{\rho_a}{r_c}\left(\frac{q}{q_o} + 1\right)\right] \\
\frac{d\rho_b}{dt} &= \frac{r_c}{t_b}\left[\frac{w_a}{w_o} - \frac{\rho_b}{r_c}\left(\frac{q}{q_o} + 1\right)\right] \qquad (103) \\
\frac{dq}{dt} &= \rho(q + q_o) - r_c q
\end{aligned}$$

where subscripts a and b designate quantities associated with the fast and slow centers respectively, and $\rho=\rho_a+\rho_b$.

In a single center, laser ρ and n are tied together by a single spontaneous lifetime. In a two-center laser where t_a and t_b are vastly different, an additional degree of freedom exists where the energy storage can be dominated by the slow centers n_b, and ρ is dominated by the fast centers through n_a/t_a even though n_a may be small. It is this separation of roles in pulsed laser operation that we would like to exploit. If one is to hope to take advantage of this duality, one must consider the relative magnitudes of the pumping rates. The effect of the relative magnitudes of the pumping rates on the electronic excitation is illustrated in Figure 17 where the contributions of each center to the electronic energy storage are given by solid lines and the contributions to gain are given by dashed lines. The first set of curves are given for $w_a > 5w_b$ where we assume a ratio of 5 between the lifetimes. In this case the laser dynamics are completely dominated by the fast centers since the contributions of the slow centers to both energy storage and to stimulated emission rate are small relative to the contributions of the fast centers.

For $w_b < w_a < 5w_b$, we arrive at the desirable situation where the energy storage is dominated by the slow centers and the stimulated emission is dominated by the fast centers. It is important not only that the stimulated emission rate attain high values but also that it react rapidly to a trigger pulse.

We have shown that one can arrange a situation where the energy storage in an initial below threshold pulse is dominated by the slow centers. In a subsequent intense narrow pulse the stimulated emission rate can be dominated by the fast centers. The question that remains, however, is whether the energy stored in the slow centers would contribute significantly to the laser spike triggered by the later narrow pulse.

In Section 7 we considered the coupling between the photon field and the electronic excitation. There we concluded [see Eq. (50)] that for a given peak stimulated emission rate, the maximum number of photons generated in the cavity is proportional to the lifetime, therefore one would like long lifetime centers. Indeed, in the case of Q-switching we found that long lifetime centers were desirable. However, in the case of a two-center laser the lifetime to be substituted for τ in Eq. (50) is an effective lifetime ${}_a\tau_1$:

$$\frac{1}{\tau_1} = \left(\frac{1}{t_a}\frac{\rho_a}{\rho} + \frac{1}{t_b}\frac{\rho_b}{\rho}\right) \tag{104}$$

From the considerations of Section 4 it is obvious that $\tau_1 \approx t_a$, i.e., the lifetime of the fast centers.

In Section 10 we obtained Eq. (77) which gives the maximum stimulated emission rate. The lifetime dependence of Eq. (77) results from Eq. (74) which can be written in the form:

$$\rho \approx \rho_o + \frac{1}{\tau_2} \left(\frac{w}{w_o} - 1 \right) \frac{t}{t_c} \tag{105}$$

where this effective lifetime is given by:

$$\frac{1}{\tau_2} = \frac{1}{t_a} + \frac{1}{t_b} \tag{106}$$

Again the performance is dominated by the fast centers. Having exhausted effects due to lifetime, we must conclude that adding slow centers has no stong effect on the transient spike operation.

In Figure 16, we use numerical integration to compare the transient spike for a two-center laser having lifetimes differing by a factor of ten with spike operations for individual lasers with single centers of either lifetime. The peak intensities for the three are comparable and no apparent advantage of the two-center laser is shown. One might suggest that some different set of parameters for the integration might demonstrate enhanced intensity for the two-center laser. However, the analytical discussion offers no encouragement. From this analysis it is apparent that any slow centers that are present can store energy better than the fast centers but in transient spike operation merely sit on the sidelines. If two types of centers are present in a given laser material, they should be converted to a single lifetime if possible.

13. CONCLUSIONS

We have succeeded in obtaining approximate analytic expressions describing a wide variety of laser pulse phenomena that can be handled using the laser rate equations. Using these expressions we can examine these phenomena without recourse to the catalogs of numerical computer data that have been the traditional approach to laser pulse phenomena.

In Table 4 we compare various pulse modes among themselves and with cw operation. For laser materials with long spontaneous lifetimes, the Q-switch mode is to be preferred since it gives the highest peak intensity. The enhancement of the peak intensity over cw is approximately equal to the ratio of the spontaneous lifetime to the cavity lifetime.

As the spontaneous lifetime approaches the cavity lifetime, the preferred mode is cavity dumping, if the residual cavity losses are small enough. In this case the enhancement over cw is proportional to the ratio of the cavity lifetime with zero output coupling to the cavity round-trip time.

Transient spike operation is useful in roughly the same range as Q-switching. However, the enhancement factor over cw operation is approximately equal to $\ln q_o$, i.e., the logarithm of the number of modes in the luminescent line width. Using a typical value for q_o gives $F \approx 22$. This is low relative to that achievable with Q-switching. Transient spike operation is useful if one is interested in moderate pulse intensities and in dispensing with extra intracavity elements or if one is principly interested in obtaining narrow pulses. If there are lasing centers of different lifetimes present, transient spike operation is dominated by the fast centers and no enhancement of peak intensity results from adding long lifetime centers for energy storage.

TABLE 4

COMPARISON OF VARIOUS MODES OF
PULSED LASER OPERATION

	PEAK INTENSITY	ENERGY	PULSE WIDTH	F
Cavity Dumping	$\frac{c}{4\ell}(wt_\ell - q_o)$	wt_ℓ	t_c	$\frac{c}{4\ell}\frac{t_\ell}{1-2\sqrt{\frac{q_o r_\ell}{w}}}$
Q-Switch	$\frac{1}{10}\frac{w^2\tau}{q_o}$	$w\tau$	t_c	$\frac{1}{10}\frac{\frac{w}{w_o}\frac{\tau}{t_c}}{1-2\sqrt{\frac{q_o r_\ell}{w}}}$
Transient Spike	$w\left[1-2\frac{q_o r_\ell}{w}\right]\ln\left[\frac{q_o\left(\frac{w}{w_o}-1\right)}{B}\right]$	$2.5\sqrt{q_o^2 r_c \tau\left(\frac{w}{w_o}-1\right)\ln\left[\frac{q_o\left(\frac{w}{w_o}-1\right)}{B}\right]}$	$\frac{2.5\sqrt{\tau t_c}}{\sqrt{\left(\frac{w}{w_o}-1\right)\ln\left[\frac{q_o\left(\frac{w}{w_o}-1\right)}{B}\right]}}$	$\ln\left[\frac{q_o\left(\frac{w}{w_o}-1\right)}{\sqrt{2\pi\frac{w_o}{w}\frac{\tau}{t_c}}}\right]$

14. REFERENCES

1. See, for example, R. Dunsmuir, J. Electronics & Control 10, 453 (1961); D.A. Kleinman, Bell System Tech. J. 43, 1505 (1964); and D.G. Carlson, JAP 39, 4369 (1968).

2. D. Roess, J. of Appl. Phys. 37, 2004 (1966).

3. Y. Miyazoe, M. Maeda, IEEE J. Quantum Electronics QET, 36 (1971).

4. A. Eranian, P. Dezauzier and O. DeWitte, Optics Communications 7, 150 (1973).

5. C. Lin and C.V. Shank, Appl. Phys. Letters 26, 389 (1975).

6. C. Lin, J. Appl. Physics 46, 4076 (1975).

7. H. Salzmann and H. Strohwald, Physics Letters 57A, 41 (1976).

SECTION V

SPECTROSCOPY OF A HIGH CONCENTRATION Al-PHOSPHATE GLASS

ABSTRACT

An Al-phosphate glass containing Nd^{3+} in concentrations ranging from 3×10^{20} to 2.7×10^{21} ions/cm^3 has been prepared and investigated spectroscopically. Different ways of measuring the $^4F_{3/2} \rightarrow {}^4I_{9/2}$ emission cross sections yield values between 1.96×10^{-20} and 2.7×10^{-20} cm^2. At the highest concentration the decay time is 50 μs, while the radiative lifetime is estimated to be $\geq$ 446 μs. Lasing experiments were performed by pumping thin platelets of glass coaxially with a dye laser. Cross sections, losses and differential efficiencies are derived from these experiments. The status of high concentration glasses vs. stoichiometric Nd compounds is viewed.

1. INTRODUCTION

In the last few years, there has been considerable activity in attempts to make small lasers which involve stoichiometric Nd compounds which contain up to 30 times the Nd content of conventional Nd laser materials such as Nd:YAG. This work has been recently reviewed by Chinn, Hong, and Pierce[1] and by Danielmeyer.[2] The most promising single crystalline materials are $LiNdP_4O_{12}$ and NdP_5O_{14}, otherwise known as meta and ultraphosphates (the ultraphosphates are also referred to in the literature as pentaphosphates).

The above compounds make use of particular crystalline lattice constraints which isolate Nd ions so that typical Nd-Nd distances are in the 0.5 - 0.7 nm range. The phosphate materials accomplish this by formation of polymer chains in which Nd ions are separated by -O-P-O- linkages.

In view of the success with crystalline stoichiometric materials the question has been recently raised whether development of high concentration glasses is another possible alternative.[3,4] This work is stimulated as much by the desirability to develop miniaturized Nd lasers as by the use of glass in fiber technology.[5,6] One possible approach is to form glasses of composition close to the meta and ultraphosphates. The Russian workers have been quite successful in obtaining glasses of composition close to the metaphosphate,[4] whereas ultraphosphate glasses have been difficult to control and are hygroscopic.*

Prior to the advent of stoichiometric materials, several groups, predominantly in the USSR and France, have been active in preparing various low concentration Nd-doped phosphate glasses for large laser applications.[7,8] The limitations which emerged from this work were due to concentration quenching and nonradiative losses attributable to OH contamination. The latter effect is quite analogous to our results on liquid hosts for Nd (namely $POCl_3$) which are extremely sensitive to water content.[9]

A number of procedures have been reported to reduce the water content of phosphate glasses by as much as two orders of magnitude.[10] These include bubbling N_2 through the liquid during founding, addition of Cl or F as getters, a prolonged founding procedure, and evacuation of the sample during founding. In general, however, this work has been limited to glasses with low Nd concentrations.

In totally unrelated work at GTE Laboratories, some aluminum phosphate glasses capable of accepting rather large concentration of rare earths

* Private communication, J. Gualtieri, Ft. Monmouth, New Jersey.

have been developed. Normally trivalent cations such as aluminum are not considered the best choice for laser glasses since they invariably lead to a rather broad fluorescence line width.[8] In this investigation we were not guided by the choice of best possible glass composition but rather by the availability of the material and need to establish a standard of reference for further work. The usefulness of such a reference is obvious when one considers that in the literature of phosphate glasses the details of the spectroscopy needed to fully describe a system are often omitted.[11]

In this paper, we describe some spectroscopic results and laser operation with high Nd concentration aluminum phosphate glasses. The results are encouraging considering that no special attempts were made to control or reduce water contamination.

2. MATERIAL PREPARATION

Neodymium-doped aluminum phosphate glasses have been prepared by heating mixtures of $Al(OH)_3$ and Nd_2O_3 in ~ 1 M H_3PO_4 to increasing temperatures in order to remove the water and to obtain a homogenous starting batch. The solid mix is fired in Al_2O_3 crucibles at 1500°C for 1 hour. The initial composition is chosen to correspond to the metaphosphate AlP_3O_9; during firing, P_2O_5 volatilization shifts the composition to the desirable glass-forming region in the vicinity of the AlP_3O_9-$AlPO_4$ eutectic which is shown in Figure 1. After pouring into graphite molds, the samples are annealed at ~ 700°C. Three samples of aluminum phosphate glass were prepared in this manner containing 31 mole % (24 weight %) Al_2O_3, and their Nd content is listed in Table 1.[12]

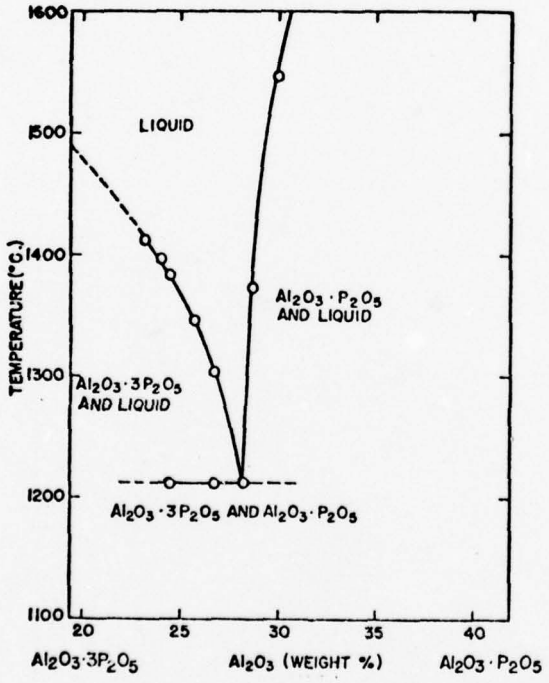

Figure 1. The Binary System $Al_2O_3 \cdot 3P_2O_5$ - $Al_2O_3 \cdot P_2O_5$ (from Ref. 12)

TABLE 1

Nd-CONTAINING ALUMINUM PHOSPHATE GLASSES

Sample	Density g/cm^3	Nd Concentration (ion/cm^3)
1	2.587	2.9×10^{20}
2	2.627	8.3×10^{20}
3	2.770	2.7×10^{21}

3. EXPERIMENTAL RESULTS

3.1 EMISSION-ABSORPTION

For spectroscopic purposes, plates of 5 x 5 mm dimension and thickness ranging from 0.025 cm to 0.6 cm were cut from the glass buttons and polished on both sides. Emission spectra were taken by using either Xe arc or dye laser excitation as shown on Figure 2. Decay times could be obtained using the same apparatus. In this case, the fluorescence in the 1.06 micron region was isolated by an interference filter and detected by a photomultiplier (PM1).

The apparatus could further be modified to obtain absorption spectra at low temperature which are needed for a correct assignment of levels. A tungsten filament lamp was imaged on the sample holder which in turn was imaged on the entrance slit. From runs made with and without a sample, a transmission curve (not corrected for reflection) could be obtained.

Figure 3 gives emission spectra at room temperature of the three glass samples excited by monochromatic radiation from the dye laser. We see that there is considerable difference between samples 2 and 3 in the resonance region (850 - 930 nm) due mostly to self-absorption. The shape of the laser transition line (1030 - 1080 nm) seems, however, hardly affected by the increase in concentration. A spectrally corrected emission intensity (using a standard lamp) for sample 2 is shown on Figure 4.

Figure 5 gives the absorbance (= α d $\log_{10}$e; α-absorption coefficient, d thickness) for sample 2 taken on a Cary 14 spectrometer. The labeling of the states is taken from Ref. 14. In making spectroscopic assignments of the various lines occurring in the emission spectrum, a room temperature absorption spectrum of the kind shown on Figure 5 is of limited usefulness because the transitions $^4I_{9/2} \rightarrow {}^4F_{3/2}$ are not resolved. In order to obtain better information on the structure of the ground state, low temperature absorption spectra had to be obtained.

Figure 6 gives the $^4I_{9/2} \rightarrow {}^2P_{1/2}$ absorption spectrum taken at liquid nitrogen temperature. Since the upper state is unsplit by the crystal field, this absorption should mirror the structure of the $^4I_{9/2}$ ground state. At 77°K, it does not seem possible to observe all the five stark components which may be expected to be present. From this spectrum, we can only identify the components Z_1, Z_2 and Z_3 of the $^4I_{9/2}$ manifold. The levels Y_i and R_i discussed below belong to the $^4I_{11/2}$ and $^4F_{3/2}$ manifold, respectively.

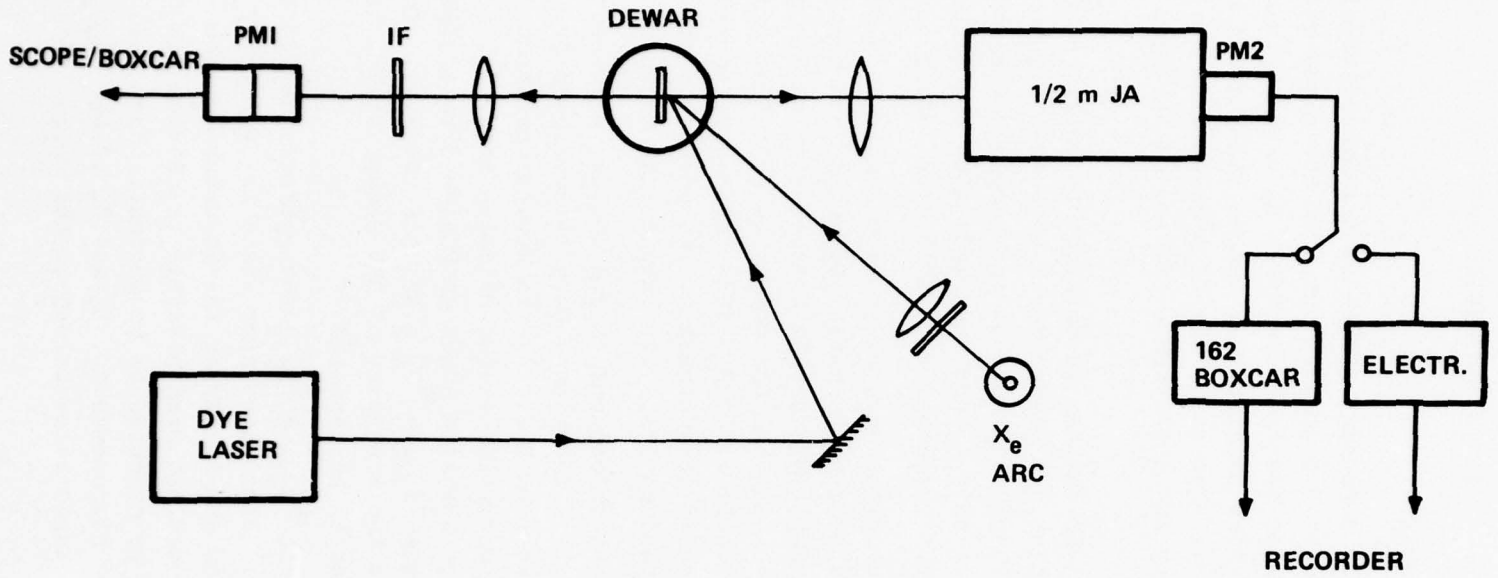

Figure 2. Schematic Layout of Apparatus for Measuring Lifetimes and Time Resolved Spectroscopy

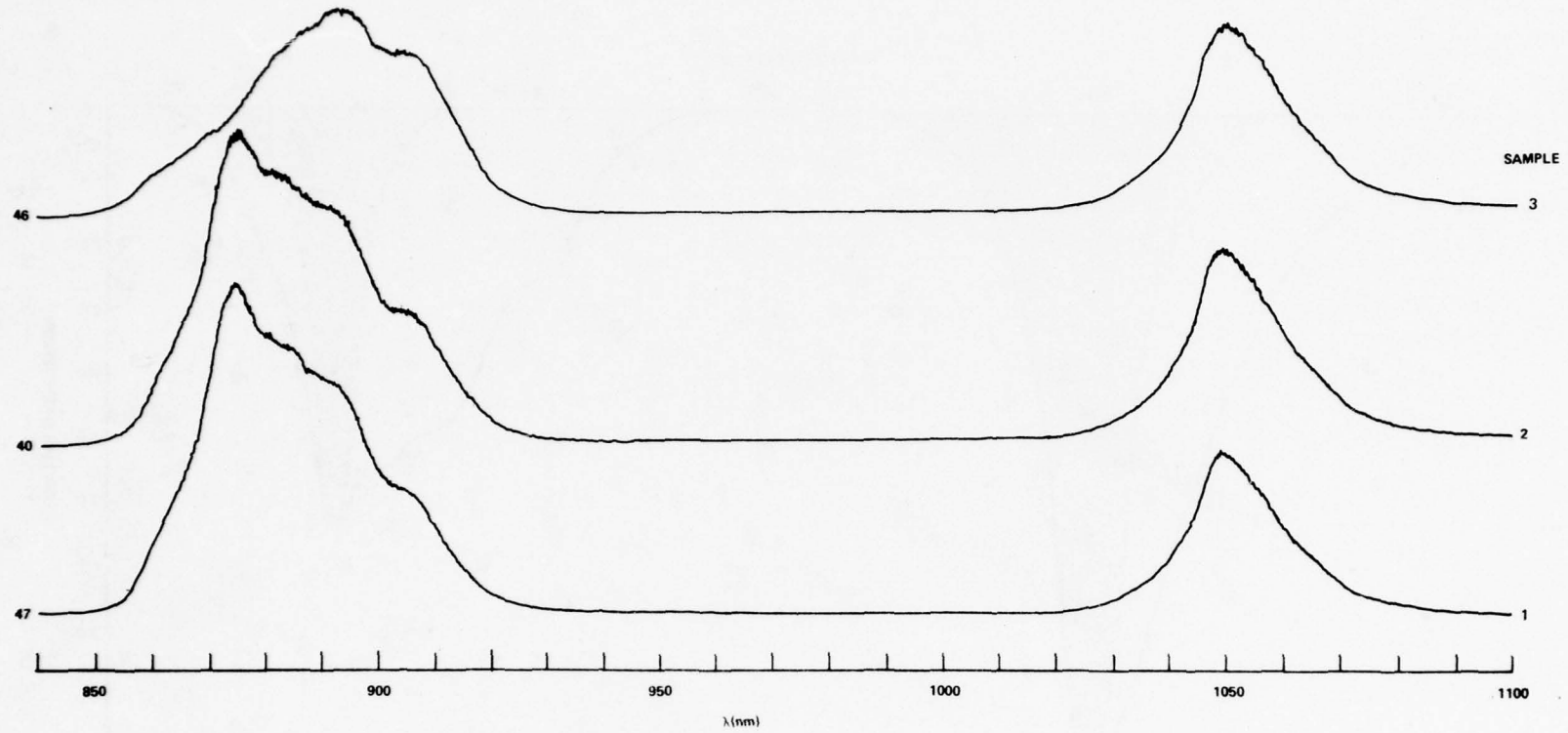

Figure 3. Emission Spectra of the Three Glass Samples (Room Temp. Monochromatic Excitation at 583.6 nm)

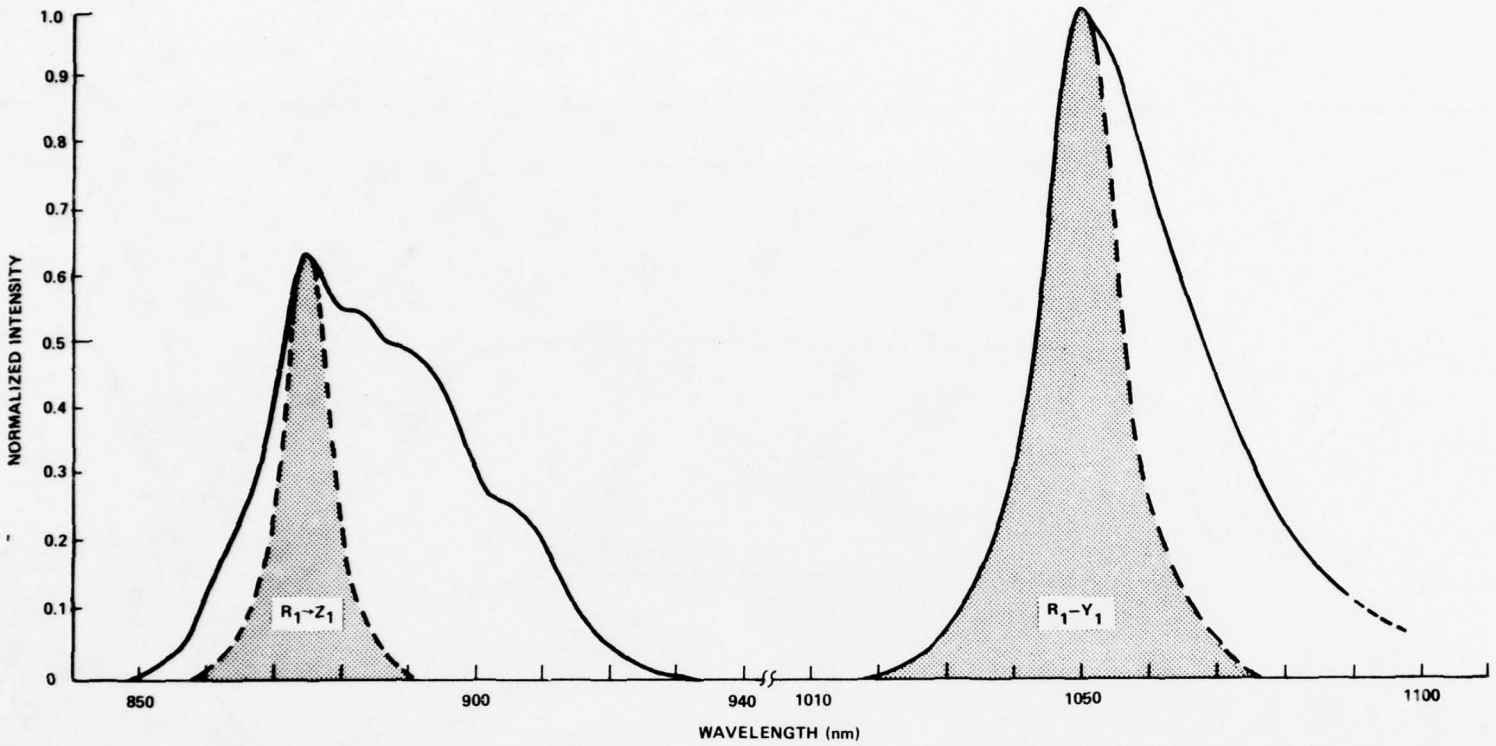

Figure 4. Spectrally Corrected Emission Spectrum of Sample 2. For meaning of Shaded Portions see Section 3.3

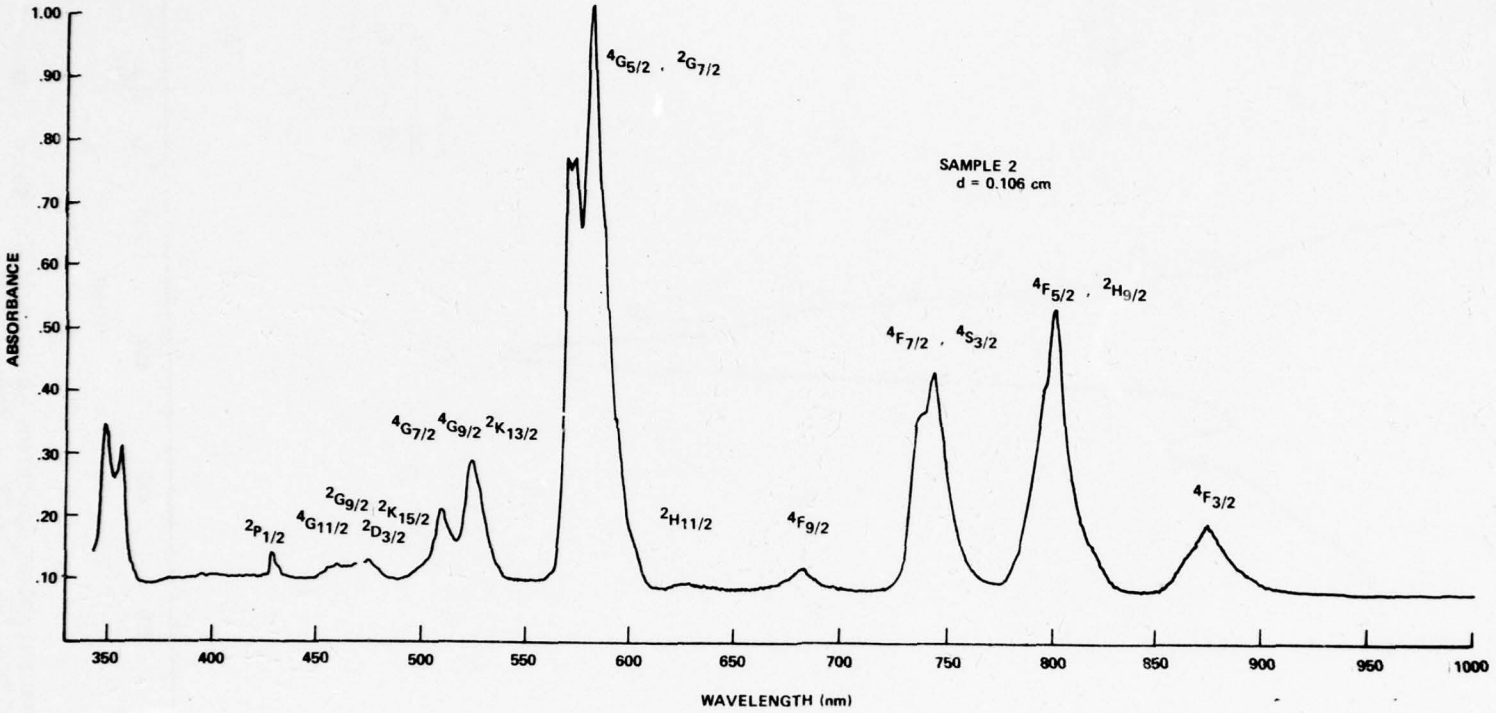

Figure 5. Absorbance Spectrum for Sample 2

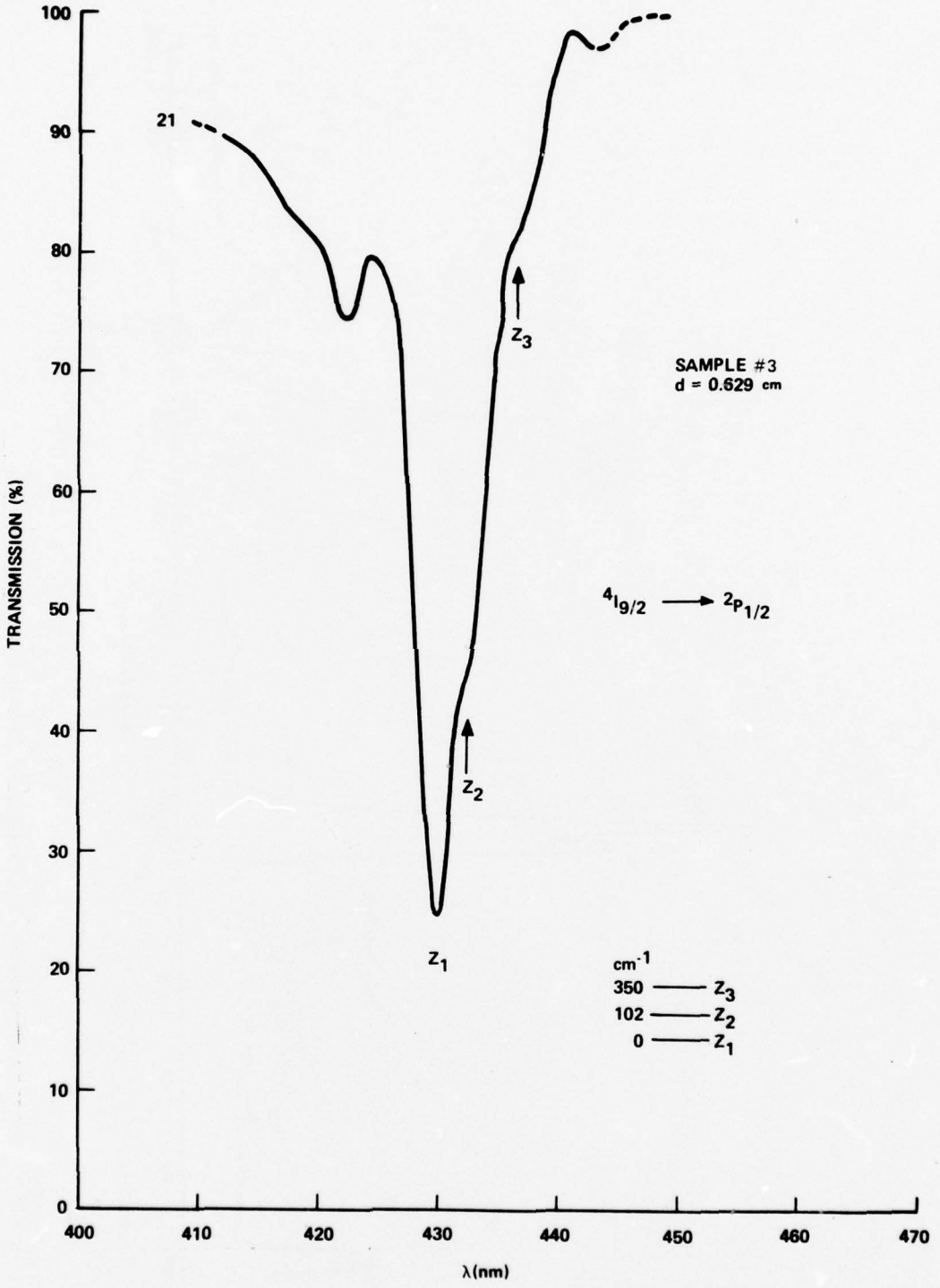

Figure 6. Transmission Spectrum at Liquid Nitrogen Temperature in the Region of the $^4I_{9/2} \rightarrow {}^4P_{1/2}$ Transition

The splitting of the $^4F_{3/2}$ manifold can be partially obtained from a low temperature spectrum taken in the region around 875 nm. This is shown on Figure 7. Since the lines are still quite broad at this temperature due to contribution from the Z_2 state, the $^4F_{3/2}$ splitting shown on the figure as 130 cm^{-1} cannot be regarded as highly accurate. A better value will be obtained by combining these data with low temperature emission spectrum shown on Figure 8.

It is well known that water (or OH) contamination of the host material introduces nonradiative quenching of the luminescence. In order to obtain some information on the water content, we have run infrared spectra of the samples in the region of 2.5 to 4 microns. An example of such a spectrum is given in Figure 9. The band at 3400 cm^{-1} marked with an arrow is attributed to OH. From the peak transmission of 82% (not corrected for reflection), we obtain an absorption constant α (3400 cm^{-1}) < 7.9 cm^{-1}. This value will be compared in the next section with measurement quoted in the literature.

3.2 SPECTROSCOPIC ASSIGNMENTS

From the data of Figures 3, 6 and 8, we can arrive at a plausible assignment of some six lines in the resonance region. Assignments in the laser transition region are more difficult because the lines are poorly resolved and we have no independent information on the structure of the ground state. There is, however, little doubt that the peak occurring at 1052 nm occurs from the lower $^4F_{3/2}$ level, R_1. Comparing Figures 3 and 8 we see that this peak remains largely unaffected by temperatures, whereas the short wavelength shoulder of the emission band sharpens considerably, leaving a small residual peak (transition from R_2) at 77°K and located at 1036 nm. The energy difference between these peaks corresponds to 147 cm^{-1} and hence is within 10 cm^{-1} of the R_1 - R_2 splitting determined from the resonance transition data (Figure 6). The summary of the assignments is given on Figure 10 and in Table 2. The extent of the $^4I_{11/2}$ state on the long wavelengths side (Y_6 level) can only be given approximately because of the tailing off response of the S1 photomultiplier.

3.3 EMISSION CROSS SECTION

From the spectroscopic data, we can determine the emission cross section for the transition $^4F_{3/2} \rightarrow {}^4I_{9/2}$. There are several ways of handling this problem, resulting in somewhat different expressions for the cross section. In each case the basic idea is to compare the

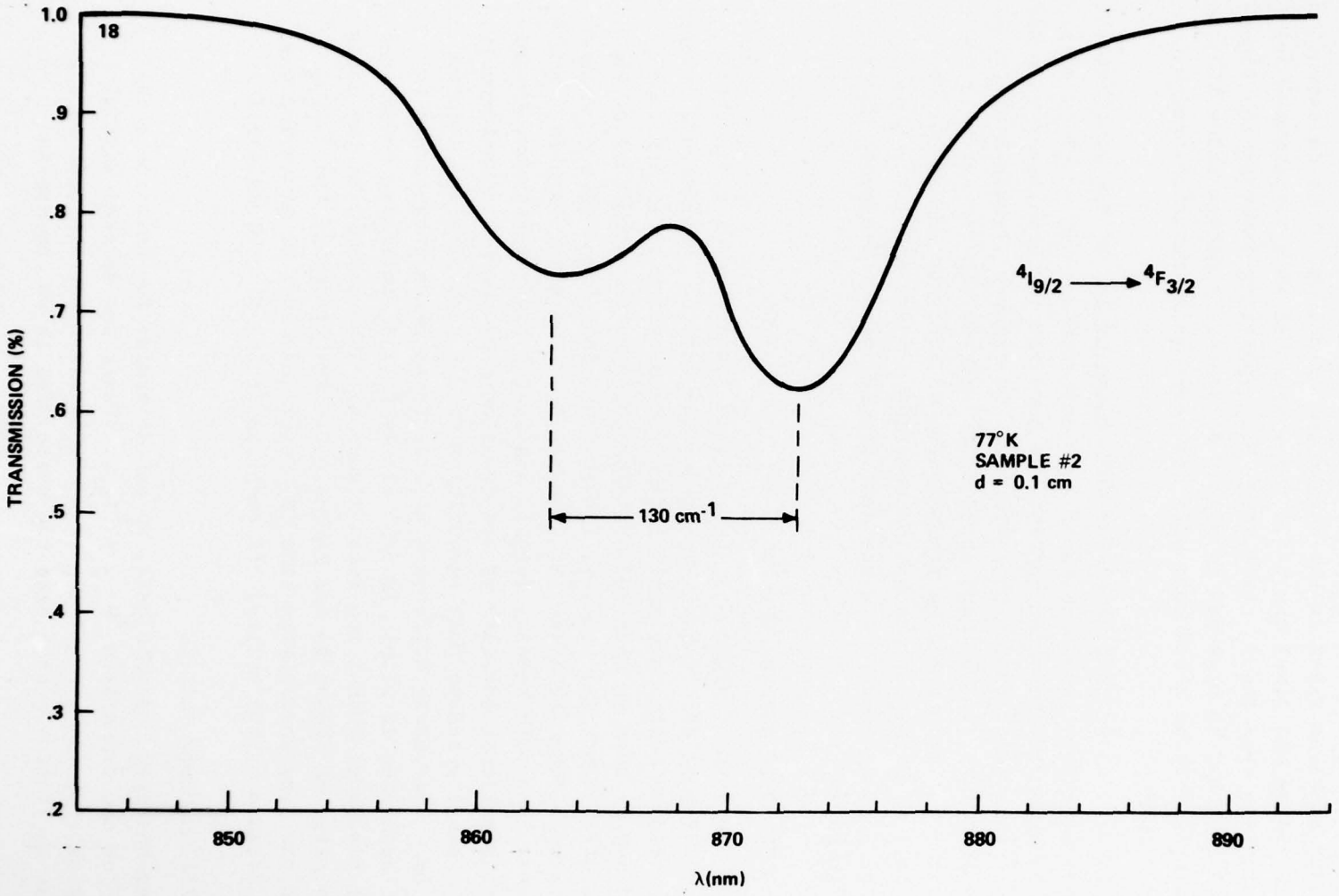

Figure 7. Transmission Spectrum at Liquid Nitrogen Temperature in the Region of the $^4I_{9/2} \rightarrow {}^4F_{3/2}$ Transition

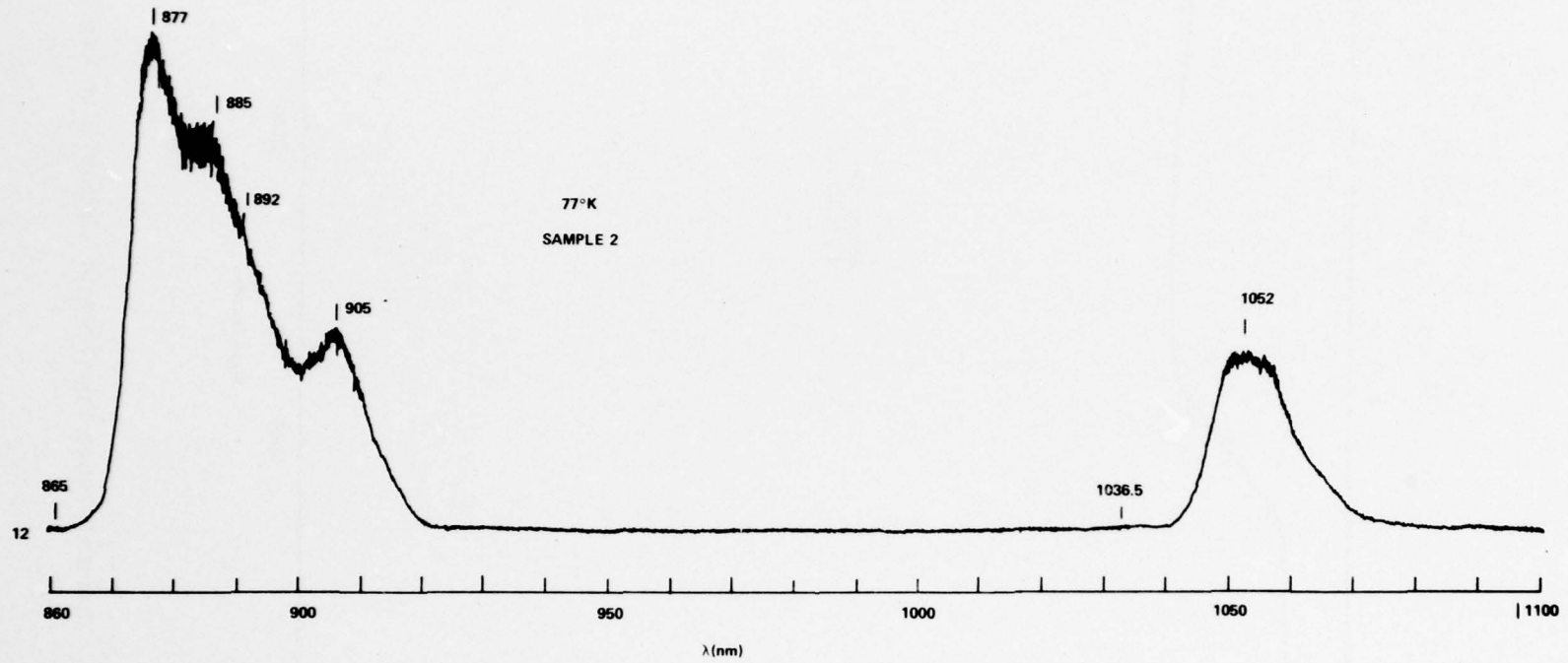

Figure 8. Emission Spectrum of Sample 2 at Liquid Nitrogen Temperature

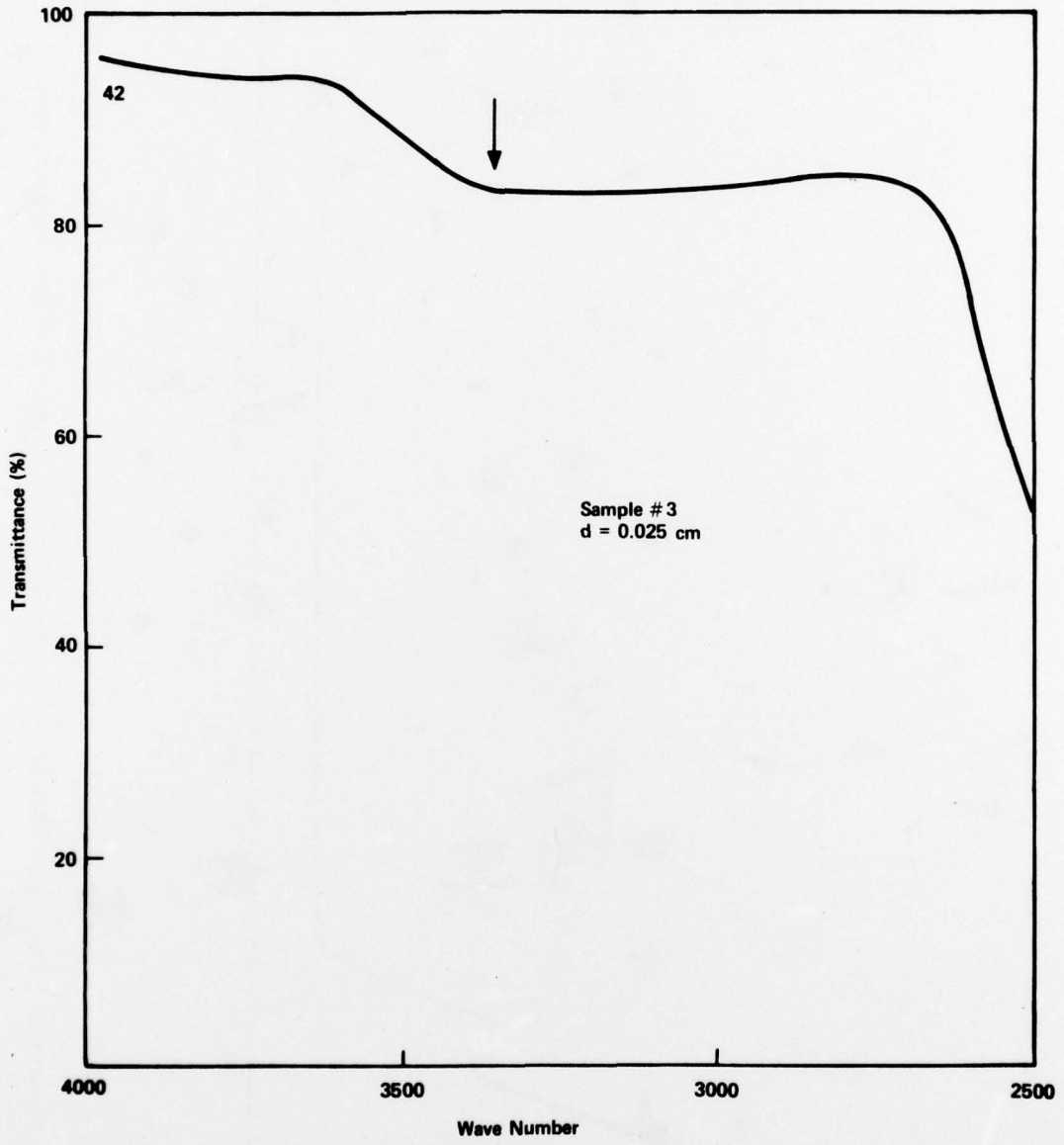

Figure 9. Transmittance Spectrum of Sample 1 in the Infrared

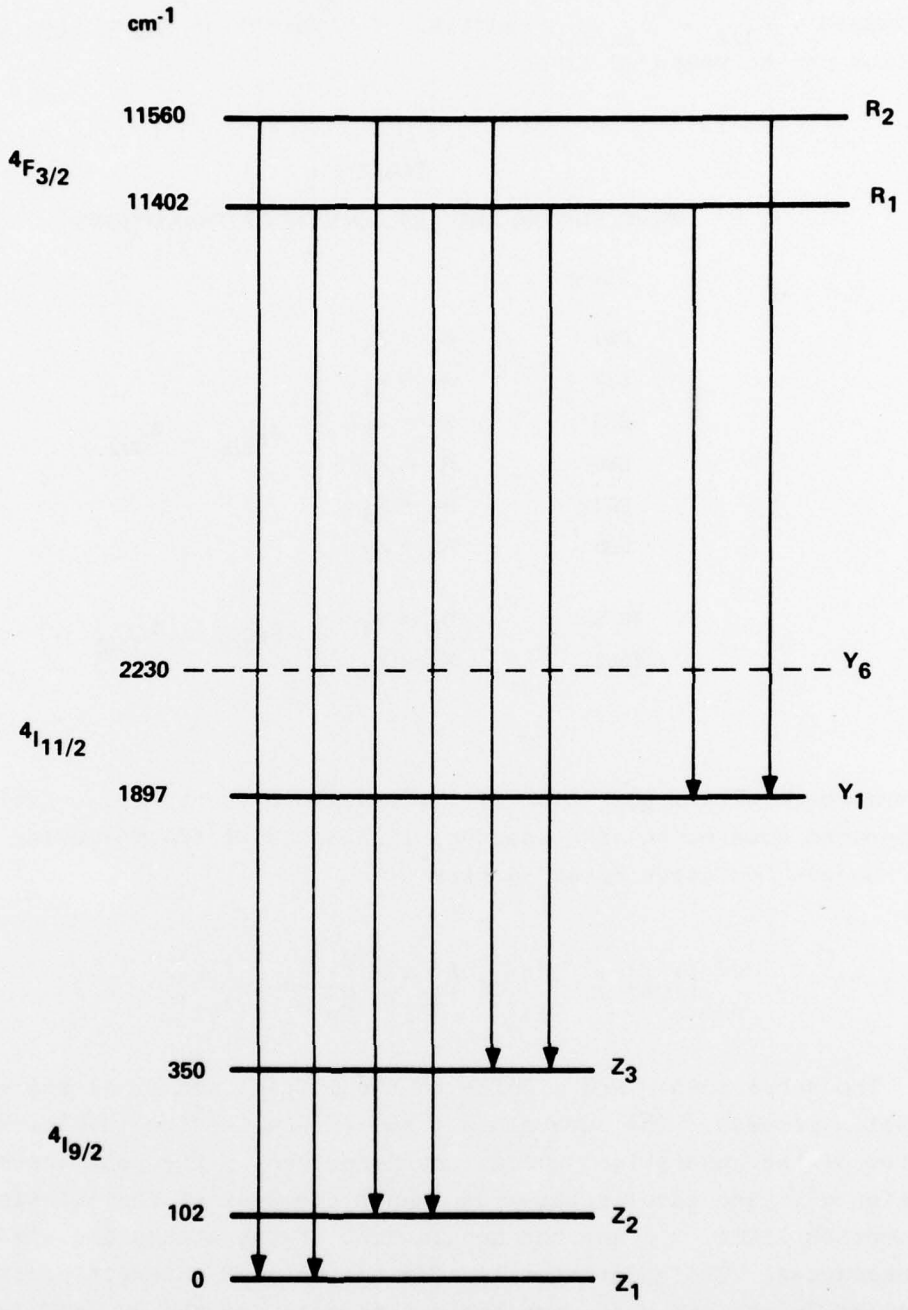

Figure 10. Energy Level Diagram Derived from Emission and Absorption Spectra

fluorescence intensities of the laser ($^4F_{3/2} \rightarrow {}^4I_{9/2}$) transition and the resonance ($^4F_{3/2} \rightarrow {}^4I_{11/2}$) transition for which the absorption cross section can be measured directly.

TABLE 2

WAVELENGTHS AND ASSIGNMENTS OF TRANSITIONS

λ(nm)		
865	$R_2 \rightarrow Z_1$	$^4F_{3/2} - {}^4I_{9/2}$
877	$R_1 \rightarrow Z_1$	
873	$R_2 \rightarrow Z_2$	
885	$R_1 \rightarrow Z_2$	
892	$R_2 \rightarrow Z_3$	
905	$R_1 \rightarrow Z_3$	
1036	$R_2 \rightarrow Y_1$	$^4F_{3/2} - {}^4I_{11/2}$
1052	$R_1 \rightarrow Y_1$	

A straightforward application of the Ladenburg-Fuchtbauer equation for the integrated absorption of a spectral line leads to the following expression for the peak emission cross section[13]

$$\sigma^E_{n\rightarrow m}\left(\lambda_{nm}\right) = \sigma^A_{i\rightarrow j}\left(\lambda_{ij}\right)\left(\frac{\lambda_{nm}}{\lambda_{ij}}\right)^5 \frac{N_j}{N_n}\frac{g_i}{g_j}\frac{I\left(\lambda_{nm}\right)}{I\left(\lambda_{ji}\right)} \quad . \tag{1}$$

The subscripts n and m refer to the initial and final states in the emission process. The subscripts i and j refer to the initial and final states of the absorption process characterized by the peak absorption cross section σ^A. The wavelengths λ designate the peak of the emission and absorption lines; N's are the populations of the states and g's are their degeneracies. The quantities I refer to the peak intensities of the emission (watts per unit wavelength interval) for the n→m and j→i lines.

Eq. (1) involves no approximations other than the equality of local field corrections for the various states[14] and is well suited for the calculation of cross sections if the n→m and i→j transition can be unambiguously assigned. Such is the case of Nd in YAG to which Eq. (1) was

applied in Ref. 13. Use of Eq. (1) for a substance like glass is not entirely justified because the lines connecting individual Stark components of the $^4F_{3/2}$, $^4I_{9/2}$ and $^4I_{11/2}$ states are not well resolved. It is, in principle, possible to follow the procedure of Mann and DeShazer[15] and decompose the broadened spectrum, but such procedure is both tedious and not necessarily unique. With this proviso it is nevertheless instructive to apply it to the glass case. From the spectroscopic assignment it appears reasonable that the peaks at 877 nm and 1052 nm correspond to the $R_1 \rightarrow Z_1$ and $R_1 \rightarrow Y_1$ transitions. If we assume that other transitions contribute negligibly to the peak intensities at these two wavelengths (a fact schematically illustrated by the shaded portions on Figure 4) then we can use the ratio of these two intensities directly in Eq. (1). We further need the absorption cross section for sample 2 corresponding to the $Z_1 \rightarrow R_1$ transition (877 nm). The peak absorption constant is measured to be 2.3 cm^{-1} for this line. The peak cross section is then given by:

$$\sigma^A = \frac{\alpha_{peak}}{N(Z_1)} \quad , \tag{2}$$

where the population of the state Z_1 is:

$$N(Z_1) = \frac{g_1 N_0 e^{-E_1/kT}}{\sum_i g_i e^{-E_i/kT}} \quad . \tag{3}$$

N_0 is the concentration of Nd^{3+} per cc and g_i is the degeneracy of the state. Using the three Z states from Figure 10 and assigning to each a Kramers degeneracy of 2, we obtain for the partition function a value of 3.59 and for the peak absorption cross section:

$$\sigma^A(Z_1 \rightarrow R_1) = 0.5 \times 10^{-20} \text{ cm}^2 \quad . \tag{4}$$

Since both emission and absorption transitions involve the same R_1 level:

$$\frac{N_j}{N_n} = 1 \quad . \tag{5}$$

From these values we obtain from Eq. (1):

$$\sigma^E(R_1 \rightarrow Y_1) = 1.96 \times 10^{-20} \text{ cm}^2 \quad . \tag{6}$$

There exists another way of calculating the emission cross section, widely used in the glass literature[16] and first formulated by Sarkies, Sandoe and Parke.[17] In this formulation the individual and unresolved Stark components of a state are all lumped together and the cross sections (both for emission and absorption) are averaged for the whole state. The result is:

$$\bar{\sigma}^E\left({}^4F_{3/2} \rightarrow {}^4I_{9/2}\right) = \left(\frac{\lambda_1}{\lambda_r}\right)^7 \frac{1}{\Delta\lambda_{eff}} \frac{5}{2} \frac{\int I_1(\lambda)d\lambda}{\int I_r(\lambda)d\lambda} \int \sigma_r^A(\lambda)d\lambda \quad . \quad (7)$$

where the subscripts 1 and r refer to the laser and resonance regions; the factor 5/2 is the ratio of degeneracies of the ground and metastable level (${}^4F_{3/2}$) and $\Delta\lambda_{eff}$ is defined by:

$$\Delta\lambda_{eff} = \frac{\int I_1(\lambda)d\lambda}{I_1(peak)} \quad . \quad (8)$$

The integrated absorption cross section appearing in Eq. (7) is obtained from an absorption spectrum similar to that of Figure 5 but taken on a sample of 0.188 cm. We obtain:

$$\int \sigma_r^A(\lambda)d\lambda = \frac{1}{N_0}\int \alpha_r(\lambda)d\lambda = 0.64 \times 10^{-26} \text{ cm}^3 \quad . \quad (9)$$

With $\Delta\lambda_{eff}$ = 28.8 nm the emission cross section is:

$$\sigma^E\left({}^4F_{3/2} \rightarrow {}^4I_{9/2}\right) = 2.7 \times 10^{-20} \text{ cm}^2 \quad . \quad (10)$$

The discrepancy between the two values of the emission cross section indicates the sensitivity of the result to the method of calculation, the assumptions that go into the use of Eqs. (1) and (7), and indeed the definition of the quantity which is often loosely called the "emission cross section."

It has been pointed out recently[18] that the averaging which goes into the derivation of Eq. (7) may be seriously at fault if the transitions between individual Stark components of initial and final states are not equal and if their populations differ significantly. Strictly speaking, Eq. (7) is only valid when the states are degenerate. It is thus difficult to pinpoint exactly the reason for the discrepancy, but the results illustrate the pitfalls of applying indiscriminately expressions taken from the literature. A possible way of obtaining more reliable values of emission

cross section has been indicated in Ref. 18 but this requires data taken at liquid helium temperature.

A comment should be made about the role of self-absorption in the determination of the cross section. Examining the spectra of Figure 3 it is obvious that the spectrum of sample 3 is heavily distorted by self-absorption in the resonance region. Samples 1 and 2, however, show almost identical spectra -- although they differ by a factor of 2.8 in Nd concentration. We have also calculated the self-absorption correction for sample 2 and concluded that it may account for an error in the resonance spectrum of less than ten percent. Neglecting self-absorption can, therefore, only result in a slight overestimate of the cross sections.

3.4 LIFETIMES

The luminescence decay times were measured for the three samples by using short pulse (dye laser) excitation at 584 nm and the boxcar averager. For the most concentrated sample 3, a slight deviation from exponential decay is observed in the early stages of decay as shown on Figure 11. Such a deviation is common in Nd doped glasses and is a consequence of the statistical distribution of ion sites.

Heat treatment of glass 3 at 750°C for 2 hrs in vacuum or in oxygen did not produce any measurable change in the lifetime. To the degree that the decay time of the most concentrated sample is due to OH contamination, much longer annealing times and possibly higher temperatures may be required to reduce this contamination.

The dependence of decay time on concentration is presented on Figure 12 (curve marked Al-Phosphate). Unfortunately, we are not certain of the limiting value of the decay time at low Nd concentration since low doped samples were not available. In the same figure we have also entered data on other materials which we shall discuss in the next section.

The radiative lifetime of the state $^4F_{3/2}$ can be obtained in terms of the cross section for a luminescent transition connecting this state to a lower state (say $^4I_{9/2}$) and the branching ratio γ for this transition,[14]

$$\tau_{Rad}\left(^4F_{3/2}\right) = \gamma_{9/2} \frac{\lambda_1^4}{8\pi c n^2 \Delta\lambda_{eff}\, \sigma^E} \qquad (11)$$

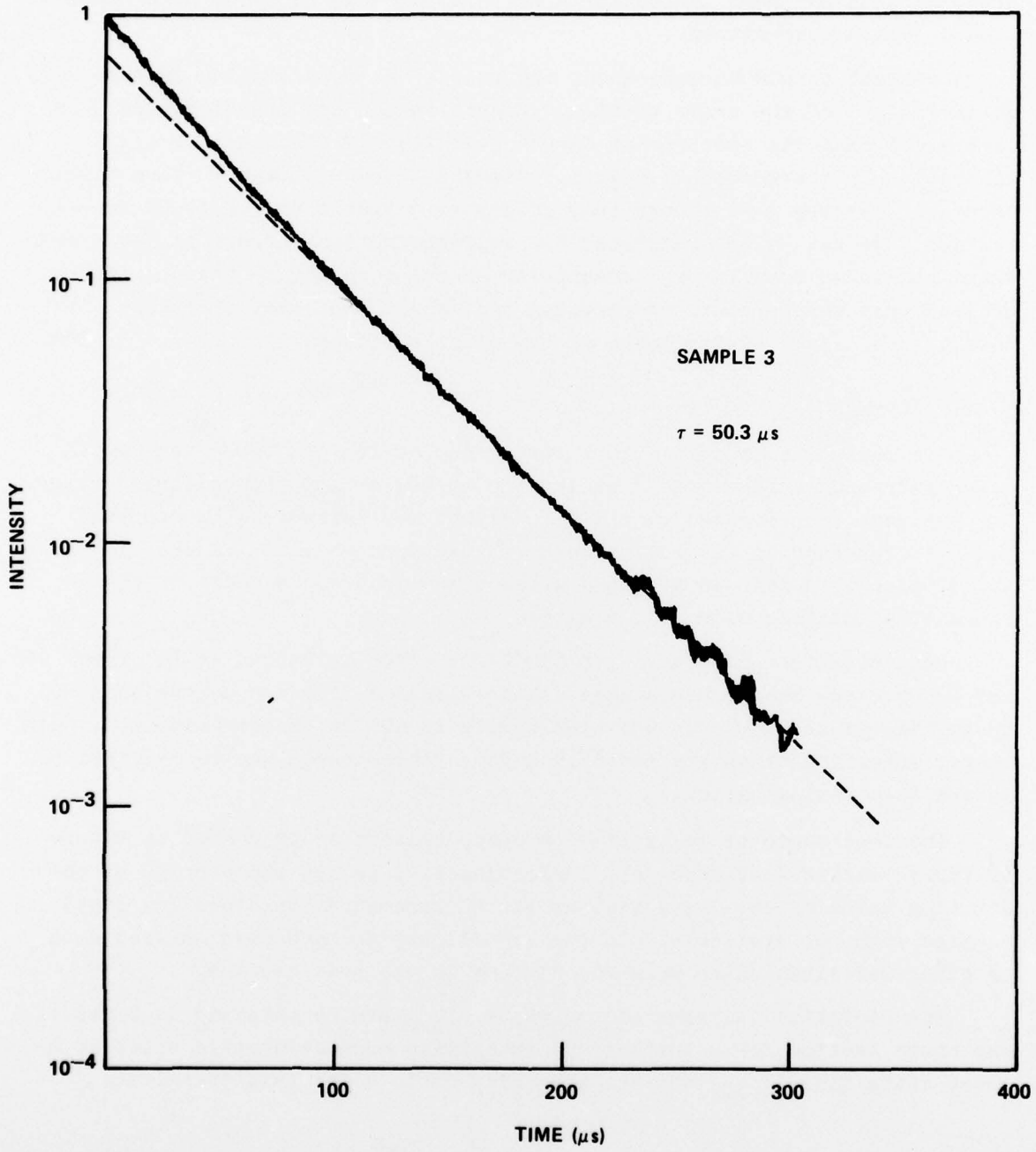

Figure 11. Decay of Fluorescence of Sample 3 at Room Temperature

where we have taken n = 1.55.[18] An accurate determination of the branching ratios require measurements of emission intensity for transitions terminating on all members of the quartet I manifold. This has not been carried out for the states $^4I_{13/2}$ and $^4I_{15/2}$. Assuming, however, reasonable values taken from the literature,[16] we obtain:

$$\gamma_{9/2} = 0.385$$
$$\gamma_{11/2} = 0.514$$
$$\gamma_{13/2} \simeq 0.1$$
$$\gamma_{15/2} \simeq 0 \qquad (12)$$

From Eq. (11) and these values we obtain:

$$\tau_{Rad} = \begin{cases} 446\ \mu s \\ 614\ \mu s \end{cases} \qquad (13)$$

depending whether the larger or smaller of the two cross sections were taken. These two values of the calculated radiative lifetime could be checked against measurements of decay time taken on very dilute samples. On the basis of available data (see Figure 16), it is not possible to say which is closer to the true value.

4. CONCLUSIONS

For the purpose of comparison, we present in Table 3 some basic data on a few representative phosphate glasses. We see from this comparison that parameters of our aluminum phosphate glass fall well within the range of those measured on other preparations.

To our knowledge, only the two last entries (Li-MP and the Al-phosphate) have been investigated at Nd concentrations substantially exceeding 10^{21} ions/cm^3, and therefore comparable to the stoichiometric Nd compounds. From Table 3 we see that these two glasses are roughly equivalent.

TABLE 3
COMPARISON OF SOME PHOSPHATE GLASSES

	LHG-5*	P107*	EV1*	L-41*	Li-MP**	Al–Phosphate
$\Delta\lambda_{eff}$ (nm)	25.5	26.5	21.7	32.5	31.0	28.8
λ_ℓ (nm)	1054	1054	1054	1056	1055	1052
τ_{rad} (μs)	351	322	314	564	330	446
σ^E (10^{-20} cm^2)	3.9	3.9	4.7	1.9	3.2	2.7

* Ref 16
** Li-Metaphosphate Ref 4

Another perspective on high concentration phosphate glasses is obtained from Figure 12. From it we see that both the aluminum phosphate and Li-MP fall between the concentration quenching curves of Nd ultraphosphate (UP)[19] and the French phosphate glasses reported in Ref. 8. The data on tellurite glasses were included in the figure since they were recently reported[6] and suggested as good candidates for minilasers.

The quenching characteristics of the Al-phosphate glass are essentially similar to the Li-MP glass. Since very dilute samples were not available at this time, we do not know to what extent the decay time would approach the calculated 446 µs radiative lifetime of the $^4F_{3/2}$ state. Should there be a substantial discrepancy, we would have to conclude that OH quenching occurs in our samples. The value of the infrared absorption constant (8 cm^{-1}), derived from Figure 9, compares favorably with values achieved by Soviet

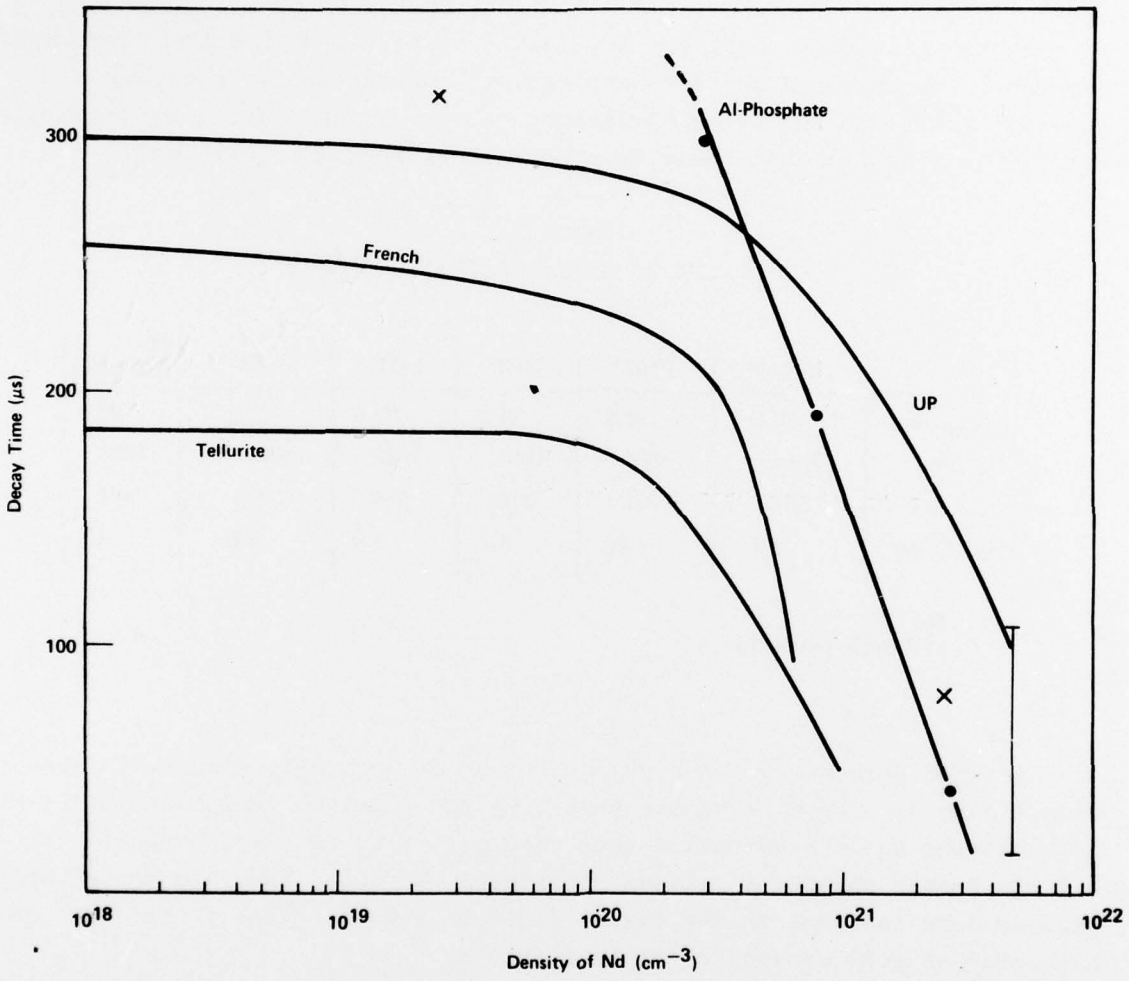

Figure 12. Concentration Quenching of Some Nd Containing Materials: ● - present Al phosphate glass; X - Li metaphosphate glass from Refs. 3 and 4; "UP" - Nd ultraphosphate from Ref. 19; "French" - phosphate glasses from Ref. 8; "Tellurite" - glass from Ref. 6

workers who used halogenization, bubbling and long founding times, since none of these procedures were attempted. It is, however, well above an absorption of 1 cm^{-1} at 3.45 microns achievable by extra care.[10] This leads us to believe that the Al-phosphate glasses do stand a chance of considerable improvement in that respect. We find it is somewhat surprising that Li-MP has much larger bandwidth than Al-phosphate, since according to the work of Deutschbein, et al.,[8] it appears that monovalent cations produce the narrowest lines, whereas trivalent cations (specifically Al) produce the largest.

For practical applications the chemical stability and resistance to moisture can be of major significance. In that respect the aluminum phosphate glass appears to be excellent. Over a period of months we have not observed any deterioration of the polished surfaces under ordinary laboratory conditions.

In summary our results indicate that high concentration glasses should not be neglected in the search for new Nd hosts since concentration quenching in these materials plays surprisingly less of a role than generally anticipated.[19] Finally, when the technology of preparation of this glass improves, the possibility of making large melts will offer a distinct advantage over one-at-a-time crystal growth.

The authors are grateful to Dr. L. Riseberg for making the Nd glass samples available. Many helpful clarifications on the chemistry aspects are due to Dr. B. McCollum. The absorption spectra were kindly supplied by Dr. P. Cukor. Dr. E.J. Johnson supplied a computer program for the correction of the spectra.

5. REFERENCES

1. S.R. Chinn, H.Y-P. Hong and J.W. Pierce, Laser Focus, 64 (May 1976).
2. H.G. Danielmeyer, Festkörperprobleme xv, 253 (1975).
3. Yu. K. Voronko, et al, Opt. Comm. 18, 88 (1976).
4. S.Kh. Batygov, et al, Sov. J. Quantum Electronics 6, 1220 (1976).
5. H.P. Weber, P.F. Liao, B.C. Tofield and P.M. Bridenbaugh, Appl. Phys. Lett. 26, 692 (1975).
6. S. Singh, L.G. van Uitert and W.H. Grodkiewicz, Opt. Comm. 17, 315 (1976).
7. P.M. Buzhinskii, M.E. Zhabotinskii, N.M. Zhavoropkov, V.G. Lebedev, B.I. Malyshev, I.U.P. Rudnitskii, V.V. Tsapkin and G.V. Ellert, Dokl. Akad Nank USSR 185, 1306 (1969).
8. O.K. Deutschbein, C.C. Pautrat and I.M. Svirchevsky, Rev. Phys. Appl. 2, 29 (1967).
9. H. Samelson and R. Kocher, "High Energy Pulsed Liquid Laser," Final Report (Aug. 1974) (Contract N0014-68-C-0110).
10. N.E. Alekseev, et al. Inorg. Mat. (USSR) 11, 270 (1975).
11. O.K. Deutschbein and C.C. Pautrat, IEEE J. Quant. Electr. QE4, 48 (1968).
12. P.E. Stone, E.P. Egan, Jr. and J.R. Lehr, J. Am. Ceram. Soc. 39, 92 (1956).
13. S. Singh, R.G. Smith and L.G. van Uitert, Phys. Rev. B10, 2566 (1974).
14. W.F. Krupke, IEEE J. Quant. Electr. QE10, 450 (1974).
15. M.M. Mann and L.G. DeShazer, J. Appl. Phys. 41, 2951 (1970).
16. R.R. Jacobs and M.J. Weber, IEEE J. Quant. Electr. QE12, 102 (1976).
17. P.H. Sarkies, J.N. Sandoe and S. Parke, J. Phys. D. Appl. Phys. 4, 1642 (1971).
18. E.M. Dianov, A. Ya. Karasik, L.S. Kornienko, A.M. Prokhorov and I.A. Shcherbakov, Sov. J. Quant. Electr. 5, 901 (1976).
19. A.Lempicki, R.M. Klein and S.R. Chinn, IEEE J. Quant. Electr., to be published.

Unclassified

SECURITY CLASSIFICATION OF THIS PAGE (When Data Entered)

REPORT DOCUMENTATION PAGE		READ INSTRUCTIONS BEFORE COMPLETING FORM
1. REPORT NUMBER 13299.3-P ✓	2. GOVT ACCESSION NO.	3. RECIPIENT'S CATALOG NUMBER
4. TITLE (and Subtitle) Nd Mini Lasers Based on Stoichiometric Rare Earths Compounds		5. TYPE OF REPORT & PERIOD COVERED 25 JUNE 75-24 JUNE 77 6. PERFORMING ORG. REPORT NUMBER
7. AUTHOR(s) A. Lempicki E. Johnson B. McCollum		8. CONTRACT OR GRANT NUMBER(s) DAAG29 75 C 0028 new use
9. PERFORMING ORGANIZATION NAME AND ADDRESS General Telephone & Electronics Laboratories Incorporated ✓ Waltham, Massachusetts 02154		10. PROGRAM ELEMENT, PROJECT, TASK AREA & WORK UNIT NUMBERS
11. CONTROLLING OFFICE NAME AND ADDRESS U. S. Army Research Office P. O. Box 12211 Research Triangle Park, NC 27709		12. REPORT DATE Apr 1978 13. NUMBER OF PAGES 157
14. MONITORING AGENCY NAME & ADDRESS(if different from Controlling Office)		15. SECURITY CLASS. (of this report) unclassified 15a. DECLASSIFICATION/DOWNGRADING SCHEDULE

16. DISTRIBUTION STATEMENT (of this Report)

Approved for public release; distribution unlimited.

17. DISTRIBUTION STATEMENT (of the abstract entered in Block 20, if different from Report)

18. SUPPLEMENTARY NOTES

The findings in this report are not to be construed as an official Department of the Army position, unless so designated by other authorized documents.

19. KEY WORDS (Continue on reverse side if necessary and identify by block number)

MICRON

20. ABSTRACT (Continue on reverse side if necessary and identify by block number)

This report contains an account of the principal results of an investigation into new stoichiometric compounds of Nd over a two-year period. The overall objective of this program was to develop new high concentration Nd materials for miniature lasers emitting at 1.06μ. At the present time there are only a few such compounds. Nd pentaphosphate being the most widely known. Although remarkable in its efficiency, relative lack of concentration quenching and high gain, the growth of pentaphosphate crystals has proved to be difficult. The crystal growth problems of the pentaphosphate coupled with the possibilities for improved performance by new materials were motivating factors in the research.

DD FORM 1 JAN 73 1473 EDITION OF 1 NOV 65 IS OBSOLETE

Unclassified